

**Revealing State Delays in Chemical Engineering:
A Control Framework for Distributed Parameter Systems**

by

Behrad ‘Brad’ Moadeli

A thesis submitted in partial fulfillment of the requirements for the degree of

Doctor of Philosophy

in

Process Control

Department of Chemical and Materials Engineering
University of Alberta

Abstract

This guide is a comprehensive resource crafted for University of Alberta students tackling their theses with LaTeX. It is designed to simplify the thesis-writing process by offering a detailed walkthrough of a custom LaTeX template tailored to meet the university's formatting requirements. The guide goes beyond mere template usage, providing step-by-step instructions, tips, and best practices for creating a well-structured thesis that adheres to academic standards.

It also delves into advanced customization techniques, allowing users to achieve specific stylistic elements and formatting nuances that suit their individual needs. Alongside these, the guide introduces JabRef, a robust reference management tool, and explains how to seamlessly integrate it with LaTeX to streamline citation management. Whether you are a novice or an experienced LaTeX user, this guide equips you with the knowledge and tools necessary to produce a polished, professional thesis. By following its clear and concise instructions, students can confidently navigate the complexities of thesis writing, ensuring their work is both technically sound and perfectly laid out. Test.

Preface

Writing a thesis is no small task, and as a graduate student at the University of Alberta, I quickly realized just how challenging it can be to meet all the formatting requirements while also producing a document that looks professional. Like many others, I started out using traditional word processors, but it didn't take long before I ran into the usual headaches—crashes, file corruption, and formatting issues that seemed to have a mind of their own.

These frustrations led me to explore L^AT_EX as an alternative. I discovered that L^AT_EX not only provided a way to keep my content and formatting separate but also offered a more reliable and consistent way to produce a high-quality thesis. The learning curve was steep, but once I got the hang of it, I found it to be a game-changer.

The original template document was born out of my experience with L^AT_EX and the desire to make the thesis-writing process a bit less daunting for others who might be in the same boat. My goal here with this new document is to provide a comprehensive guide that not only walks you through the basics of L^AT_EX but also gives you practical examples and best practices¹ to follow.

I built this template and class from the ground up with the aim of reducing the typical L^AT_EX learning curve. I have tried to keep it as simple as possible

¹These might not be the “best” practices, however, these are practices that I follow to make my work more constant.

while still making it powerful enough to handle everything you'll need for a thesis. I hope this document makes your life a little easier and that you find L^AT_EX as useful as I have.

Disclaimer: This guide provides practical insights and tips for writing a thesis, based on the information available at the time of writing. However, it remains *your responsibility* to verify the accuracy of all content, conclusions, and interpretations. Official university guidelines, requirements, and advice *always* takes precedence over this guide. I assume *no responsibility* for any potential inaccuracies, misrepresentations, or unintended consequences resulting from the use of any material presented in this guide or the supporting documentation and files.

To...

“Etiam ac leo a risus tristique nonummy. Donec dignissim tincidunt nulla. Vestibulum rhoncus molestie odio. Sed lobortis, justo et pretium lobortis, mauris turpis condimentum augue, nec ultricies nibh arcu pretium enim. Nunc purus neque, placerat id, imperdiet sed, pellentesque nec, nisl. Vestibulum imperdiet neque non sem accumsan laoreet. In hac habitasse platea dictumst. Etiam condimentum facilisis libero. Suspendisse in elit quis nisl aliquam dapibus. Pellentesque auctor sapien. Sed egestas sapien nec lectus. Pellentesque vel dui vel neque bibendum viverra. Aliquam porttitor nisl nec pede. Proin mattis libero vel turpis. Donec rutrum mauris et libero. Proin euismod porta felis. Nam lobortis, metus quis elementum commodo, nunc lectus elementum mauris, eget vulputate ligula tellus eu neque. Vivamus eu dolor.”

- Author of the Quote

Acknowledgements

While I would love to acknowledge every individual who has influenced this document, I realize that doing so might mean this document never gets finished.

I want to extend my deepest gratitude to my friends and family for their unwavering support throughout all my accomplishments.

A special thank-you goes out to the developers and other L^AT_EX users who have contributed to the L^AT_EX community. Without their work, this guide wouldn't exist in its current form.

I am also incredibly thankful to everyone who provided feedback and support along the way, including those new to L^AT_EX. Your fresh perspectives were invaluable in motivating the transformation from the previous version of this template into a full-fledged class, template, and this newly added guide to writing a thesis, complete with examples of the most requested elements to include.

Table of Contents

Abstract	ii
Preface	iii
Acknowledgements	vi
List of Tables	xii
List of Figures	xvii
List of Symbols	xviii
Abbreviations	xviii
Glossary of Terms	xx
Chapter 1: Introduction	1
1.1 Background	1
1.2 Objectives	2
1.3 Scope and Limitations	2
1.4 Organization of the Thesis	5
1.5 Summary	6
Chapter 2: Continuous-time Estimation and Optimal Control for the Isothermal System	7
2.1 Introduction	7
2.2 Open-loop System	13
2.2.1 System model	13

2.2.2	PDE representation of the delay term	15
2.2.3	Adjoint operator	17
2.2.4	Eigenvalue problem	17
2.3	Linear Quadratic Regulator Design	22
2.3.1	Full-state feedback regulator	22
2.3.1.1	Operator Riccati equation	22
2.3.1.2	Obtaining \mathfrak{B} and \mathfrak{B}^*	23
2.3.1.3	Matrix Riccati equation	24
2.3.2	Output feedback compensator	25
2.4	Results and Discussion	29
2.4.1	Full-state feedback regulator FDM representation	30
2.4.2	Observer-based regulator FDM representation	32
2.4.3	Parameter sensitivity analysis	37
2.5	Conclusion	39
	References	41

Chapter 3: Discrete-time Estimation and Model-Predictive Control for the Isothermal System	44	
3.1	Introduction	44
3.2	Mathematical Modeling of the Reactor System	47
3.2.1	Model representation	47
3.2.2	Adjoint system	52
3.2.3	Resolvent operator	52
3.2.4	Cayley–Tustin Time Discretization	56
3.3	Estimation and Control	56
3.3.1	Model predictive control design, full-state availability	56
3.3.2	Continuous-Time Observer Design	59
3.3.3	Discrete-Time Observer Design	60
3.3.4	Model predictive control design, output feedback implementation	61
3.4	Simulation Results	63
3.4.1	Full-State Feedback MPC Performance	64
3.4.2	Observer-Based Output Feedback MPC	66
3.5	Conclusion	68

References	69
Chapter 4: Non-isothermal System: Moving Horizon Estimation and Model Predictive Control	73
4.1 Introduction	73
4.2 Model Representation	76
4.2.1 Non-linear System Model with State Delays	76
4.2.2 State Delays as Transport PDEs	78
4.2.3 Steady-State Analysis	82
4.2.4 Linearized Model	82
4.3 Infinite-dimensional Representation	86
4.3.1 System Operators	86
4.3.2 Spectral Analysis	88
4.3.3 Adjoint System and Biorthogonal Basis	89
4.4 Cayley–Tustin Time Discretization	91
4.4.1 Resolvent Operator	92
4.4.2 Operator Mapping	98
4.5 Control and Estimation	100
4.5.1 Model Predictive Control	100
4.5.2 Moving Horizon Estimation	103
4.5.3 Closed Loop MHE-MPC Implementation	107
4.6 Simulation Results	107
4.6.1 Full-State MPC (Case I)	110
4.6.2 Output Feedback MHE–MPC (Case II)	111
4.7 Conclusion	115
References	116
Chapter 5: Concluding Remarks	120
5.1 Introduction	120
5.2 Inserting Figures	121
5.3 Tables and Tabularx	124
5.4 Advanced Table Features	125
5.5 Additional Packages for Enhanced Table Functionality	125
5.6 Conclusion	126

Bibliography	128
Appendix A: Additional Example Figures	134
Appendix B: Additional Example Tables	140
B.1 Section 1	140
B.2 Section 2	141
Appendix C: Including Code Listings	142
C.1 Using the <code>listings</code> Package	142
C.1.1 Basic Usage	142
C.1.2 Customizing Listings	143
C.2 Advanced Features	144
C.2.1 Including External Files	144
C.2.2 Handling Special Characters	144
C.3 Line Breaks in Long Code Lines	145
C.4 Conclusion	145
Appendix D: Including PDFs	146
D.1 How to Insert a Portrait PDF	147
D.2 How to Insert a Landscape PDF	150
Appendix E: Math Lettering	153

List of Tables

1.1	List of Other Available Templates	3
2.1	Physical parameters for the system	21
3.1	Physical Parameters for the System	51
4.1	Parameters used in the steady-state analysis for Case I (Unstable) and Case II (Stable)	84
4.2	Proposed MHE–MPC Algorithm	108
E.1	Math Mode Greek Letters	154
E.2	Blackboard Bold Letters	155
E.3	Calligraphic Letters	156
E.4	Fraktur Letters	157

List of Figures

2.1	Axial tubular reactor with recycle stream.	13
2.2	Eigenvalues of operator \mathfrak{A} obtained by solving Equation (2.11).	19
2.3	First few eigenmodes of \mathfrak{A} and \mathfrak{A}^*	20
2.4	Full-state feedback gain $K(\zeta)$ utilizing the first N modes of the system given by Equation (2.20).	26
2.5	Block diagram representation of the optimal full-state feedback control system.	26
2.6	Observer gain $L(\zeta)$	28
2.7	Eigenvalues of the observer-based controller, full-state feedback controller, and open-loop system.	28
2.8	Block diagram representation of the observer-based output feedback control system.	29
2.9	Input response of the system under full-state feedback control given by Equation (2.21), utilizing the feedback gain obtained in Figure 2.4.	31
2.10	2D cross-section plots of the full-state feedback input response at various ζ positions, utilizing the feedback gain obtained in Figure 2.4b.	31
2.11	Input response of the system under observer-based output feedback control given by Equation (??), utilizing the observer gain obtained in Figure 2.6 and the feedback gain obtained in Figure 2.4b.	33
2.12	2D cross-section plots of the input response at various ζ positions, utilizing the observer gain obtained in Figure 2.6 and the feedback gain obtained in Figure 2.4b.	34

2.13	Error dynamics of the observer-based regulator utilizing the observer gain obtained in Figure 2.6 and the feedback gain obtained in Figure 2.4b.	35
2.14	2D cross-section plots of the error dynamics of the observer-based regulator at various ζ positions, utilizing the observer gain obtained in Figure 2.6 and the feedback gain obtained in Figure 2.4b.	36
2.15	Measured output of the systems with different time delays τ , under observer-based output feedback control utilizing the observer gain obtained in Figure 2.6 and the feedback gain obtained in Figure 2.4b, where $\tau = 80$ s.	38
3.1	Axial tubular reactor with recycle stream.	47
3.2	Eigenvalues of operator \mathfrak{A}	51
3.3	Proposed full-state feedback model predictive control system. .	57
3.4	The effect of various observer gains $\mathfrak{L}_c = f(\zeta, l_{obs})$ on the eigenvalues of state reconstruction error dynamics λ_o	60
3.5	Block diagram representation of the observer-based MPC. . .	61
3.6	Open-loop concentration profile along the reactor.	64
3.7	Stabilized reactor concentration profile under the proposed full-state MPC.	65
3.8	Input profile and reactor output under full-state MPC, subject to constraints.	65
3.9	Stabilized reactor concentration profile under the proposed observer-based MPC.	67
3.10	Input profile and reactor output under observer-based MPC. .	67
3.11	State reconstruction error profile along the reactor.	67
4.1	Non-isothermal axial dispersion tubular reactor with recycle stream.	77
4.2	Steady-state solutions for Case I. Solid and dashed lines represent reactor and recycle stream profiles, respectively.	83
4.3	Steady-state solution for Case II. Solid and dashed lines represent reactor and recycle stream profiles, respectively.	83

4.4	Eigenvalue distribution in the complex plane for Case I (Unstable) and Case II (Stable).	89
4.5	3D profile of the state $x(\zeta, t)$ evolution over space and time (ζ, t) for Case I system with zero input.	110
4.6	Profiles of plant output $y(t)$ and control input $u(t)$ over time for Case I system with full-state feedback MPC.	111
4.7	3D profile of the state $x(\zeta, t)$ evolution over space and time (ζ, t) for Case I system with full-state feedback MPC.	112
4.8	Profiles of plant output $y(t)$ and estimated output $\hat{y}(t)$ (left), and control input $u(t)$ (right) over time for Case II system with output feedback MHE-MPC.	113
4.9	3D profile of the true state $x(\zeta, t)$ over time for Case II system with output feedback MHE-MPC.	114
4.10	3D profile of the estimated state $\hat{x}(\zeta, t)$ over time for Case II system with output feedback MHE-MPC.	114
4.11	3D profile of the state estimation error $e(\zeta, t) = x(\zeta, t) - \hat{x}(\zeta, t)$ over time for Case II system with output feedback MHE-MPC.	115
5.1	This is an example of a single figure similar to that produced by Listing 5.1.	122
5.2	This is an example of a double image figure similar to that produced by Section 5.2.	123
A.1	This is an example of a double image figure.	135
A.2	This is an example of a triple image figure.	136
A.3	This is a second example of a triple image figure.	137
A.4	This is an example of a quad image figure.	138

List of Symbols

Constants

ϵ_0	Permittivity of Free Space.	$\epsilon_0 = 8.854 \times 10^{-12} \text{ F/m}$
\hbar	Reduced Planck Constant.	$\hbar = 1.055 \times 10^{-34} \text{ Js}$
μ_0	Permeability of Free Space.	$\mu_0 = 4\pi \times 10^{-7} \text{ H/m}$
π	Mathematical Constant Pi.	$\pi \approx 3.14159$
R_e	Rankine Number.	$R_e = \frac{Lv\rho}{\mu}$
c	Speed of light in a vacuum.	$299,792,458 \text{ m/s}$
g	Acceleration due to Gravity.	$g = 9.81 \text{ m/s}^2$
h	Planck constant.	$6.62607015E - 34 \text{ Js}$
k	Boltzmann Constant.	$k = 1.380649 \times 10^{-23} \text{ J/K}$
R	Gas Constant.	$R = 8.314 \text{ J/(mol}\cdot\text{K)}$

Latin

A	Cross-sectional Area.
a	Acceleration
D	Diameter.
d	Distance
E	Young's Modulus

F	Force.
G	Shear Modulus.
I	Area Moment of Inertia.
K	Elastic Constant
L	Length.
M	Moment.
m	Mass
P	Pressure.
T	Temperature.
T	Torque
t	Thickness.
V	Volume.
v	Velocity

Greek

α	Primary Angle
δ	Deflection.
λ	Wavelength.
σ	Normal Stress.
τ	Shear Stress.
ε	Strain

Abbreviations

AC Armor Class.

AL Adventurers League.

AoE Area of Effect.

AoO Attack of Opportunity.

BAB Base Attack Bonus.

BBEG Big Bad Evil Guy.

CHA Charisma.

CON Constitution.

CoS Curse of Strahd.

CR Challenge Rating.

CRPG Computer Role-Playing Game.

D&D Dungeons & Dragons.

DEX Dexterity.

DM Dungeon Master.

DMG Dungeon Master's Guide.

DMPC Dungeon Master Player Character.

DnD Dungeons & Dragons.

DPR Damage Per Round.

DR Damage Reduction.

ECL Effective Character Level.

HD Hit Dice.

HP Hit Points.

IC In Character.

INT Intelligence.

LA Level Adjustment.

LFG Looking For Group.

LoS Line of Sight.

LR Long Rest.

MM Monster Manual.

NPC Non-Player Character.

OGL Open Game License.

OOC Out Of Character.

PB Proficiency Bonus.

PC Player Character.

PHB Player's Handbook.

PP Passive Perception.

RAI Rules As Intended.

RAW Rules As Written.

RNG Random Number Generator.

RP Roleplaying.

SR Spell Resistance.

SRD System Reference Document.

STR Strength.

THAC0 To Hit Armor Class 0.

TPK Total Party Kill.

TTRPG Tabletop Role-Playing Game.

VTT Virtual Tabletop.

WIS Wisdom.

WotC Wizards of the Coast.

XP Experience Points.

Glossary of Terms

Ability Score One of six numbers (Strength, Dexterity, Constitution, Intelligence, Wisdom, Charisma) that represent a character's physical and mental attributes.

AC (Armor Class) A number representing how difficult it is to hit a character in combat.

Advantage/Disadvantage A mechanic where a player rolls two d20s and takes the higher (advantage) or lower (disadvantage) result.

Alignment A character's ethical and moral perspective, such as Lawful Good or Chaotic Evil.

Arcane A type of magic derived from study, such as wizardry.

Backstory The history and background of a character before the campaign begins.

Bonus Action An additional action a character can take during their turn, often granted by class features or spells.

Cantrip A spell that can be cast at will without using a spell slot.

Chaotic Free-spirited and sometimes unpredictable. Can also be reckless or reactionary.

Charisma (CHR) Social skills and sometimes physical appearance.

Class The primary archetype of a character, such as Fighter, Wizard, or Rogue, which determines abilities and progression.

Combat A structured sequence where characters and enemies take turns performing actions like attacking or casting spells.

Concentration A mechanic where certain spells require ongoing focus, and taking damage can force a concentration check to maintain the spell.

Constitution (CON) Physical resilience. This affects hit points and some physical resistances.

d20 A 20-sided die, the primary die used in D&D for most rolls.

Damage Types One of the thirteen (13) categories of damage: acid, bludgeoning, cold, fire, force, lightning, necrotic, piercing, poison, psychic, radiant, slashing, and thunder.

Dexterity (DEX) Agility and accuracy. This affects ranged attacks and dodging.

Dungeon Master (DM) The person who runs the game, narrates the story, and controls the world and NPCs.

Encounter Any situation where players must overcome a challenge, such as combat, puzzles, or social interaction.

Equipment The gear and items a character carries, including weapons, armor, and adventuring tools.

Evil Wicked and often selfish or oppressive.

Experience Points (XP) Points gained from overcoming challenges, used to level up a character.

Familiar A magical creature that assists a spellcaster, often summoned by the spell *Find Familiar*.

Feat A special ability or skill a character can choose instead of an ability score increase at certain levels.

Flanking A tactical position where a character attacks an enemy from the opposite side of an ally, often granting a combat advantage (this rule is optional and varies by DM).

Good Having a respect for life, altruism, and selflessness.

Grapple A combat action where a character attempts to grab and restrain an opponent.

Group Check A mechanic where the success of the party depends on the number of successful rolls among the group.

Hit Points (HP) A measure of a character's health, reduced when taking damage.

Hit Dice (HD) Dice used to determine a character's hit points at each level and for healing during short rests.

Initiative A roll made at the start of combat to determine the order of turns..

Inspiration A DM-awarded bonus that allows a player to gain advantage on a roll.

Intelligence (INT) The ability to process problems and wield certain magic. INT affects the number of skill points received.

Ki A resource used by monks to perform special abilities.

Lawful Abides by a core morality or honor system. Can also be judgmental and close-minded.

Level A measure of a character's progression, determining access to new abilities, spells, and increased hit points.

Long Rest A period of downtime (usually 8 hours) where characters recover hit points and spell slots.

Melee Combat at close range, typically involving hand-to-hand or short-ranged weapons.

Metagaming Using out-of-game knowledge within the game, often discouraged as it can break immersion.

Multiclassing The practice of taking levels in more than one class, allowing a character to gain abilities from multiple classes.

Neutral A balance between Lawful & Chaotic or Good & Evil.

NPC (Non-Player Character) Characters controlled by the DM that players interact with, such as villagers, shopkeepers, or enemies.

Opportunity Attack A reaction that allows a character to make a melee attack against a creature that moves out of their reach.

Party The group of player characters (PCs) adventuring together.

Perception A skill representing a character's ability to notice hidden things, typically rolled as a Wisdom check.

Proficiency Bonus A bonus added to rolls where a character has proficiency, such as with certain skills, weapons, or saving throws.

Quiver A container for holding arrows or bolts, typically used by archers and ranged combatants.

Ranged Attack An attack made with a ranged weapon or spell, targeting an enemy at a distance.

Reaction An instant response to a trigger, such as casting *Counterspell* or making an opportunity attack.

Saving Throw A roll made to resist a spell, trap, or other effect.

Short Rest A brief period of downtime (usually 1 hour) where characters can spend Hit Dice to recover hit points.

Skill Check A roll made to determine the outcome of an action related to a skill, such as Stealth or Acrobatics.

Spell Slot A resource that determines how many spells a character can cast at each level.

Strength (STR) The character's physical strength. This effects the potency of melee attacks.

Turn A player's time to act during a round of combat, typically consisting of movement, an action, and possibly a bonus action or reaction.

Vision Types Various levels of sight in D&D, such as Darkvision, Blindsight, and Truesight.

Weapon Proficiency Determines which weapons a character can use effectively, adding their proficiency bonus to attack rolls.

Wisdom An ability score representing a player character's insight, perception, and willpower.

Wisdom (WIS) Common sense and spirituality.

XP (Experience Points) See Experience Points.

Chapter 1

Introduction

1.1 Background

As a graduate student from the University of Alberta, I am familiar with the challenging task of writing a thesis that adheres to the GPS Minimum Thesis Formatting Requirements. Using a traditional word processor to create a long document filled with equations and figures can be frustrating due to frequent crashes, file corruption, unpredictable formatting changes, and the inability to output a document in the required PDF/A format for submission to GPS.

To overcome these issues, many students turn to L^AT_EX as an alternative to conventional word processors.

L^AT_EX allows students and researchers to focus separately on the content and the formatting of their documents. Because the writing is independent of the formatting, documents can be written in lightweight text editors or L^AT_EX editors, which also facilitate the compilation of the documents. These editors can often save work after every keystroke, and due to the plaintext format, they are less prone to file corruption. Moreover, L^AT_EX ensures a consistent and professional appearance throughout the document.

1.2 Objectives

The main objectives of this thesis are:

1. To provide a comprehensive guide on writing a thesis using L^AT_EX.
2. To assist students and researchers in mastering the nuances of L^AT_EX document preparation.
3. To showcase best practices for structuring and formatting a thesis in L^AT_EX.

1.3 Scope and Limitations

Although there are existing templates for writing a thesis in L^AT_EX for the University of Alberta (see [Table 1.1](#) for a list of available templates), none seem to provide all the necessary information for creating an outstanding thesis. Most templates apply “band-aid” solutions to existing classes, such as `report` or `book`, offering a customized title page and methods for including prefatory pages. However, these templates often fall short by not providing tips and best practices on how to include the various sections and parts that make up a thesis. They also fail to offer a solid foundation for those who are new to L^AT_EX. Many of these templates involve extensive patching and fixing, resulting in a large *preamble* section at the beginning of the template that can be confusing to new L^AT_EX users and add to the already steep learning curve.

Developer	Last Updated	Link to Template Source
Shivam Garg	May 29, 2023	https://github.com/svmgrg/ualberta_thesis_template
Henry Brausen	Feb 11, 2022	https://github.com/henrybrausen/thesis_template
Bernard Llanos	Oct 05, 2019	https://drive.google.com/file/d/1wKS8fu5e6qiVDRt0VUzEtIW8p7uMyz1T/view?usp=sharing
John Bowman	Sep 30, 2019	https://github.com/vectorgraphics/uofathesis
Hongtao Yang & Benjamin Bernard GAME	Sep 28, 2017	https://github.com/adrs0049/ThesisTemplate
Hongtao Yang	Feb 03, 2016	https://www.ualberta.ca/computing-science/media-library/grad/candidacy-template.tex
Steven Taschuk	Mar 21, 2012	https://github.com/stebulus/ualberta-math-stat-templates/tree/master/thesis
CMENG	Jul 19, 1999	https://sites.ualberta.ca/CMENG/research/new-control/stythes.html

Table 1.1: List of Other Available Templates.

This template, document class, and guide aim to address these shortcomings by providing all the necessary information to create a well-structured thesis, along with examples to assist in formatting your thesis written in L^AT_EX. To ensure the robustness and ease of maintenance, I developed the class file from the ground up keeping the additional required packages to a minimum. This makes this L^AT_EX solution easier to maintain, update, and customize to suit different needs from different areas of the University of Alberta. A key goal with this was to reduce the traditionally steep learning curve associated with L^AT_EX to ensure that anyone could create an outstanding thesis.

While the class file (`ualberta.cls`) deserves its own comprehensive documentation, this document will focus on more specifically on the template file (`ualberta.tex`), as well as the following points:

- Installation and basic usage of L^AT_EX.
- Document structure and formatting.
- Inclusion of figures and tables.
- Inclusion of plots and graphs.
- Handling mathematical equations.
- Citations and references using BibTeX.
- Use of JabRef—Reference Manager.
- Inclusion of Code and PDF's.
- And more.

This guide does not cover advanced L^AT_EX programming or extensive customization of document classes. Instead, the class file `ualberta.cls` provides all the major document and formatting requirements as provided by GPS, while this document offers references on how to include the various elements that might be required in a thesis. This includes all of the explanations of the packages and macros needed to perform the examples.

1.4 Organization of the Thesis

The thesis is organized into several chapters, each addressing a specific aspect of writing a thesis in L^AT_EX. The breakdown is as follows:

- ?: ?: ?
- ?: ?: ?
- **Chapter 5: Concluding Remarks**
- ?: ?: ?
- ?: ?: ?
- ?: ?: ?
- ?: ?: ?

Each chapter provides detailed information, examples, and recommendations to help you navigate the thesis writing process within the L^AT_EX ecosystem.

1.5 Summary

This chapter introduced the background, objectives, scope, and organization of the thesis. The subsequent chapters delve into specific topics, offering practical guidance and examples for mastering the art of writing a thesis in L^AT_EX. Through this process, you will develop an understanding of how to create a thesis and manipulate content within the L^AT_EX ecosystem to produce an exceptional document.

Chapter 2

CONTINUOUS-TIME ESTIMATION AND OPTIMAL CONTROL FOR THE ISOTHERMAL SYSTEM¹

2.1 Introduction

Many chemical, petrochemical, and biochemical unit operation processes are modelled as distributed parameter systems (DPS), ranging from tubular reactors, heat exchangers, and separation columns to processes like digesters in the pulp and paper industry and fluid flow in pipeline networks. When these processes are described using first-principle modelling, they result in a class of partial differential equations (PDEs) to effectively capture diffusion, transport, and reaction phenomena, leading to infinite-dimensional state space representations [2]. This characteristic presents significant challenges, making the control and estimation of DPS inherently more complex than finite-dimensional

¹This chapter has been published as B. Moadeli *et al.*, “Optimal control of axial dispersion tubular reactors with recycle: Addressing state-delay through transport PDEs,” *The Canadian Journal of Chemical Engineering*, vol. 103, no. 8, pp. 3751–3766, 2025, ISSN: 0008-4034. DOI: [10.1002/cjce.25629](https://doi.org/10.1002/cjce.25629).

systems. Two primary methods have emerged for addressing DPS control. One is early lumping, which approximates the infinite-dimensional system with a finite-dimensional model [3, 4]. While this method enables the use of standard regulator design techniques, mismatches between the dynamical properties of the original DPS and the approximate lumped parameter model can occur, negatively affecting the performance of the designed regulator [5]. The second method is late lumping, which directly tackles the infinite-dimensional system before applying numerical solutions. This approach introduces a challenging yet fertile direction of research, leading to many meaningful contributions that address various aspects of control and estimation of infinite-dimensional systems.

Among notable studies utilizing late lumping method for control of convection-reaction chemical systems resulting in first order hyperbolic PDEs, Christofides explored the robust control of quasi-linear first-order hyperbolic PDEs, providing explicit controller synthesis formulas for uncertainty decoupling and attenuation [6]. Krstic and Smyshlyaev extended boundary feedback stabilization techniques for first-order hyperbolic PDEs using a backstepping method, converting the unstable PDE into a system for finite-time convergence [7]. Relevant applications of reaction-convection systems other than tubular reactors have also been addressed within this field, resulting in regulator/observer design strategies for chemical systems governed by first order hyperbolic PDEs. Xu and Dubljevic addressed the state feedback regulator problem for a countercurrent heat exchanger system, utilizing an infinite-dimensional approach to ensure that the controlled output tracks a reference signal [8]. Xie and Dubljevic developed a discrete-time output regulator for gas pipeline networks, em-

phasizing the transformation of continuous-time models into discrete-time systems while preserving essential continuous-time properties [9]. This work was further extended by Zhang *et al.*, who proposed a tracking model predictive control and moving horizon estimation design for pipeline systems, addressing the challenges of state and parameter estimation in an infinite-dimensional chemical system governed by first order hyperbolic PDEs [10]. For a similar convection-reaction system, Zhang *et al.* proposed a model predictive control strategy, incorporating a Luenberger observer to achieve output constrained regulation in a system modelled by nonlinear coupled hyperbolic PDEs [11].

Additionally, diffusion-convection-reaction systems resulting in parabolic PDEs are also addressed in several works. For example, Christofides addressed order reduction methods for diffusion-convection-reaction type of reactors [12]. Dubljevic *et al.* utilized modal decomposition to capture dominant modes of a DPS to construct a reduced order finite dimensional system, which enables the design of a low dimensional controller for a diffusion-convection-reaction type reactor described by second order parabolic PDEs [13]. Cassol *et al.* designed and compared the performance of a full-state and output feedback controller for a diffusion–convection heat exchanger system [14]. In Khatibi *et al.*’s work, an axial dispersion tubular reactor equipped with recycle stream is considered as a second order parabolic DPS, with a predictive controller being utilized to optimally control the reactor. Although the presence of recycle is common in industrial reactor designs, their study has thus far been one of the few contributions in this field addressing a diffusion-convection-reaction system equipped with a recycle stream [15].

Moreover, continuous-time optimal control design is a well-developed con-

cept for distributed parameter systems, particularly when the system generator is either a self-adjoint operator or can be transformed into one through a proper linear transformation [16]. However, there are distributed parameter systems that do not possess this property. Instead, the system generator belongs to the class of Riesz-spectral operators. Rather than an orthonormal basis for the function-space, these generators introduce a bi-orthonormal set of eigenfunctions as the basis. Optimal controller design for these systems was initially addressed by Curtain and Zwart [17]. Since then, significant work has been done in this field; for instance, continuous-time optimal control design for a cracking catalytic reactor, another convection-reaction system governed by first-order hyperbolic PDEs, has been achieved by solving an operator Riccati equation (ORE)[18]. This work has been further extended to time-varying PDEs of the same class[18]. The same approach has been applied to develop a full-state feedback[19] and output feedback[20] linear quadratic (LQ) optimal regulator for a boundary-controlled convection-reaction system, utilizing the properties of a Riesz-spectral generator for the system.

On top of those dynamic systems that are distributed in space, delay systems are another example of distributed parameter systems [17]. Although delay is commonly represented in the form of delay differential equations (DDEs), it can also be modelled as a transport partial differential equation (PDE), which offers advantages in more complex scenarios or when employing alternative norms on infinite-dimensional states. This approach allows for a smoother transition to problems involving more intricate PDE dynamics while maintaining notational consistency [21]. Input/output delay with relevant applications in chemical engineering has been addressed previously in the field of

control theory for DPS. For example, time-delayed boundary observation is considered while addressing an output feedback regulator for a tubular reactor [22]. However, the notion of state-delay (as opposed to delayed-inputs or delayed-measurements) seems to be less addressed in this field compared to other relevant fields like signal processing, self-driving cars, or network control theory (NCT). This is probably due to the fact that not many applications in the field of distributed parameter chemical engineering systems can be described by state delays in the first place. Cassol *et al.*'s work is one of the few instances that addressed a delayed-state distributed parameter chemical engineering system, where they designed a full-state and output feedback regulator for a system of heat exchangers [14]. The notion of state-delay comes from the time it takes for a stream to leave one pass of the heat exchanger and enter the next pass. As stated previously, not much work is published addressing chemical reactors equipped with recycle as distributed parameter systems. Even in Khatibi *et al.*'s work, the recycle is assumed to be instantaneous [15]; a simplifying assumption that does not resonate well with reality. In fact, taking the time it takes for the recycle stream to re-enter the reactor input can be another instance for the rare concept of a delayed state DPS in the field of chemical engineering. In another attempt, Qi *et al.* addressed the challenge of state delay imposed by a recycle stream in a system modelled by interconnected first-order hyperbolic partial integro differential equations (PIDEs), introducing a transport PDE to account for the in-domain recycle delay [23]. However, the diffusion term was not addressed, leaving a gap in the literature regarding diffusion-convection-reaction systems with a recycle stream imposing state delay.

The present work focuses on the control of an axial tubular reactor equipped with a recycle stream—a configuration common in industrial processes such as catalytic reactors, polymerization units, and biochemical fermenters—but one that is inadequately addressed in the literature. Unlike previous studies that assumed instantaneous recycle, this work incorporates the time delay associated with the recycle stream re-entering the reactor, presenting a rare example of state-delay in the field of chemical engineering DPS. The model comprises a second-order parabolic PDE to capture the diffusion-convection-reaction nature of the reactor, coupled with a first-order hyperbolic PDE to account for the delay. The boundary conditions are chosen as Danckwerts boundary conditions, which are particularly suitable for this type of reactor. The system results in a non-self-adjoint operator. However, by utilizing the bi-orthogonal theorem, given that the generator is Riesz-spectral, a full-state feedback optimal LQ regulator is developed, followed by an output feedback regulator. The control feedback is derived by solving an operator Riccati equation (ORE) in order to implement a late lumping approach. Actuation and observation are applied at the boundaries, making it a boundary-actuated system involving finite-dimensional dynamics for an infinite-dimensional DPS. These contributions are presented in the following order: In **Section 2.2**, the system analysis is first addressed by modelling the delay infinite-dimensional system (DPS) and transforming it into a system of coupled PDEs using the delay-transport approach. The system’s characteristics are explored by examining the system generator and its eigenvalues, followed by analyzing the adjoint operator and its spectrum, which allows introducing the bi-orthogonal basis for the infinite-dimensional system. Consequently in **Section 2.3.1**, the

design strategy for an optimal full-state regulator is developed by formulating the infinite-time horizon LQ control problem, converting the ORE into matrix Riccati equations (MRE), and calculating the feedback gain. Practical limitations of the full-state feedback mechanism are then addressed in **Section 2.3.2** by introducing a Luenberger observer for state reconstruction, followed by the design of an output feedback regulator. Finally, numerical simulations are illustrated in **Section 2.4** to showcase the results of the developed theoretical concepts, demonstrating closed-loop responses of the system equipped with both full-state feedback regulator and output feedback compensator in various settings.

2.2 Open-loop System

2.2.1 System model

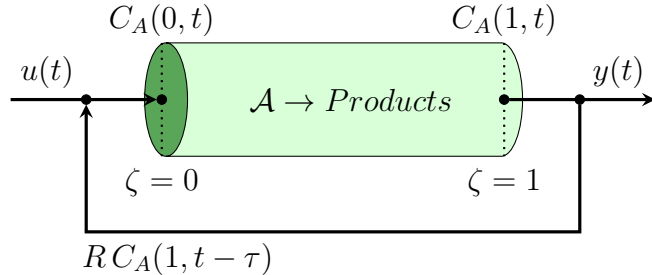


Figure 2.1: Axial tubular reactor with recycle stream.

The chemical process illustrated in Figure 2.1 represents an axial dispersion tubular reactor, which incorporates diffusion, convection, and a chemical reaction where reactant A is converted into products [24]. The reactor is equipped with a recycle mechanism, allowing a fraction of the product stream to re-enter the reactor to ensure the consumption of any unreacted substrate. By applying first-principle modelling through relevant mass balance relations on

an infinitesimally small section of the reactor, the dynamics of the reactant concentration can be described by the PDE given in Equation (2.1), belonging to the class of second order parabolic PDEs commonly used to characterize diffusion-convection-reaction systems [25] in chemical engineering.

$$\dot{C}_A(\zeta, t) = D\partial_{\zeta\zeta}C_A(\zeta, t) - v\partial_{\zeta}C_A(\zeta, t) + r(C_A) \quad (2.1)$$

Here, $C_A(\zeta, t)$ denotes the concentration of reactant A along the reactor. The physical parameters D and v correspond to the diffusion coefficient and flow velocity along the reactor, respectively. It is worth noting that the system properties are assumed to be constant against changes in temperature and pressure. The spatial and temporal coordinates of the system are represented by ζ and t , where $\zeta \in [0, 1]$ and $t \in [0, \infty)$. In addition, $r(C_A)$ is the reaction rate by which the reactant is consumed. Considering the reaction term in general can be non-linear, the model is further linearized around its steady-state, followed by replacing the reactant concentration C_A with its deviations from the steady-state concentration $C_{A,ss}$. The result is given in Equation (3.1).

$$\dot{c}(\zeta, t) = D\partial_{\zeta\zeta}c(\zeta, t) - v\partial_{\zeta}c(\zeta, t) - k_r c(\zeta, t) \quad (2.2)$$

where $c(\zeta, t) \equiv C_A(\zeta, t) - C_{A,ss}(\zeta)$ is the deviation from the steady-state concentration and the linearized reaction coefficient is defined as $k_r \equiv \left. \frac{\partial r(C_A)}{\partial C_A} \right|_{C_{A,ss}}$ in the vicinity of the steady-state. The system output is assumed to be the deviation of the reactant concentration from the steady-state measured at the reactor outlet, while the control input is set to be equal to the deviation of the reactant concentration from the steady-state, applied at the reactor inlet after being mixed with the delayed state resulting from the recycled portion of the

flow occurring τ time units ago. Incorporating input, output, and state delay in addition to the assumption of Danckwerts boundary condition will result in Equation (3.3) that describe the boundary conditions of the system.

$$\begin{cases} D\partial_\zeta c(0, t) - vc(0, t) = -v [Rc(1, t - \tau) + (1 - R)u(t)] \\ \partial_\zeta c(1, t) = 0 \\ y(t) = c(1, t) \end{cases} \quad (2.3)$$

Here, parameters R and τ correspond to the recycle ratio and the residence time along the recycle stream, respectively. Accounting for deviations from perfect mixing and piston flow and assuming negligible transport lags in connecting lines [26], the Danckwerts boundary conditions have become an inseparable part of modelling axial tubular reactors in the field of chemical engineering process control and dynamics. While capturing physical significance, Danckwerts boundary conditions maintain generality without unnecessarily simplifying the model as they belong to the general class of Robin boundary conditions.

2.2.2 PDE representation of the delay term

One effective method for addressing delay in systems is to represent the delay using an alternative transport partial differential equation (PDE). This approach is particularly advantageous when the problem already involves similar forms of PDEs, as is the case in the current study. To specifically address the delay in the system under consideration, the state variable $c(\zeta, t)$ is expanded into a vector of functions $x(\zeta, t) \equiv [x_1(\zeta, t), x_2(\zeta, t)]^T$, where $x_1(\zeta, t)$ is the same as $c(\zeta, t)$, while $x_2(\zeta, t)$ is introduced as a new state variable to account for the concentration along the recycle stream. The delay is thus modelled as

a pure transport process, as if the first state $x_1(\zeta, t)$ is being transported from the reactor outlet to the inlet, experiencing a delay of τ time units while in the recycle stream. As a result, Equations 3.1 and 3.3 may be re-formulated as follows:

$$\partial_t \begin{bmatrix} x_1(\zeta, t) \\ x_2(\zeta, t) \end{bmatrix} = \begin{bmatrix} D\partial_{\zeta\zeta} - v\partial_\zeta + k_r & 0 \\ 0 & \frac{1}{\tau}\partial_\zeta \end{bmatrix} \begin{bmatrix} x_1(\zeta, t) \\ x_2(\zeta, t) \end{bmatrix} \quad (2.4)$$

$$\begin{cases} D\partial_\zeta x_1(0, t) - vx_1(0, t) = -v[Rx_2(0, t) + (1-R)u(t)] \\ \partial_\zeta x_1(1, t) = 0 \\ x_1(1, t) = x_2(1, t) \\ y(t) = x_1(1, t) \end{cases} \quad (2.5)$$

With all state variables now expressed explicitly at a specific time instance t —in contrast to the previous representation where states at t were directly involved with states at $(t - \tau)$ —the open-loop system can be described in the standard state-space form of an infinite-dimensional linear time-invariant (LTI) system as $\dot{x} = \mathfrak{A}x$. Here, \mathfrak{A} is a linear operator $\mathcal{L}(X)$ acting on a Hilbert space $X : L^2[0, 1] \times L^2[0, 1]$ and $x(\zeta, t)$, as defined previously, is the vector of functions describing the states of the system. The operator \mathfrak{A} and its domain are defined in detail as shown in Equation (2.6):

$$\begin{aligned} \mathfrak{A} &\equiv \begin{bmatrix} D\partial_{\zeta\zeta} - v\partial_\zeta + k_r & 0 \\ 0 & \frac{1}{\tau}\partial_\zeta \end{bmatrix} \\ \mathcal{D}(\mathfrak{A}) &= \left\{ x = [x_1, x_2]^T \in X : x(\zeta), \partial_\zeta x(\zeta), \partial_{\zeta\zeta} x(\zeta) \text{ a.c.,} \right. \\ &\quad \left. D\partial_\zeta x_1(0) - vx_1(0) = -v[Rx_2(0) + (1-R)u], \right. \\ &\quad \left. \partial_\zeta x_1(1) = 0, x_1(1) = x_2(1) \right\} \end{aligned} \quad (2.6)$$

2.2.3 Adjoint operator

The adjoint operator \mathfrak{A}^* plays a critical role in analyzing the spectral properties of the system. It is obtained in Equation (2.7):

$$\begin{aligned} \langle \mathfrak{A}\phi, \psi \rangle = \langle \phi, \mathfrak{A}^*\psi \rangle \Rightarrow \\ \mathfrak{A}^* = \begin{bmatrix} D\partial_{\zeta\zeta} + v\partial_\zeta + k_r & 0 \\ 0 & -\frac{1}{\tau}\partial_\zeta \end{bmatrix} \\ \mathcal{D}(\mathfrak{A}^*) = \left\{ y = [y_1, y_2]^T \in Y : y(\zeta), \partial_\zeta y(\zeta), \partial_{\zeta\zeta} y(\zeta) \text{ a.c.,} \right. \\ \left. D\partial_\zeta y_1(1) + vy_1(1) = \frac{1}{\tau}y_2(1) \right. \\ \left. Rvy_1(0) = \frac{1}{\tau}y_2(0) \right. \\ \left. \partial_\zeta y_1(0) = 0 \right\} \end{aligned} \quad (2.7)$$

where $\phi_i(\zeta) = [\phi_{i,1}(\zeta), \phi_{i,2}(\zeta)]^T$ and $\psi_i(\zeta) = [\psi_{i,1}(\zeta), \psi_{i,2}(\zeta)]^T$ are the eigenfunction of \mathfrak{A} and \mathfrak{A}^* , respectively. Given that \mathfrak{A} is not self-adjoint (i.e., $\mathfrak{A} \neq \mathfrak{A}^*$), their combined eigenmodes may still form a bi-orthonormal basis, typical of a Riesz-spectral operator [17]. Therefore their spectral properties must be determined by solving their characteristic equations.

2.2.4 Eigenvalue problem

The eigenvalue problem for \mathfrak{A} is formulated as follows:

$$\mathfrak{A}\phi_i(\zeta) = \lambda_i\phi_i(\zeta) \quad (2.8)$$

where $\lambda_i \in \mathbb{C}$ is the i^{th} eigenvalue. To obtain the characteristic equation, the system of PDEs shall be reduced to the ODE system in Equation (2.9)
 $\forall i \geq 0$:

$$\partial_\zeta \begin{bmatrix} \phi_1 \\ \partial_\zeta \phi_1 \\ \phi_2 \end{bmatrix} = \begin{bmatrix} 0 & 1 & 0 \\ \frac{\lambda - k_r}{D} & \frac{v}{D} & 0 \\ 0 & 0 & \tau\lambda \end{bmatrix} \begin{bmatrix} \phi_1 \\ \partial_\zeta \phi_1 \\ \phi_2 \end{bmatrix} \quad (2.9)$$

which is in the form of $\tilde{\phi}_\zeta = \tilde{\mathfrak{A}}\tilde{\phi}$, with the solution stated in Equation (2.10):

$$\begin{bmatrix} \phi_1 \\ \partial_\zeta \phi_1 \\ \phi_2 \end{bmatrix}_{\zeta=1} = \begin{bmatrix} \Lambda_{1,1} & \Lambda_{1,2} & \Lambda_{1,3} \\ \Lambda_{2,1} & \Lambda_{2,2} & \Lambda_{2,3} \\ \Lambda_{3,1} & \Lambda_{3,2} & \Lambda_{3,3} \end{bmatrix} \begin{bmatrix} \phi_1 \\ \partial_\zeta \phi_1 \\ \phi_2 \end{bmatrix}_{\zeta=0} \quad (2.10)$$

where the 3×3 matrix $\Lambda_{(m,n)}$ is defined as $\Lambda \equiv e^{\tilde{\mathfrak{A}}(\zeta-0)} \Big|_{\zeta=1}$. By applying the boundary conditions to Equation (2.10), the algebraic system of equations in Equation (2.11) is obtained:

$$\begin{bmatrix} -v & D & Rv \\ \Lambda_{2,1} & \Lambda_{2,2} & \Lambda_{2,3} \\ (\Lambda_{1,1} - \Lambda_{3,1}) & (\Lambda_{1,2} - \Lambda_{3,2}) & (\Lambda_{1,3} - \Lambda_{3,3}) \end{bmatrix} \begin{bmatrix} \phi_1 \\ \partial_\zeta \phi_1 \\ \phi_2 \end{bmatrix}_{\zeta=0} = \tilde{\Lambda} \tilde{\phi} \Big|_{\zeta=0} = 0 \quad (2.11)$$

where $\tilde{\Lambda}$ is defined as the square matrix shown in Equation (2.11). Equation (2.11) suggests that the matrix $\tilde{\Lambda}$ must be rank-deficient for appropriate values of λ_i . Attempts to analytically solve the characteristic equation $\det(\tilde{\Lambda}) = 0$ have failed; therefore, it is solved numerically using the parameters in Table 2.1. The resulting eigenvalue distribution is depicted in Figure 2.2 in the complex plane.

Following the same procedure for \mathfrak{A}^* shows that the eigenvalues of \mathfrak{A} match the ones of its adjoint, confirming that \mathfrak{A} and \mathfrak{A}^* form a bi-orthogonal basis according to Equation (2.12):

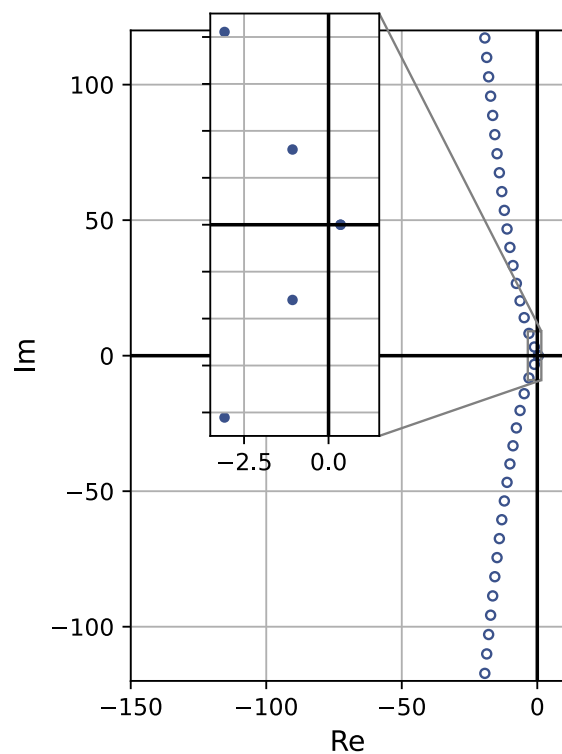


Figure 2.2: Eigenvalues of operator \mathfrak{A} obtained by solving Equation (2.11).

$$\langle \mathfrak{A}\phi_i, \psi_j \rangle = \langle \lambda_i \phi_i, \psi_j \rangle = \lambda_i \langle \phi_i, \psi_j \rangle$$

$$\text{L.H.S.} = \langle \phi_i, \mathfrak{A}^* \psi_j \rangle = \langle \phi_i, \lambda_j^* \psi_j \rangle = \overline{\lambda_j^*} \langle \phi_i, \psi_j \rangle \quad (2.12)$$

$$\lambda_i = \overline{\lambda_i^*} \Rightarrow \langle \phi_i, \psi_j \rangle = \delta_{ij}$$

The eigenfunctions $\{\phi_i(\zeta), \psi_i(\zeta)\}$ (for \mathfrak{A} and \mathfrak{A}^* , respectively) may be obtained following the calculation of eigenvalues. The first 3 eigenfunctions are plotted in Figure 2.3.

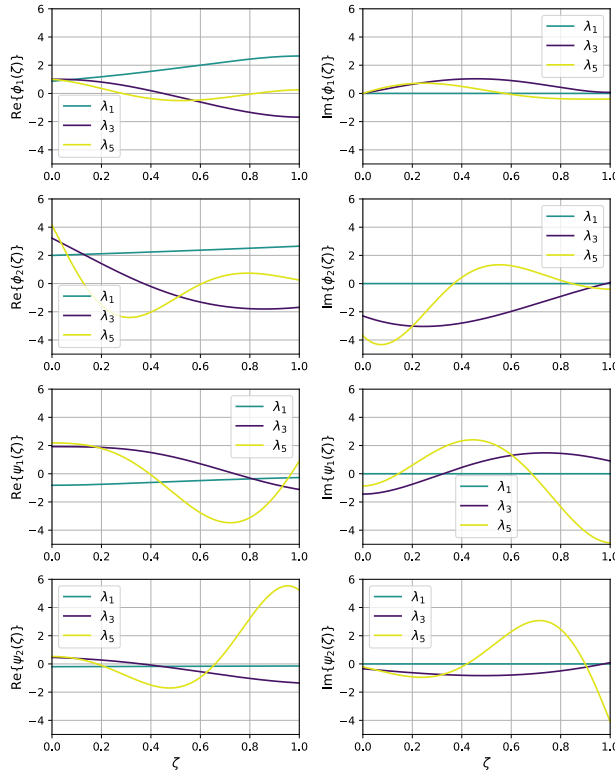


Figure 2.3: First few eigenmodes of \mathfrak{A} and \mathfrak{A}^* .

The parameters of the system are carefully chosen to highlight all its key characteristics simultaneously—namely, significant diffusion, convection, and reaction occurring within the reactor—while also ensuring that the delay term and recycle ratio have a pronounced effect on system dynamics. Addition-

Table 2.1: Physical parameters for the system.

Parameter	Symbol	Value	Unit
Diffusivity	D	2×10^{-5}	m^2/s
Velocity	v	0.01	m/s
Reaction constant	k_r	-1.5	s^{-1}
Recycle residence time	τ	80	s
Recycle ratio	R	0.3	-

ally, the parameters are deliberately selected to introduce instability into the system, emphasizing the proposed control strategy's ability to stabilize an inherently unstable system. While no isothermal reactor can truly exhibit exponential instability due to the finite availability of reactants, such systems can still become unstable near the steady state. In this context, deviations from the steady state may cause the system to transition toward a different steady state, thereby altering the underlying dynamics and invalidating the original model used for system design and control optimization.

It has been observed that for the linearized system to have an unstable steady state, the reaction coefficient, k_r , must be negative. Although rare, this scenario can arise in certain reaction mechanisms where the reaction rate decreases as the reactant concentration increases, such as autocatalytic reactions, enzyme-catalyzed reactions, or reactions involving inhibitory effects. This instability can be qualitatively understood as follows: a negative reaction coefficient causes a decline in the reaction rate as the reactant accumulates, leading to further reactant accumulation and thus, driving the system away from its steady state. Quantitative confirmation of this behaviour can be achieved through eigenvalue analysis, where the presence of at least one eigen-

value with a positive real part indicates the fact that the open-loop linearized system is exponentially unstable.

2.3 Linear Quadratic Regulator Design

2.3.1 Full-state feedback regulator

The bi-orthogonal basis generated by the Riesz-spectral operator \mathfrak{A} in the LTI system $\Sigma(\mathfrak{A}, \mathfrak{B}, \mathfrak{C}, -)$ provides the foundation for solving the operator Riccati equation (ORE), a crucial step in the design of a linear quadratic regulator (LQR). The objective is to determine an offline feedback control law that drives the system's states from an arbitrary initial condition to zero, thereby maintaining the system at its steady state. This is achieved within an optimal control framework, minimizing the infinite-time cost function defined in Equation 2.13. In this context, \mathfrak{Q} and \mathfrak{R} are self-adjoint coercive operators that penalize state deviations and control actions, respectively.

$$J(x_0, u) = \int_{t=0}^{\infty} \langle x(s), \mathfrak{Q}x(s) \rangle + \langle u(s), \mathfrak{R}u(s) \rangle ds \quad (2.13)$$

2.3.1.1 Operator Riccati equation

The LQR problem is solved by finding the unique positive semi-definite operator $\mathbf{\Pi}$, which satisfies the ORE presented in Equation 2.14. This operator is then used to compute the feedback gain that ensures optimal control of the system.

$$\langle \mathfrak{A}^* \mathbf{\Pi} x, y \rangle + \langle \mathbf{\Pi} \mathfrak{A} x, y \rangle - \langle \mathbf{\Pi} \mathfrak{B} \mathfrak{R}^{-1} \mathfrak{B}^* \mathbf{\Pi} x, y \rangle + \langle \mathfrak{Q} x, y \rangle = 0 \quad (2.14)$$

Given that the solution to the ORE is unique for any set of functions in the domain of operator \mathfrak{A} , we can arbitrarily set $x = \phi_m$ and $y = \phi_n$, that is, the eigenfunctions of \mathfrak{A} . Applying this choice, and noting that $\mathbf{\Pi}$ is self-adjoint, leads to the simplified Equation 2.15.

$$\langle \mathbf{\Pi}\phi_m, \mathfrak{A}\phi_n \rangle + \langle \mathfrak{A}\phi_m, \mathbf{\Pi}\phi_n \rangle - \mathfrak{R}^{-1} \langle \mathfrak{B}^*\mathbf{\Pi}\phi_m, \mathfrak{B}^*\mathbf{\Pi}\phi_n \rangle + \langle \mathfrak{Q}\phi_m, \phi_n \rangle = 0 \quad (2.15)$$

To ensure that the domain and range of $\mathbf{\Pi}$ match those of \mathfrak{A} and \mathfrak{A}^* , respectively, $\mathbf{\Pi}$ can be expressed as an infinite series, as shown in Equation 2.16. The coefficients $p_{i,j}$ can be interpreted as elements of an infinite-dimensional matrix \tilde{P} , which represents the operator $\mathbf{\Pi}$. This forms the first step in converting the ORE to the corresponding matrix Riccati equation (MRE).

$$\mathbf{\Pi}x \equiv \sum_{i=1}^{\infty} \sum_{j=1}^{\infty} p_{i,j} \langle x, \psi_j \rangle \psi_i \quad \forall i, j : \quad p_{i,j} \in \mathbb{C} \quad (2.16)$$

2.3.1.2 Obtaining \mathfrak{B} and \mathfrak{B}^*

Before further simplifying the ORE, it is essential to define the operators \mathfrak{B} and \mathfrak{B}^* . Given the boundary-control nature of the system as seen in Equation 3.3, \mathfrak{B} is defined to properly project the control input $u \in \mathbb{R}^1$ onto the state space $X : L^2[0, 1] \times L^2[0, 1]$, as outlined in Equation 2.17.

$$\mathfrak{B}u \equiv v(1 - R) \begin{bmatrix} \delta(\zeta) \\ 0 \end{bmatrix} \cdot u \quad (2.17)$$

where $\delta(\zeta)$ denotes the Dirac delta function. The adjoint operator \mathfrak{B}^* is obtained by leveraging the properties of \mathfrak{A} and \mathfrak{A}^* , that is, their expressions as well as their domains (as shown in Equations 3.5 and 3.6), after applying

integration by parts to the result of the inner products, as summarized in Equation 2.18.

$$\begin{aligned} \langle \mathfrak{A}x + \mathfrak{B}u, y \rangle &= \langle \mathfrak{A}x, y \rangle + \langle \mathfrak{B}u, y \rangle = \langle x, \mathfrak{A}^*y \rangle + \langle u, \mathfrak{B}^*y \rangle \\ \langle u, \mathfrak{B}^*y \rangle &= \langle \mathfrak{A}x + \mathfrak{B}u, y \rangle - \langle x, \mathfrak{A}^*y \rangle \Rightarrow \dots \\ \Rightarrow \mathfrak{B}^*(\cdot) &= \left[v(1-R) \int_0^1 \delta(\zeta)(\cdot) d\zeta \quad , \quad 0 \right] \end{aligned} \quad (2.18)$$

2.3.1.3 Matrix Riccati equation

Using the expression for $\mathbf{\Pi}$ in Equation 2.16, along with the derived \mathfrak{B}^* from Equation 2.18, and the eigenvalue problem $\mathfrak{A}\phi_i = \lambda_i\phi_i$, the ORE can be reformulated as the MRE shown in Equation 2.19. Here, $\gamma_i \equiv v(1-R) \left. \psi_1^{(i)} \right|_{\zeta=0}$, and $q_{m,n} = \langle \mathfrak{Q}\phi_m, \phi_n \rangle$.

$$p_{n,m}(\lambda_m + \overline{\lambda_n}) - \mathfrak{R}^{-1} \left\langle \sum_{i=1}^{\infty} p_{i,m} \gamma_i, \sum_{i=1}^{\infty} p_{i,n} \gamma_i \right\rangle + q_{m,n} = 0 \quad (2.19)$$

Due to the infinite-dimensional nature of \tilde{P} , a numerical solution is impractical. This challenge is addressed by selecting the first N eigenmodes of the system as its dominant modes. This translates to truncating the infinite sums in the MRE and reducing the infinite-dimensional system to a finite set of nonlinear algebraic equations that can be solved to obtain an equivalent $N \times N$ matrix P , that is, a truncated approximation of matrix \tilde{P} . The optimal full-state feedback gain is then calculated using Equation 2.20, ensuring closed-loop stability.

$$\begin{aligned}
u(t) &= -\langle K(\zeta), x(\zeta, t) \rangle = -\mathfrak{B}^* \mathbf{\Pi} x(\zeta, t) \\
&= -\sum_{i=1}^N \sum_{j=1}^N p_{i,j} \langle x(\zeta, t), \psi_j(\zeta) \rangle \gamma_i \\
&= -\sum_{i=1}^N \sum_{j=1}^N p_{i,j} \gamma_i \int_0^1 x(\zeta, t) \cdot \overline{\psi_j}(\zeta) d\zeta \\
&= -\int_0^1 \sum_{i=1}^N \sum_{j=1}^N p_{i,j} \gamma_i \overline{\psi_j}(\zeta) \cdot x(\zeta, t) d\zeta \\
\Rightarrow K(\zeta) &\equiv \sum_{i=1}^N \sum_{j=1}^N p_{i,j} \gamma_i \overline{\psi_j}(\zeta)
\end{aligned} \tag{2.20}$$

The computed gain is a function of space and is calculated offline. The control action at any given time instance is the inner product of this gain with the current state of the system, thus justifying the term “full-state” feedback. The dynamics of the resulting closed-loop full-state feedback system may be described by the state-space representation shown in Equation 2.21.

$$\begin{aligned}
\dot{x}(\zeta, t) &= \mathfrak{A}x(\zeta, t) + \mathfrak{B}u(t) \\
&= (\mathfrak{A} - \mathfrak{B}K)x(\zeta, t) \\
&= \mathfrak{A}_{reg}x(\zeta, t)
\end{aligned} \tag{2.21}$$

By selecting $\mathfrak{Q} = 0.05$ as a constant function over $\zeta = [0, 1]$, and $\mathfrak{R} = 50$, the full-state feedback gain is obtained and represented in Figure 2.4. The obtained gains are used to design the optimal full-state feedback regulator to stabilize the control system. A block diagram representation of the full-state feedback control system is shown in Figure 3.3.

2.3.2 Output feedback compensator

Thus far, the optimal regulator is designed under the assumption that it has full access to the system’s states. However, this assumption is not feasible in

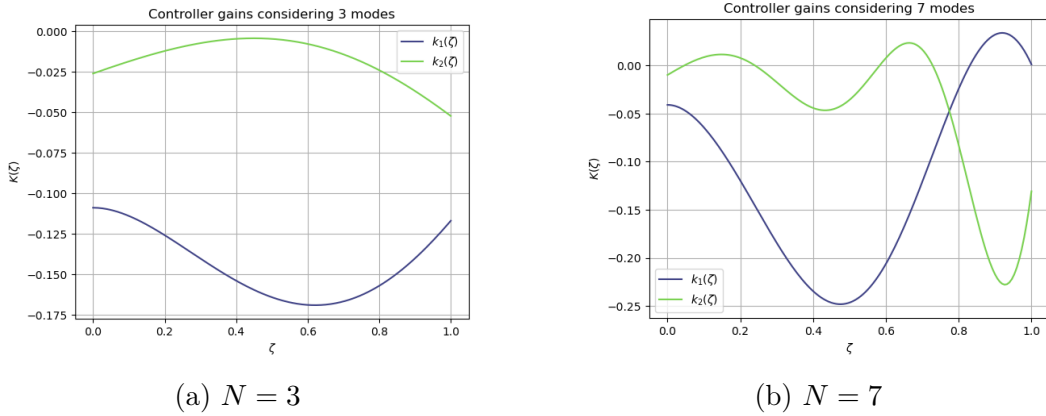


Figure 2.4: Full-state feedback gain $K(\zeta)$ utilizing the first N modes of the system given by Equation (2.20).

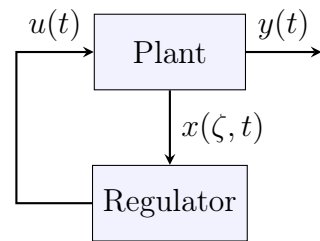


Figure 2.5: Block diagram representation of the optimal full-state feedback control system.

realistic applications. To address this, an observer is introduced to estimate and reconstruct the states by measuring the system's output in real time, and providing the regulator with the reconstructed states to further stabilize the system. The output, in this context, is taken as the concentration at the reactor outlet, as defined in Equation 3.3. This leads to the definition of the output operator \mathfrak{C} in the linear time-invariant (LTI) system $\Sigma(\mathfrak{A}, \mathfrak{B}, \mathfrak{C}, -)$, which is subsequently used to determine the observer gain, $L(\zeta)$. The formulation is shown in Equation 2.22:

$$\mathfrak{C} \equiv \left[\int_0^1 \delta(\zeta - 1)(\cdot) d\zeta \quad , \quad 0 \right] \quad (2.22)$$

where $\delta(\zeta)$ denotes the Dirac delta function. Regarding the choice of observer, Luenberger-based observers are well-suited for infinite-dimensional systems when the system parameters are perfectly known [27]. Among the various methods to compute the gain for this class of observers, pole-placement is a solid, straightforward, and reliable approach for state reconstruction. To ensure that the state reconstruction dynamics converge more quickly than the regulation dynamics, the poles of the observer-based controller are placed to the left of the poles of the full-state feedback controller. This practice is common in the design of observer-based controllers for infinite-dimensional systems [16]. The observer gain in Figure 2.6 is obtained by limiting the eigenmodes of the observer-based controller to have real parts that are at least 3 times more negative than the real part of the dominant eigenmodes of the full-state feedback system. This is done for the case where the first 7 modes of the system are considered for designing the controller. The first few eigenvalues of the observer-based controller and the full-state feedback controller, along with the

eigenvalues of the open-loop system are shown in Figure 2.7 to demonstrate the pole placement strategy explained above. It can be confirmed that both control systems have eigenvalues with negative real parts, ensuring stability. Note that the eigenvalues of both control systems are identical after the 7th mode, as the real parts of these eigenvalues are already sufficiently negative.

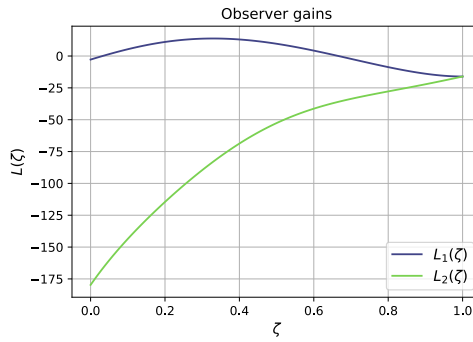


Figure 2.6: Observer gain $L(\zeta)$.

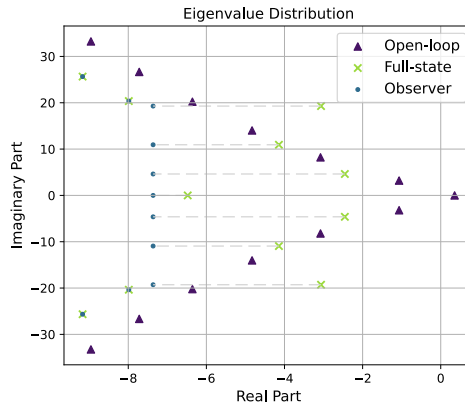


Figure 2.7: Eigenvalues of the observer-based controller, full-state feedback controller, and open-loop system.

The dynamics of the augmented observer-controller system are described by the state-space representation shown in Equation ??, where $\hat{x}(\zeta, t)$ and $e(\zeta, t)$ refer to the estimated state and the state estimation error, respectively. A

block diagram representation of the output feedback control system is also shown in Figure 2.8.

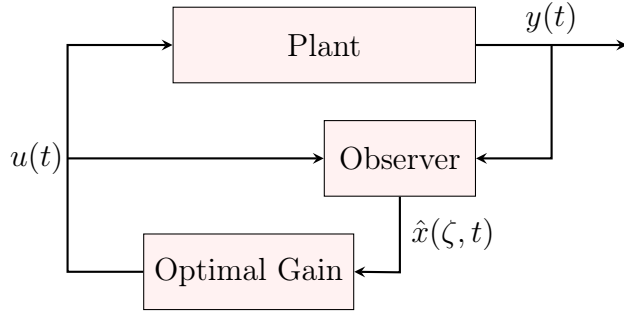


Figure 2.8: Block diagram representation of the observer-based output feedback control system.

2.4 Results and Discussion

In this section, the obtained control strategies are applied to a finite-difference method (FDM) representation of the system to evaluate its dynamic response. The system is discretized in space using a uniform grid with 100 equidistributed points, resulting in a system of ordinary differential equations (ODEs) with respect to time. This spatial discretization is introduced solely at the evaluation stage to numerically approximate the system's behaviour under the influence of the optimal control input and is not involved in the design of the control law. The control law is derived directly in the infinite-dimensional space, fully capturing the continuous nature of the original system.

To solve the resulting ODEs, an adaptive Runge–Kutta method of order 5(4), commonly referred to as RK45, is employed. This method dynamically adjusts time steps to balance accuracy and computational efficiency, ensuring a reliable numerical solution while evaluating the system at specific points as required [28, 29]. The implementation of this method is facilitated using the

`solve_ivp` function from Python's SciPy library [30], which provides a robust framework for handling time integration of ODEs.

Employing the outlined approach to evaluate the dynamic response of the systems under consideration, a comparative analysis is conducted between two identical systems with full-state access, differing only in the number of eigenmodes employed to compute the optimal full-state feedback gains. Subsequently, the performance of the proposed observer-based controller is assessed, with particular attention given to the dynamics of state reconstruction errors. Finally, a sensitivity analysis is performed to examine the impact of key parameters on the model behaviour and the effectiveness of the control strategy. Across all simulations presented, $\mathfrak{Q} = 0.05 \cdot \mathfrak{I}$ and $\mathfrak{R} = 50$ are used as the deviation penalty and control effort weight operators, respectively, where \mathfrak{I} denotes the identity operator matching the size of \mathfrak{A} .

2.4.1 Full-state feedback regulator FDM representation

Initially, the input response of the system provided by the full-state feedback is explored using the mentioned FDM setup. Two configurations are compared where the optimal feedback gain is obtained using different numbers of eigenmodes: one with $N = 3$ and another with $N = 7$, according to Figure 2.4. The state profile versus time and space is illustrated for both cases in Figure 2.9.

In order to offer a clearer representation of the state trajectory in time, spatial cross-sectional plots are provided in Figure 2.10 for the $N = 7$ case at different lengths of the domain. The delay-imposing state, that is, the concentration along the recycle stream $x_2(\zeta, t)$, is provided only in Figure 2.10 for the sake of conciseness.

Both optimal feedback gains are able to successfully stabilize the system

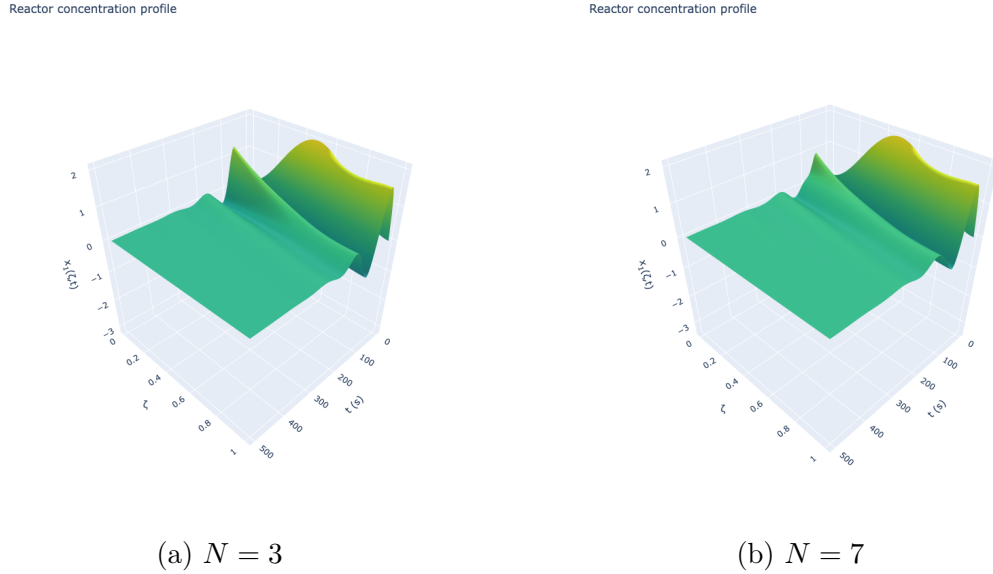


Figure 2.9: Input response of the system under full-state feedback control given by Equation (2.21), utilizing the feedback gain obtained in Figure 2.4.

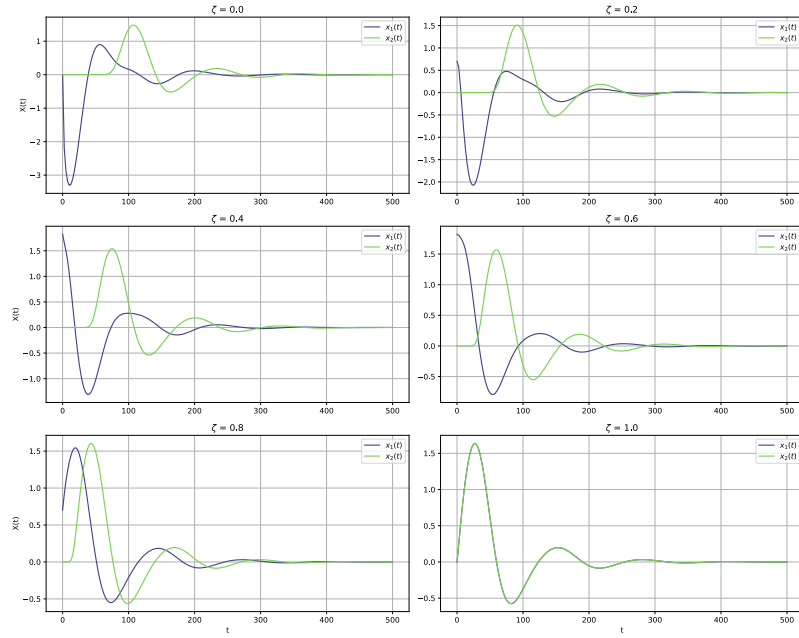


Figure 2.10: 2D cross-section plots of the full-state feedback input response at various ζ positions, utilizing the feedback gain obtained in Figure 2.4b.

within finite time horizon. However, the case where more eigenmodes are considered in the controller design shows better performance, as the higher dimensional controller is able to stabilize the system quicker with lower cost function values in general.

2.4.2 Observer-based regulator FDM representation

Omitting the need to have full access to system states, the observer-based regulator is evaluated using the same FDM representation. The states reconstruction is done by applying the observer gain obtained in Figure 2.6 to the system output. The estimated states are now used with the previously obtained optimal feedback gain with $N = 7$ eigenmodes to calculate the input. Similar to the previous case, the state profile $x_1(\zeta, t)$ is illustrated in Figure 2.11, as well as cross-sectional plots for both states in Figure 2.12 for better visualization of state trajectories in time.

In the next step, the state estimation error dynamics of the observer are plotted in Figures 2.13 and 2.14 to demonstrate the performance of the observer. The error dynamics are calculated as the squared difference between the true state and the estimated state at each grid point and time instance.

While the performance of the observer-based controller is slightly more sluggish compared to that of the full-state feedback regulator, it successfully stabilizes the system within a finite time horizon using only output measurements instead of full state information. In the absence of uncertainty in the system model, the observer gain can theoretically be designed so that the state estimation error converges to zero very fast compared to full-state feedback regulator dynamics. In practice, however, the observer gain is constrained by factors such as noise in the system output and plant–model mismatches.

Estimated state profile

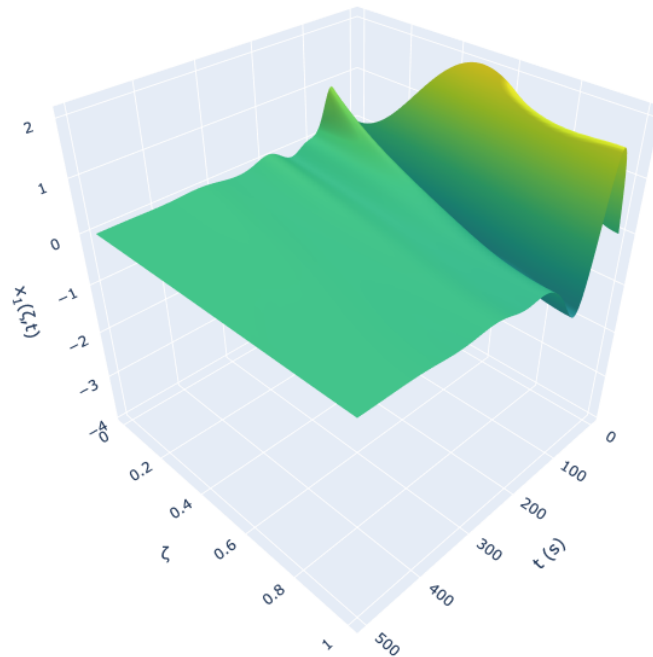


Figure 2.11: Input response of the system under observer-based output feedback control given by Equation (??), utilizing the observer gain obtained in Figure 2.6 and the feedback gain obtained in Figure 2.4b.

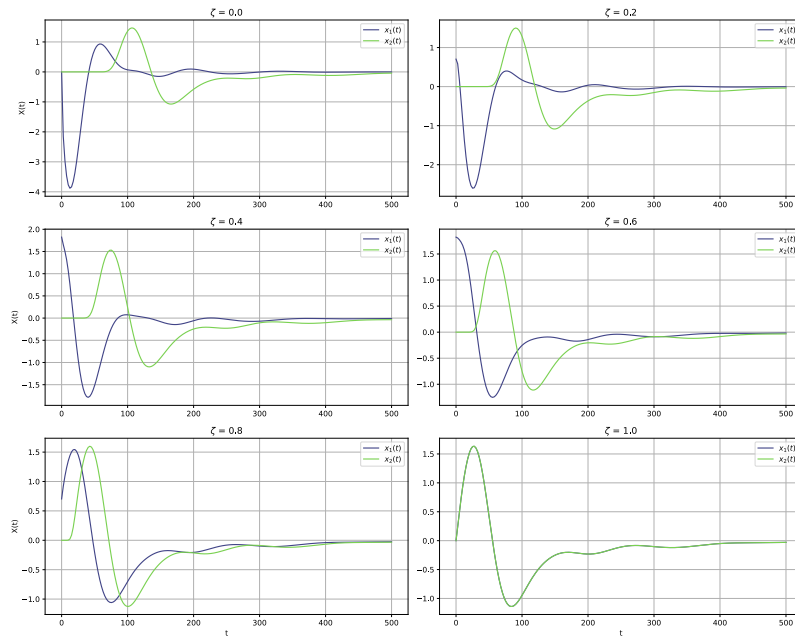


Figure 2.12: 2D cross-section plots of the input response at various ζ positions, utilizing the observer gain obtained in Figure 2.6 and the feedback gain obtained in Figure 2.4b.

State reconstruction error profile

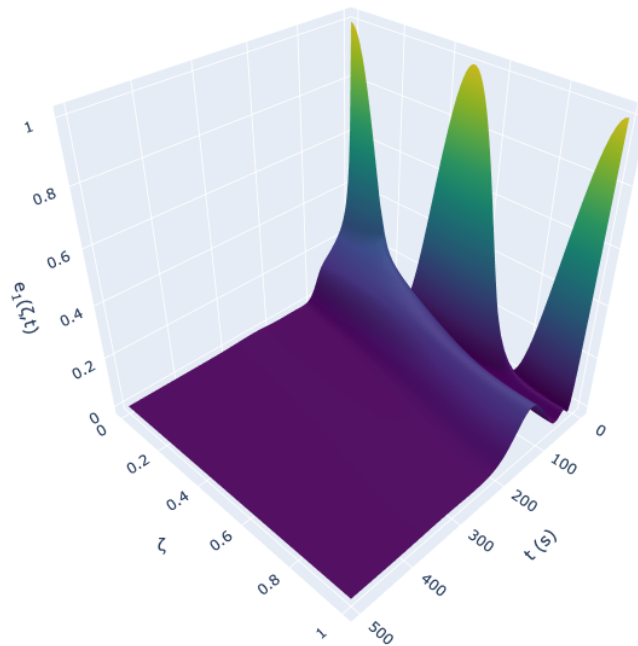


Figure 2.13: Error dynamics of the observer-based regulator utilizing the observer gain obtained in Figure 2.6 and the feedback gain obtained in Figure 2.4b.

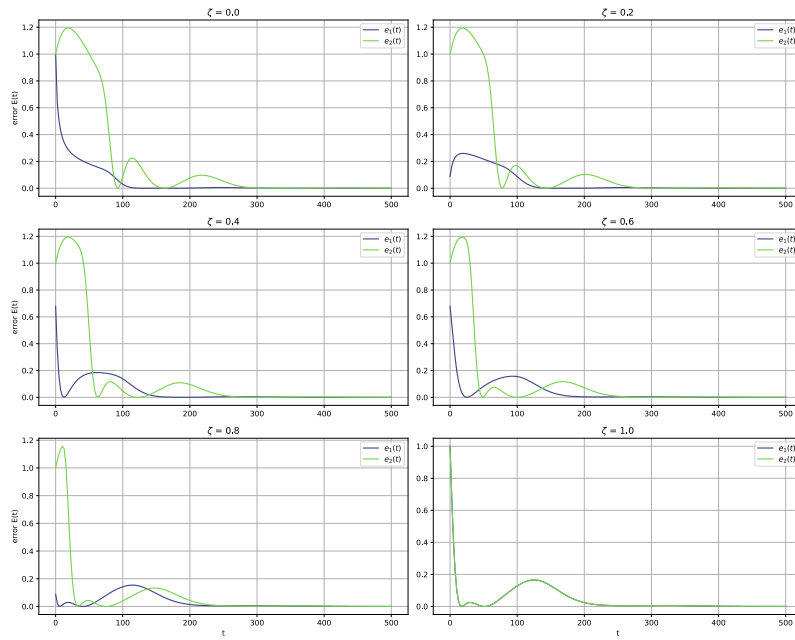


Figure 2.14: 2D cross-section plots of the error dynamics of the observer-based regulator at various ζ positions, utilizing the observer gain obtained in Figure 2.6 and the feedback gain obtained in Figure 2.4b.

Despite these challenges, the proposed observer design mechanism achieves system stabilization with reasonable performance.

2.4.3 Parameter sensitivity analysis

Followed by showcasing the ability of the proposed controller to stabilize an unstable system using merely output measurements, a brief parameter sensitivity analysis of the model dynamics and controller performance is conducted at the end of this section. The effects of varying the recycle ratio R and mass transfer Peclet number (i.e., the ratio of convection to diffusion, $Pe = v/D$) were explored during initial simulations. In addition, as it is central to this work, the effect of varying time delay τ on the response of the system under the original controller design is investigated in more detail.

Regarding the effect of recycle ratio on system dynamics and controller performance, it was observed that as the recycle ratio approaches unity, the open-loop system exhibits behaviour similar to that of a well-mixed reactor, with concentration profiles flattening. This also influences the controller performance as it becomes more challenging to affect the system dynamics with the control input as the controller's action becomes diluted at the reactor inlet due to mixing with the recycle stream. For changes in mass Peclet number and its effect on the system dynamics, it was observed that a decrease in the Peclet number causes the eigenvalues of the system generator to shift closer to the real axis of the complex plane. This implies that greater diffusion relative to convection dampens the oscillatory behaviour of the system that is originally imposed as the result of the delayed recycle stream.

Finally, the effect of varying time delay τ on the system dynamics is also investigated, as it is a key parameter in the model and controller design within

this work. Input responses of several systems with different time delays are compared in Figure 2.15, where the input for all cases is calculated assuming $\tau = 80$ s, which results in the same output feedback gain as the one obtained in Section 2.4.2.

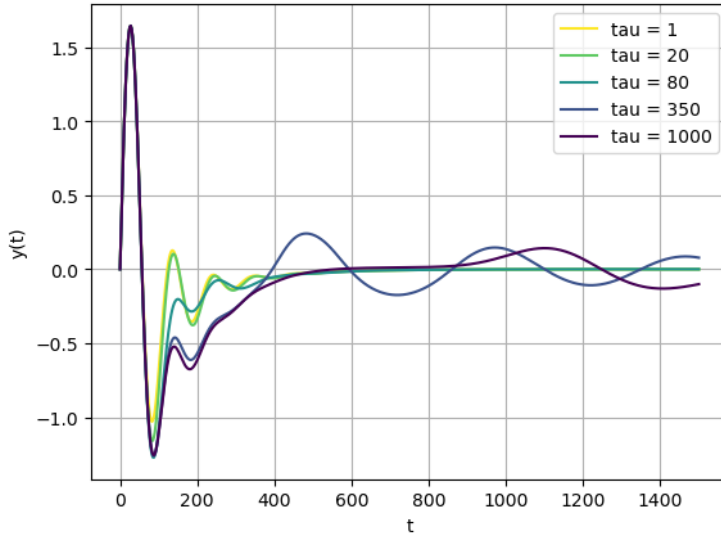


Figure 2.15: Measured output of the systems with different time delays τ , under observer-based output feedback control utilizing the observer gain obtained in Figure 2.6 and the feedback gain obtained in Figure 2.4b, where $\tau = 80$ s.

It can be seen that as long as the actual time delay of a system is less than the assumed delay used in the controller design, the controller is still able to stabilize the system within a finite time horizon, although transient deviations from the desired behaviour are observed. However, as the actual delay increases, the response of the system starts to deviate significantly from the desired behaviour, especially after a certain threshold close to the actual recycle delay of the system. This shows the importance of including the time delay in the controller design to ensure the stability of the system within an

optimal framework.

Although further parameter sensitivity analysis is possible as it naturally raises readers' curiosity, expanding the analysis to include more detailed investigations would risk exceeding the scope of this work, which is to offer a novel modeling and control framework for a certain class of distributed parameter systems in chemical engineering. Nonetheless, the proposed modelling and control strategy is able to effectively stabilize the system over a broad range of parameter sets, including but not limited to variations in the imposed time delay, Peclet number, and recycle ratio, ensuring the practicality of the proposed framework across different system configurations.

2.5 Conclusion

The control of an axial tubular reactor equipped with recycle stream is addressed as a significant class of distributed parameter systems in chemical engineering industries. The notion of time delay introduced by the recycle process has not been adequately addressed in the literature despite being a common and intrinsic feature of such systems; introducing a rare example of state-delay in this field. By converting the notion of delay into an equivalent transport PDE, the DPS is formulated as a system of coupled parabolic and hyperbolic PDEs. The infinite-dimensional system is assumed to be boundary controlled, with the control input acting on the reactor inlet. Particularly suited for the class of axial tubular reactors, Danckwerts boundary conditions are considered. A continuous-time linear quadratic optimal regulator is then developed to stabilize the system.

To address the infinite-dimensional nature of the system, a late lumping

approach is employed, ensuring that the infinite-dimensional characteristics of the system are preserved in the control design. The system's Riesz-spectral properties are utilized to derive the full-state feedback regulator by solving the ORE, utilizing dominant modes of the system to obtain low-dimensional feedback gains. Recognizing practical limitations of the full-state feedback strategy, an observer-based regulator is also introduced to reconstruct the system states using boundary measurements, addressing the challenge of limited state access in real-world applications.

The proposed framework may be extended to more complex diffusion-convection reactor configurations, such as non-isothermal reactors. More complex control strategies may also be considered for this framework, such as model-predictive control (MPC) strategy, enabling constraints to be incorporated into the control design. The proposed observer-based control strategy may also be extended to handle measurement noise as well as plant-model mismatches, which are common in real-world applications. Another interesting aspect to explore is the briefly described impact that picking different numbers of eigenmodes may have on the optimality of controller design. This could be further investigated to provide a more comprehensive understanding of the effects of this choice on the controller's performance.

In summary, this research introduces a comprehensive optimal control strategy for a novel yet practically significant class of distributed parameter systems, that is, axial tubular reactors with delayed recycle streams. A late-lumping approach is employed to address the infinite-dimensional nature of the system, leveraging the Riesz-spectral properties of the system generator to derive an optimal feedback law utilizing both full-state and estimated states of

the system, setting the stage for future advancements in this area of research.

References

- [1] B. Moadeli, G. O. Cassol, and S. Dubljevic, “Optimal control of axial dispersion tubular reactors with recycle: Addressing state-delay through transport PDEs,” *The Canadian Journal of Chemical Engineering*, vol. 103, no. 8, pp. 3751–3766, 2025, ISSN: 0008-4034. DOI: [10.1002/cjce.25629](https://doi.org/10.1002/cjce.25629).
- [2] W. H. Ray, *Advanced process control*. McGraw-Hill: New York, NY, USA, 1981.
- [3] E. Davison, “The robust control of a servomechanism problem for linear time-invariant multivariable systems,” *IEEE transactions on Automatic Control*, vol. 21, no. 1, pp. 25–34, 1976, ISSN: 0018-9286. DOI: [10.1109/tac.1976.1101137](https://doi.org/10.1109/tac.1976.1101137).
- [4] B. A. Francis, “The linear multivariable regulator problem,” *SIAM Journal on Control and Optimization*, vol. 15, no. 3, pp. 486–505, 1977, ISSN: 0363-0129. DOI: [10.1137/0315033](https://doi.org/10.1137/0315033).
- [5] A. A. Moghadam, I. Aksikas, S. Dubljevic, and J. F. Forbes, “Infinite-dimensional LQ optimal control of a dimethyl ether (DME) catalytic distillation column,” *Journal of Process Control*, vol. 22, no. 9, pp. 1655–1669, 2012, ISSN: 0959-1524. DOI: [10.1016/j.jprocont.2012.06.018](https://doi.org/10.1016/j.jprocont.2012.06.018).
- [6] P. D. Christofides, “Robust control of parabolic PDE systems,” *Chemical Engineering Science*, vol. 53, no. 16, pp. 2949–2965, 1998, ISSN: 2324-9749. DOI: [10.1007/978-1-4612-0185-4_5](https://doi.org/10.1007/978-1-4612-0185-4_5).
- [7] M. Krstic and A. Smyshlyaev, “Backstepping boundary control for first-order hyperbolic PDEs and application to systems with actuator and sensor delays,” *Systems & Control Letters*, vol. 57, no. 9, pp. 750–758, 2008, ISSN: 0167-6911. DOI: [10.1016/j.sysconle.2008.02.005](https://doi.org/10.1016/j.sysconle.2008.02.005).
- [8] X. Xu and S. Dubljevic, “The state feedback servo-regulator for counter-current heat-exchanger system modelled by system of hyperbolic PDEs,” *European Journal of Control*, vol. 29, pp. 51–61, 2016, ISSN: 0947-3580. DOI: [10.1016/j.ejcon.2016.02.002](https://doi.org/10.1016/j.ejcon.2016.02.002).
- [9] J. Xie and S. Dubljevic, “Discrete-time modeling and output regulation of gas pipeline networks,” *Journal of Process Control*, vol. 98, pp. 30–40, 2021, ISSN: 0959-1524. DOI: [10.1016/j.jprocont.2020.12.002](https://doi.org/10.1016/j.jprocont.2020.12.002).

- [10] L. Zhang, J. Xie, and S. Dubljevic, “Tracking model predictive control and moving horizon estimation design of distributed parameter pipeline systems,” *Computers & Chemical Engineering*, vol. 178, p. 108381, 2023, ISSN: 0098-1354. DOI: [10.1016/j.compchemeng.2023.108381](https://doi.org/10.1016/j.compchemeng.2023.108381).
- [11] L. Zhang, J. Xie, and S. Dubljevic, “Dynamic modeling and model predictive control of a continuous pulp digester,” *AICHE Journal*, vol. 68, no. 3, e17534, 2022. DOI: [10.22541/au.164841554.43817131/v1](https://doi.org/10.22541/au.164841554.43817131/v1).
- [12] P. D. Christofides, *Nonlinear and robust control of PDE systems* (Systems & Control: Foundations & Applications). New York, NY: Springer, Oct. 2012.
- [13] S. Dubljevic, N. H. El-Farra, P. Mhaskar, and P. D. Christofides, “Predictive control of parabolic PDEs with state and control constraints,” *International Journal of Robust and Nonlinear Control*, vol. 16, no. 16, pp. 749–772, 2006, ISSN: 1049-8923. DOI: [10.1002/rnc.1097](https://doi.org/10.1002/rnc.1097).
- [14] G. O. Cassol, D. Ni, and S. Dubljevic, “Heat exchanger system boundary regulation,” *AICHE Journal*, vol. 65, no. 8, e16623, 2019, ISSN: 0001-1541. DOI: [10.1002/aic.16623](https://doi.org/10.1002/aic.16623).
- [15] S. Khatibi, G. O. Cassol, and S. Dubljevic, “Model predictive control of a non-isothermal axial dispersion tubular reactor with recycle,” *Computers & Chemical Engineering*, vol. 145, p. 107159, 2021, ISSN: 0098-1354. DOI: [10.1016/j.compchemeng.2020.107159](https://doi.org/10.1016/j.compchemeng.2020.107159).
- [16] K. A. Morris, *Controller design for distributed parameter systems*. Springer, 2020. DOI: [10.1007/978-3-030-34949-3_7](https://doi.org/10.1007/978-3-030-34949-3_7).
- [17] R. Curtain and H. Zwart. Springer Nature, 2020. DOI: [10.1007/978-1-0716-0590-5_1](https://doi.org/10.1007/978-1-0716-0590-5_1).
- [18] I. Aksikas, L. Mohammadi, J. F. Forbes, Y. Belhamadia, and S. Dubljevic, “Optimal control of an advection-dominated catalytic fixed-bed reactor with catalyst deactivation,” *Journal of Process Control*, vol. 23, no. 10, pp. 1508–1514, 2013, ISSN: 0959-1524. DOI: [10.1016/j.jprocont.2013.09.016](https://doi.org/10.1016/j.jprocont.2013.09.016).
- [19] L. Mohammadi, I. Aksikas, S. Dubljevic, and J. F. Forbes, “LQ-boundary control of a diffusion-convection-reaction system,” *International Journal of Control*, vol. 85, no. 2, pp. 171–181, 2012, ISSN: 0959-1524. DOI: [10.1080/00207179.2011.642308](https://doi.org/10.1080/00207179.2011.642308).
- [20] I. Aksikas, “Spectral-based optimal output-feedback boundary control of a cracking catalytic reactor PDE model,” *International Journal of Control*, vol. 97, no. 12, pp. 1–10, 2024, ISSN: 0020-7179. DOI: [10.1080/00207179.2024.2302057](https://doi.org/10.1080/00207179.2024.2302057).

- [21] M. Krstić (Systems & control). Birkhäuser, 2009.
- [22] G. O. Cassol and S. Dubljevic, “Discrete output regulator design for a mono-tubular reactor with recycle,” in *2019 American Control Conference (ACC)*, IEEE, 2019, pp. 1262–1267. DOI: [10.23919/acc.2019.8815250](https://doi.org/10.23919/acc.2019.8815250).
- [23] J. Qi, S. Dubljevic, and W. Kong, “Output feedback compensation to state and measurement delays for a first-order hyperbolic PIDE with recycle,” *Automatica*, vol. 128, p. 109565, 2021, ISSN: 0005-1098. DOI: [10.1016/j.automatica.2021.109565](https://doi.org/10.1016/j.automatica.2021.109565).
- [24] O. Levenspiel, *Chemical reaction engineering*. John Wiley & Sons, 1998.
- [25] K. F. Jensen and W. H. Ray, “The bifurcation behavior of tubular reactors,” *Chemical Engineering Science*, vol. 37, no. 2, pp. 199–222, 1982, ISSN: 0009-2509. DOI: [10.1016/0009-2509\(82\)80155-3](https://doi.org/10.1016/0009-2509(82)80155-3).
- [26] P. V. Danckwerts, “Continuous flow systems: Distribution of residence times,” *Chemical Engineering Science*, vol. 2, no. 1, pp. 1–13, 1953, ISSN: 0009-2509. DOI: [10.1016/0009-2509\(53\)80001-1](https://doi.org/10.1016/0009-2509(53)80001-1).
- [27] J. M. Ali, N. H. Hoang, M. A. Hussain, and D. Dochain, “Review and classification of recent observers applied in chemical process systems,” *Computers & Chemical Engineering*, vol. 76, pp. 27–41, 2015, ISSN: 0098-1354. DOI: [10.1016/j.compchemeng.2015.01.019](https://doi.org/10.1016/j.compchemeng.2015.01.019).
- [28] J. R. Dormand and P. J. Prince, “A family of embedded Runge-Kutta formulae,” *Journal of computational and applied mathematics*, vol. 6, no. 1, pp. 19–26, 1980, ISSN: 0377-0427. DOI: [10.1016/0771-050x\(80\)90013-3](https://doi.org/10.1016/0771-050x(80)90013-3).
- [29] L. F. Shampine, “Some practical Runge-Kutta formulas,” *Mathematics of computation*, vol. 46, no. 173, pp. 135–150, 1986, ISSN: 0025-5718. DOI: [10.2307/2008219](https://doi.org/10.2307/2008219).
- [30] P. Virtanen *et al.*, “SciPy 1.0: Fundamental Algorithms for Scientific Computing in Python,” *Nature Methods*, vol. 17, no. 3, pp. 261–272, 2020, ISSN: 1548-7091. DOI: [10.1038/s41592-019-0686-2](https://doi.org/10.1038/s41592-019-0686-2).

Chapter 3

DISCRETE-TIME ESTIMATION AND MODEL-PREDICTIVE CONTROL FOR THE ISOTHERMAL SYSTEM¹

3.1 Introduction

Many chemical and petrochemical processes, such as reactions in tubular reactors, heat transfer in exchangers, and separations in columns, involve states distributed in space and time. These systems, known as distributed parameter systems (DPS), are often modeled using partial differential equations (PDEs) to describe distributed state dynamics. Due to their infinite-dimensional nature, the control and estimation of DPSs are inherently more challenging compared to the well-established control theories for finite-dimensional systems [2], making this field an active area of research. Two primary methods,

¹This chapter is inspired by two of our works that are published as B. Moadeli and S. Dubljevic, “Model predictive control of axial dispersion tubular reactors with recycle: Addressing state-delay through transport PDEs,” in *2025 American Control Conference (ACC)*, 2025 and B. Moadeli and S. Dubljevic, “Observer-based MPC design of an axial dispersion tubular reactor: Addressing recycle delays through transport PDEs,” in *2025 European Control Conference (ECC)*, 2025.

“Early Lumping” and “Late Lumping,” have been proposed to address DPS control in the literature. The first, “Early Lumping,” reduces the infinite-dimensional system to a finite-dimensional one through spatial discretization during the modeling phase [3]. While this enables standard control strategies, it often compromises model accuracy due to mismatches between the original and reduced-order systems [5]. In contrast, “Late Lumping” preserves the infinite-dimensional system until the final numerical implementation stage, resulting in more accurate but computationally complex control strategies [2].

State reconstruction for DPSs has also been addressed using discrete-time Luenberger observers without spatial discretization, a key feature consistent with the late lumping paradigm [27, 33–35]. Numerous studies have employed Late Lumping approaches to control infinite-dimensional systems in the field of chemical engineering. These efforts primarily focus on convection-reaction systems governed by first-order hyperbolic PDEs and diffusion-convection-reaction systems governed by second-order parabolic PDEs. For example, robust control of first-order hyperbolic PDEs was explored in [36], where a plug flow reactor system was stabilized under distributed input. Similarly, boundary feedback stabilization using the backstepping method was proposed in [7] for such systems. State feedback regulator design for a countercurrent heat exchanger, another example of a chemical engineering DPS, was addressed in [8]. Introducing the effects of dispersion in tubular reactors, robust control of second-order parabolic PDEs was studied in [6]. Modal decomposition methods for designing low-dimensional predictive controllers for diffusion-convection-reaction systems have also been applied in [37], while observer-based model predictive control (MPC) was developed in [15] for axial

dispersion tubular reactors, considering recycle stream effects.

Delay systems represent another class of infinite-dimensional systems studied extensively [17]. Commonly modeled using delay differential equations (DDEs), delays can alternatively be described using transport PDEs, offering advantages in complex scenarios [21]. In chemical engineering DPS control, input/output delays have been widely addressed, as industrial processes often feature both measurement and actuation delays. Such delays are typically handled by modeling them as transportation lag blocks, resulting in cascade PDE systems [19, 22, 38]. State delays, though less common, have been investigated in specific applications, such as heat exchangers with stream delays between passes [14], and plug flow tubular reactors with recycle delays [23]; with the effect of dispersion not being addressed in any of these works. Even in [15], where the effect of recycle is studied for an axial dispersion tubular reactor, the recycle is assumed to be instantaneous, leaving a gap in the literature regarding state delays in diffusion-convection-reaction systems with recycle streams.

In this work, an axial dispersion reactor with recycle is modeled as a diffusion-convection-reaction DPS. The reactor dynamics are described by a second-order parabolic PDE, coupled with a first-order hyperbolic transport PDE to account for the recycle stream's state delay. A Late Lumping approach is employed, obtaining the system's resolvent in a closed operator form without spatial discretization. To implement MPC as a digital controller, the system is discretized using the Cayley-Tustin method, a Crank-Nicolson-type discretization that conserves the continuous system's characteristics, avoiding the need for model reduction. Numerical simulations demonstrate that the proposed

controller stabilizes an unstable system optimally under input constraints. A discrete-time infinite-dimensional Luenberger observer is designed to reconstruct unmeasured states, enabling output feedback MPC. Simulations show that the proposed controller successfully stabilizes the otherwise unstable system under input constraints.

3.2 Mathematical Modeling of the Reactor System

3.2.1 Model representation

The chemical process depicted in Fig. 4.1 illustrates a chemical reaction within an axial dispersion tubular reactor [24] where reactant A is converted into products. The reactor features a recycle mechanism, allowing a portion of the product stream to re-enter the reactor, ensuring the consumption of any unreacted substrate. The dynamics of the reactant concentration can be described by the second-order parabolic PDE given by (3.1), a common class of equations used to characterize diffusion-convection-reaction systems [25]. The resulting PDE that describes the reactor model is obtained by utilizing first-principle modeling through relevant mass balance relations on an infinitesimally thin disk element along the longitudinal axis of the reactor.

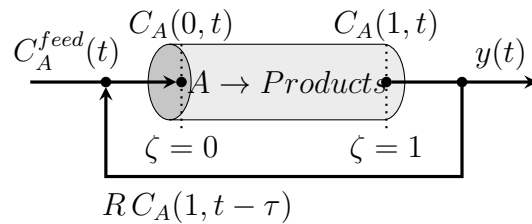


Figure 3.1: Axial tubular reactor with recycle stream.

$$\dot{C}_A(\zeta, t) = D\partial_{\zeta}\zeta C_A(\zeta, t) - v\partial_{\zeta}C_A(\zeta, t) - r(C_A) \quad (3.1)$$

Here, $C_A(\zeta, t)$ is the concentration of reactant A along the reactor. The physical parameters D and v represent the diffusion coefficient and flow velocity along the reactor, respectively. Physical parameters are assumed to be constant, hence changes in temperature or pressure will not affect the reactor model. The coordinate system in space and time is represented by ζ and t , where $\zeta \in [0, 1]$ and $t \in [0, \infty)$. In addition, $r(C_A)$ is the reaction rate of the reactant in general, which is often a non-linear function of C_A . Therefore, the model is further linearized around its steady-state, followed by introducing the deviation variable $c(\zeta, t) = C_A(\zeta, t) - C_{A,ss}(\zeta)$, where $C_{A,ss}(\zeta)$ is the steady-state concentration of the reactant. The linearized model is then given by (3.2).

$$\dot{c}(\zeta, t) = D\partial_{\zeta}\zeta c(\zeta, t) - v\partial_{\zeta}c(\zeta, t) - k_r c(\zeta, t) \quad (3.2)$$

Here, $k_r \equiv \left. \frac{\partial r(C_A)}{\partial C_A} \right|_{C_{A,ss}}$ is the linearized reaction rate coefficient in the vicinity of the steady-state. The system input is defined as $u(t) \equiv C_A^{feed} - C_{A,ss}^{feed}$, representing the deviation of the concentration of the reactant being fed into the reactor from its steady-state value. The output of the system is also considered as the deviation of the concentration of the reactant being measured at the reactor outlet from its steady-state value, denoted as $y(t)$.

To accurately represent the behavior of the given axial dispersion tubular reactor, Dankwerts boundary conditions are applied; as they effectively capture deviations from ideal mixing and piston flow while assuming negligible transport lags in connecting lines [26]. The inlet boundary condition is modi-

fied to reflect the mixing of the input stream with the delayed state, i.e. the recycled reactant concentration coming from the reactor outlet, occurring τ seconds earlier. These boundary conditions are therefore summarized in (3.3), with R and τ denoting the recycle ratio and the residence time in the recycle stream, respectively. The system output will consequently be defined as $y(t) = x_1(1, t)$.

$$\begin{cases} D\partial_\zeta c(0, t) - vc(0, t) = -v [Rc(1, t - \tau) + (1 - R)u(t)] \\ \partial_\zeta c(1, t) = 0 \\ y(t) = c(1, t) \end{cases} \quad (3.3)$$

In the case where the problem involves similar forms of PDEs, an effective general practice to address delays in systems is to reformulate the problem such that the notion of delay is replaced with an alternative transport PDE. Therefore, a new state variable $\underline{x}(\zeta, t) \equiv [x_1(\zeta, t), x_2(\zeta, t)]^T$ is defined as a vector of functions, where $x_1(\zeta, t)$ represents the concentration within the reactor—analogous to $c(\zeta, t)$ —and $x_2(\zeta, t)$ is introduced as a new state variable to account for the concentration along the recycle stream. The delay is thus modeled as a pure transport process, wherein the first state $x_1(\zeta, t)$ is transported from the reactor outlet to the inlet, experiencing a delay of τ time units while in the recycle stream. This makes all state variables expressed explicitly at a specific time instance t , resulting in the standard state-space form for a given infinite-dimensional linear time-invariant (LTI) system given in (3.4).

$$\begin{aligned} \dot{\underline{x}}(\zeta, t) &= \mathfrak{A}\underline{x}(\zeta, t) + \mathfrak{B}u(t) \\ y(t) &= \mathfrak{C}\underline{x}(\zeta, t) + \mathfrak{D}u(t) \end{aligned} \quad (3.4)$$

Here, \mathfrak{A} is a linear operator $\mathcal{L}(X)$ acting on a Hilbert space $X : L^2[0, 1] \times L^2[0, 1]$ and $\underline{x}(\zeta, t)$, as defined previously, is the vector of functions describing

the states of the system. Input operator \mathfrak{B} is a linear operator that maps the scalar input from input-space onto the state space. Output operator \mathfrak{C} on the other hand, is a linear operator that maps the infinite-dimensional state space onto the finite-dimensional output space, resulting in a scalar output. The operator \mathfrak{D} is the direct transmission operator, which is set to zero in this case as there is no direct transmission from the input to the output in the continuous-time system. The operators (\mathfrak{A} , \mathfrak{B} , \mathfrak{C} , and \mathfrak{D}) are shown in (3.5) for the infinite-dimensional LTI system.

$$\begin{aligned}
 \mathfrak{A} &\equiv \begin{bmatrix} D\partial_{\zeta\zeta} - v\partial_{\zeta} + k_r & 0 \\ 0 & \frac{1}{\tau}\partial_{\zeta} \end{bmatrix} \\
 D(\mathfrak{A}) &= \left\{ \underline{x}(\zeta) = [x_1(\zeta), x_2(\zeta)]^T \in X : \right. \\
 &\quad \underline{x}(\zeta), \partial_{\zeta}\underline{x}(\zeta), \partial_{\zeta\zeta}\underline{x}(\zeta) \quad \text{a.c.,} \\
 &\quad D\partial_{\zeta}x_1(0) - vx_1(0) = -vRx_2(0), \\
 &\quad \left. \partial_{\zeta}x_1(1) = 0, x_1(1) = x_2(1) \right\} \tag{3.5} \\
 \mathfrak{B} &\equiv \begin{bmatrix} \delta(\zeta) \\ 0 \end{bmatrix} v(1 - R) \\
 \mathfrak{C} &\equiv \begin{bmatrix} \int_0^1 \delta(\zeta - 1)(\cdot)d\zeta & 0 \end{bmatrix} \\
 \mathfrak{D} &= 0
 \end{aligned}$$

where $\delta(\zeta)$ is dirac delta function. This will enable the derivation of the system's spectrum using the eigenvalue problem. The characteristics equation of the system is obtained by solving the equation $\det(\mathfrak{A} - \lambda_i I) = 0$ for λ_i , where $\lambda_i \in \mathbb{C}$ is the i^{th} eigenvalue of the system and I is the identity operator. Attempts to analytically solve this equation have failed; therefore, it is solved numerically using the parameters in Table I. These parameters are carefully

chosen to reflect key characteristics of the system, i.e. diffusion, convection, reaction, and delayed recycle.

Similar to [1], a negative reaction coefficient (k_r) is used to induce instability for analysis, a condition uncommon for isothermal reactors but possible in specific cases like autocatalytic or inhibitory reactions. Figure 2 depicts the resulting eigenvalue distribution in the complex plane, confirming instability of the linearized model near its steady state.

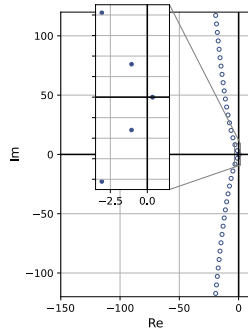


Figure 3.2: Eigenvalues of operator \mathfrak{A} .

Table 3.1: Physical Parameters for the System

Parameter	Symbol	Value	Unit
Diffusivity	D	2×10^{-5}	m^2/s
Velocity	v	0.01	m/s
Reaction Constant	k_r	-1.5	s^{-1}
Recycle Residence Time	τ	80	s
Recycle Ratio	R	0.3	—

3.2.2 Adjoint system

Next step is to obtain the adjoint system operators \mathfrak{A}^* and \mathfrak{B}^* . Utilizing the relation $\langle \mathfrak{A}\underline{x} + \mathfrak{B}u, \underline{y} \rangle = \langle \underline{x}, \mathfrak{A}^*\underline{y} \rangle + \langle u, \mathfrak{B}^*\underline{y} \rangle$, the adjoint operators \mathfrak{A}^* and \mathfrak{B}^* are obtained as shown in (3.6) and (3.7), respectively.

$$\begin{aligned} \mathfrak{A}^* &= \begin{bmatrix} D\partial_{\zeta\zeta} + v\partial_\zeta - k_r & 0 \\ 0 & -\frac{1}{\tau}\partial_\zeta \end{bmatrix} \\ D(\mathfrak{A}^*) &= \left\{ \underline{y} = [y_1, y_2]^T \in Y : \right. \\ &\quad \underline{y}(\zeta), \partial_\zeta \underline{y}(\zeta), \partial_{\zeta\zeta} \underline{y}(\zeta) \text{ a.c.,} \\ &\quad D\partial_\zeta y_1(1) + vy_1(1) = \frac{1}{\tau}y_2(1), \\ &\quad \left. Rvy_1(0) = \frac{1}{\tau}y_2(0), \partial_\zeta y_1(0) = 0 \right\} \end{aligned} \quad (3.6)$$

$$\mathfrak{B}^*(\cdot) = \left[v(1-R) \int_0^1 \delta(\zeta)(\cdot) d\zeta \quad , \quad 0 \right] \quad (3.7)$$

Once the adjoint operators are determined, the eigenfunctions $\{\underline{\phi}_i(\zeta), \underline{\psi}_i(\zeta)\}$ (for \mathfrak{A} and \mathfrak{A}^* , respectively) may be obtained and properly scaled following the calculation of eigenvalues. The set of scaled eigenfunctions will then form a bi-orthonormal basis for the Hilbert space X ; which will be later used in the controller design. It is important to note that the system is not self adjoint, as the obtained adjoint operator and its domain are not the same as the original operator and its domain.

3.2.3 Resolvent operator

One must obtain the resolvent operator of the system $\mathfrak{R}(s, \mathfrak{A}) = (sI - \mathfrak{A})^{-1}$ prior to constructing the discrete-time representation of the system. One way to obtain it is by utilizing the modal characteristics of the system, resulting in

an infinite-sum representation of the operator. While being a common practice in the literature, truncating the infinite-sum representation for numerical implementation may lead to a loss of accuracy. Another way to express the resolvent operator is by treating it as an operator that maps either the initial condition of the system $\underline{x}(\zeta, 0)$ or the input $u(t)$, to the Laplace transform of the state of the system $\underline{X}(\zeta, s)$. This approach, although more computationally intensive, results in a closed form expression for the resolvent operator, preserving the infinite-dimensional nature of the system. In (3.8), Laplace transform is applied to the LTI representation of the system for both zero-input response and zero-state response to obtain a general expression for the resolvent operator.

$$\begin{aligned} \dot{\underline{x}}(\zeta, t) &= \mathfrak{A}\underline{x}(\zeta, t) + \mathfrak{B}u(t) \xrightarrow{\mathcal{L}} \\ s\underline{X}(\zeta, s) - \underline{x}(\zeta, 0) &= \mathfrak{A}\underline{X}(\zeta, s) + \mathfrak{B}U(s) \\ \begin{cases} \xrightarrow{u=0} & \underline{X}(\zeta, s) = (sI - \mathfrak{A})^{-1}\underline{x}(\zeta, 0) = \mathfrak{R}(s, \mathfrak{A})\underline{x}(\zeta, 0) \\ \xrightarrow{\underline{x}(0, \zeta)} & \underline{X}(\zeta, s) = (sI - \mathfrak{A})^{-1}\mathfrak{B}U(s) = \mathfrak{R}(s, \mathfrak{A})\mathfrak{B}U(s) \end{cases} \end{aligned} \tag{3.8}$$

The goal is to obtain the solution for $\underline{X}(\zeta, s)$ and compare it with the general expression obtained in (3.8) to get the closed form expression for the resolvent operator. First step is to apply Laplace transform to the original system of PDEs in (3.5). The second order derivative term is decomposed to two first order PDEs, constructing a new 3×3 system of first order ODEs with respect to ζ after Laplace transformation, as shown in (3.9).

$$\begin{aligned}
 & \overbrace{\partial_\zeta \begin{bmatrix} X_1(\zeta, s) \\ \partial_\zeta X_1(\zeta, s) \\ X_2(\zeta, s) \end{bmatrix}}^{\tilde{X}(\zeta, s)} = \underbrace{\begin{bmatrix} 0 & 1 & 0 \\ \frac{s+k_r}{D} & \frac{v}{D} & 0 \\ 0 & 0 & s\tau \end{bmatrix}}_{P(s)} \begin{bmatrix} X_1(\zeta, s) \\ \partial_\zeta X_1(\zeta, s) \\ X_2(\zeta, s) \end{bmatrix} \\
 & + \underbrace{\begin{bmatrix} 0 \\ -\frac{x_1(\zeta, 0)}{D} + v(1-R)\delta(\zeta)U(s) \\ -\tau x_2(\zeta, 0) \end{bmatrix}}_{Z(\zeta, s)} \\
 \Rightarrow \partial_\zeta \tilde{X}(\zeta, s) &= P(s) \tilde{X}(\zeta, s) + Z(\zeta, s)
 \end{aligned} \tag{3.9}$$

with solution given by (3.10).

$$\tilde{X}(\zeta, s) = \underbrace{e^{P(s)\zeta}}_{T(\zeta, s)} \tilde{X}(0, s) + \int_0^\zeta \underbrace{e^{P(s)(\zeta-\eta)}}_{F(\zeta, \eta)} Z(\eta, s) d\eta \tag{3.10}$$

Since the boundary conditions are not homogeneous, $\tilde{X}(0, s)$ needs to be obtained by solving the system of algebraic equations given in (3.11); which is the result of applying Danckwerts boundary conditions to the Laplace transformed system of PDEs at $\zeta = 1$.

$$\begin{aligned}
 & \overbrace{\begin{bmatrix} -v & D & Rv \\ T_{11}(1, s) & T_{12}(1, s) & -T_{33}(1, s) \\ T_{21}(1, s) & T_{22}(1, s) & 0 \end{bmatrix}}^{M^{-1}(s)} \tilde{X}(0, s) = \\
 & \underbrace{\int_0^1 \begin{bmatrix} 0 \\ F_{33}(1, \eta)Z_3(\eta, s) - F_{12}(1, \eta)Z_2(\eta, s) \\ -F_{22}(1, \eta)Z_2(\eta, s) \end{bmatrix} d\eta}_{b(s)} \\
 \Rightarrow \tilde{X}(0, s) &= M(s)b(s)
 \end{aligned} \tag{3.11}$$

Having access to $\tilde{X}(0, s)$, the solution for $\underline{X}(\zeta, s)$ can be explicitly derived. The resolvent operator for zero-input and zero-state cases are therefore obtained in a closed form as shown in (3.12) and (3.13), respectively.

$$\begin{aligned}
 U(s) = 0 \Rightarrow \mathfrak{R}(s, \mathfrak{A})\underline{\cdot} &= \begin{bmatrix} \mathfrak{R}_{11} & \mathfrak{R}_{12} \\ \mathfrak{R}_{21} & \mathfrak{R}_{22} \end{bmatrix} \begin{bmatrix} (\cdot)_1 \\ (\cdot)_2 \end{bmatrix} \Rightarrow \\
 \mathfrak{R}_{11} &= \sum_{j=1}^2 \frac{T_{1j}(\zeta)}{D} \int_0^1 [M_{j2}F_{12}(1, \eta) + M_{j3}F_{22}(1, \eta)] (\cdot)_1 d\eta \\
 &\quad - \frac{1}{D} \int_0^\zeta F_{12}(\zeta, \eta) (\cdot)_1 d\eta \\
 \mathfrak{R}_{12} &= \sum_{j=1}^2 -\tau T_{1j}(\zeta) \int_0^1 M_{j2}F_{33}(1, \eta) (\cdot)_2 d\eta \\
 \mathfrak{R}_{21} &= \frac{T_{33}(\zeta)}{D} \int_0^1 [M_{32}F_{12}(1, \eta) + M_{33}F_{22}(1, \eta)] (\cdot)_1 d\eta \\
 \mathfrak{R}_{22} &= -\tau T_{33}(\zeta) \int_0^1 M_{32}F_{33}(1, \eta) (\cdot)_2 d\eta \\
 &\quad - \tau \int_0^\zeta F_{33}(\zeta, \eta) (\cdot)_2 d\eta
 \end{aligned} \tag{3.12}$$

$$\begin{aligned}
 \underline{x}(\zeta, 0) = 0 \Rightarrow \mathfrak{R}(s, \mathfrak{A})\mathfrak{B}(\cdot) &= \begin{bmatrix} \mathfrak{R}_1 \mathfrak{B} \\ \mathfrak{R}_2 \mathfrak{B} \end{bmatrix} (\cdot) \Rightarrow \\
 \mathfrak{R}_1 \mathfrak{B} &= -v(1-R) \left[\sum_{j=1}^2 T_{1j}(\zeta) (M_{j2}T_{12}(1) + M_{j3}T_{22}(1)) \right. \\
 &\quad \left. - T_{12}(\zeta) \right] (\cdot) \tag{3.13}
 \end{aligned}$$

$$\mathfrak{R}_2 \mathfrak{B} = -v(1-R) [T_{33}(\zeta)(M_{32}T_{12}(1) + M_{33}T_{22}(1))] (\cdot)$$

Since the system generator \mathfrak{A} is not self-adjoint, the resolvent operator for the adjoint system shall also be obtained. This is done in a similar manner as the original system, resulting in a closed-form expression for the adjoint resolvent operator $\mathfrak{R}^*(s, \mathfrak{A}^*)$. To avoid redundancy, the derivation of the resolvent operator for the adjoint system is not included in this manuscript.

3.2.4 Cayley–Tustin Time Discretization

To implement the system on digital controllers, it is necessary to transition to a discrete-time framework while preserving critical properties such as stability and controllability. The Cayley–Tustin time-discretization method achieves this by mapping the continuous-time system to the discrete domain [39, 40]. This Crank–Nicolson type of discretization is also known as the lowest order symplectic integrator in Gauss quadrature-based Runge–Kutta methods [41]. Considering Δt as the sampling time, and assuming a piecewise constant input within time intervals (zero-order hold), the discrete-time representation $\underline{x}(\zeta, k) = \mathfrak{A}_d \underline{x}(\zeta, k-1) + \mathfrak{B}_d u(k)$ is obtained, with discrete-time operators \mathfrak{A}_d , \mathfrak{B}_d , \mathfrak{C}_d , and \mathfrak{D}_d defined in (3.14), where $\alpha = 2/\Delta t$.

$$\begin{bmatrix} \mathfrak{A}_d & \mathfrak{B}_d \\ \mathfrak{C}_d & \mathfrak{D}_d \end{bmatrix} = \begin{bmatrix} -I + 2\alpha \mathfrak{R}(\alpha, \mathfrak{A}) & \sqrt{2\alpha} \mathfrak{R}(\alpha, \mathfrak{A}) \mathfrak{B} \\ \sqrt{2\alpha} \mathfrak{C} \mathfrak{R}(\alpha, \mathfrak{A}) & \mathfrak{C} \mathfrak{R}(\alpha, \mathfrak{A}) \mathfrak{B} \end{bmatrix} \quad (3.14)$$

As required for systems with nonself-adjoint generators, the adjoint discrete-time operators \mathfrak{A}_d^* and \mathfrak{B}_d^* are also obtained in a similar manner, as shown in (3.15).

$$\begin{bmatrix} \mathfrak{A}_d^* & \mathfrak{B}_d^* \end{bmatrix} = \begin{bmatrix} -I + 2\alpha \mathfrak{R}^*(\alpha, \mathfrak{A}^*) & \sqrt{2\alpha} \mathfrak{B}^* \mathfrak{R}^*(\alpha, \mathfrak{A}^*) \end{bmatrix} \quad (3.15)$$

3.3 Estimation and Control

3.3.1 Model predictive control design, full-state availability

The proposed full-state feedback model predictive control strategy, as shown in Fig. 3.3, is developed in this section with the goal of stabilizing the given

unstable infinite-dimensional system within an optimal framework while satisfying input constraints. An infinite-time open-loop objective function sets the foundation of the controller design in the discrete-time setting at each sampling instant k , which consists of a weighted sum of state deviations and actuation costs for all future time instances, subject to the system dynamics and input constraints, as shown in (3.16).

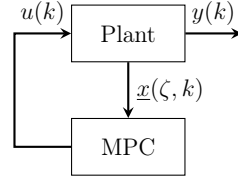


Figure 3.3: Proposed full-state feedback model predictive control system.

$$\begin{aligned}
 \min_U & \sum_{l=0}^{\infty} \langle \underline{x}(\zeta, k+l|k), \mathfrak{Q} \underline{x}(\zeta, k+l|k) \rangle \\
 & + \langle u(k+l+1|k), \mathfrak{F} u(k+l+1|k) \rangle
 \end{aligned} \tag{3.16}$$

$$\text{s.t. } \underline{x}(\zeta, k+l|k) = \mathfrak{A}_d \underline{x}(\zeta, k+l-1|k) + \mathfrak{B}_d u(k+l|k)$$

$$u^{min} \leq u(k+l|k) \leq u^{max}$$

where \mathfrak{Q} and \mathfrak{F} are positive definite operators of appropriate dimensions, responsible for penalizing state deviations and actuation costs, respectively. The notation $(k+l|k)$ indicates the future time states or input instance $k+l$ obtained at time k . The infinite-time optimization problem may be reduced to a finite-time setup by assigning zero-input beyond a certain control horizon N , resulting in the optimization problem in (3.17).

$$\begin{aligned}
 \min_U \quad & \sum_{l=0}^{N-1} \langle \underline{x}(\zeta, k+l|k), \mathfrak{Q}\underline{x}(\zeta, k+l|k) \rangle \\
 & + \langle u(k+l+1|k), \mathfrak{F}u(k+l+1|k) \rangle \\
 & + \langle \underline{x}(\zeta, k+N|k), \mathfrak{P}\underline{x}(\zeta, k+N|k) \rangle
 \end{aligned} \tag{3.17}$$

$$\text{s.t. } \underline{x}(\zeta, k+l|k) = \mathfrak{A}_d \underline{x}(\zeta, k+l-1|k) + \mathfrak{B}_d u(k+l|k)$$

$$u^{min} \leq u(k+l|k) \leq u^{max}$$

$$\langle \underline{x}(\zeta, k+N|k), \underline{\phi}_u(\zeta) \rangle = 0$$

Obtained as the solution to the discrete-time Lyapunov equation, \mathfrak{P} is the terminal cost operator as shown in (3.18); which can be proven to be positive definite only if the terminal state $\underline{x}(\zeta, k+N|k)$ is in a stable subspace. Therefore, an equality constraint is introduced to guarantee that the resulting quadratic optimization problem is convex. The terminal constraint is enforced by setting the projection of the terminal state onto the unstable subspace of the system to zero [15, 17, 40]. Here, $\underline{\phi}_u(\zeta)$ is the set of unstable eigenfunctions of the system, for all eigenvalues where $\text{Re}(\lambda_u) \geq 0$.

$$\mathfrak{P}(\cdot) = \sum_{m=0}^{\infty} \sum_{n=0}^{\infty} -\frac{\langle \underline{\phi}_m, \mathfrak{Q}\underline{\psi}_n \rangle}{\lambda_m + \bar{\lambda}_n} \langle (\cdot), \underline{\psi}_n \rangle \phi_m \tag{3.18}$$

One may further process the optimization problem in (3.17) to obtain a standard format for quadratic programming (QP) solvers by substituting the future states in terms of the current state and the sequence of future inputs using system dynamics expression. The resulting QP problem is given in (4.46). The optimal input sequence U is then obtained by solving the QP problem at each sampling instant k . To implement a receding horizon control

strategy, only the first input of the optimal sequence $u(k+1|k)$ is applied to the system, and the optimization problem is solved again at the next sampling instant $k+1$.

$$\min_U J = U^T \langle I, H \rangle U + 2U^T \langle I, P\underline{x}(\zeta, k|k) \rangle$$

$$\text{s.t. } U^{min} \leq U \leq U^{max}$$

$$T_u \underline{x}(\zeta, k|k) + S_u U = 0$$

with $H =$

$$\begin{aligned} & \left[\begin{array}{cccc} \mathfrak{B}_d^* \mathfrak{P} \mathfrak{B}_d + \mathfrak{F} & \mathfrak{B}_d^* \mathfrak{A}_d^* \mathfrak{P} \mathfrak{B}_d & \cdots & \mathfrak{B}_d^* \mathfrak{A}_d^{*N-1} \mathfrak{P} \mathfrak{B}_d \\ \mathfrak{B}_d^* \mathfrak{P} \mathfrak{A}_d \mathfrak{B}_d & \mathfrak{B}_d^* \mathfrak{P} \mathfrak{B}_d + \mathfrak{F} & \cdots & \mathfrak{B}_d^* \mathfrak{A}_d^{*N-2} \mathfrak{P} \mathfrak{B}_d \\ \vdots & \vdots & \ddots & \vdots \\ \mathfrak{B}_d^* \mathfrak{P} \mathfrak{A}_d^{N-1} \mathfrak{B}_d & \mathfrak{B}_d^* \mathfrak{P} \mathfrak{A}_d^{N-2} \mathfrak{B}_d & \cdots & \mathfrak{B}_d^* \mathfrak{P} \mathfrak{B}_d + \mathfrak{F} \end{array} \right] \\ & P = \left[\mathfrak{B}_d^* \mathfrak{P} \mathfrak{A}_d \quad \mathfrak{B}_d^* \mathfrak{P} \mathfrak{A}_d^2 \quad \cdots \quad \mathfrak{B}_d^* \mathfrak{P} \mathfrak{A}_d^N \right]^T \\ & T_u(\cdot) = \left[\langle \mathfrak{A}_d^N(\cdot), \underline{\phi}_u \rangle \right] \\ & S_u = \left[\langle \mathfrak{A}_d^{N-1} \mathfrak{B}_d, \underline{\phi}_u \rangle \quad \langle \mathfrak{A}_d^{N-2} \mathfrak{B}_d, \underline{\phi}_u \rangle \quad \cdots \quad \langle \mathfrak{B}_d, \underline{\phi}_u \rangle \right] \\ & U = \left[u(k+1|k) \quad u(k+2|k) \quad \cdots \quad u(k+N|k) \right]^T \end{aligned} \tag{3.19}$$

3.3.2 Continuous-Time Observer Design

For the purpose of state reconstruction of a diffusion-convection-reaction system, where the feedforward term \mathfrak{D} is generally absent, the continuous-time observer dynamics are given by (??), where $\hat{x}(\zeta, t)$ is the reconstructed state of the original system and \mathfrak{L}_c is the continuous-time observer gain. By subtracting the observer dynamics from the original system dynamics, the error dynamics $e(\zeta, t)$ are obtained as shown in (3.20).

$$\dot{e}(\zeta, t) = (\mathfrak{A} - \mathfrak{L}_c \mathfrak{C}) e(\zeta, t) \equiv \mathfrak{A}_o e(\zeta, t) \tag{3.20}$$

The goal is to design the observer gain \mathfrak{L}_c such that the error dynamics are exponentially stable, i.e. $\max\{\text{Re}(\lambda_o)\} < 0$ where $\{\lambda_o\}$ is the set of eigenvalues of the error dynamics operator \mathfrak{A}_o . Three different forms of the observer gain are considered as spatial functions $\mathfrak{L}_c = f(\zeta, l_{obs})$ with the effect of the scalar coefficient l_{obs} on $\max\{\text{Re}(\lambda_o)\}$ shown in Fig. 3.4.

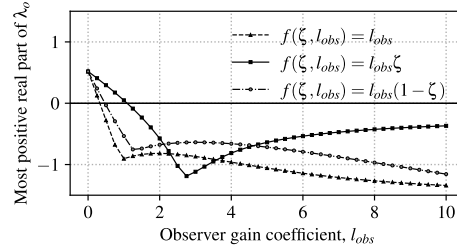


Figure 3.4: The effect of various observer gains $\mathfrak{L}_c = f(\zeta, l_{obs})$ on the eigenvalues of state reconstruction error dynamics λ_o .

3.3.3 Discrete-Time Observer Design

Once an appropriate continuous-time observer gain is determined, the discrete-time observer gain \mathfrak{L}_d may be obtained using the same Cayley-Tustin time discretization approach, as shown in (3.21).

$$\begin{aligned}\hat{x}(\zeta, k) &= \mathfrak{A}_d \hat{x}(\zeta, k-1) + \mathfrak{B}_d u(k) + \mathfrak{L}_d [y(k) - \hat{y}(k)] \\ \hat{y}(k) &= \mathfrak{C}_{d,o} \hat{x}(\zeta, k-1) + \mathfrak{D}_{d,o} u(k) + \mathfrak{M}_{d,o} y(k)\end{aligned}\tag{3.21}$$

with \mathfrak{A}_d and \mathfrak{B}_d defined in (3.14), and $\mathfrak{C}_{d,o}$, $\mathfrak{D}_{d,o}$, $\mathfrak{M}_{d,o}$, and \mathfrak{L}_d are given in (3.22).

$$\begin{aligned}\mathfrak{C}_{d,o}(\cdot) &= \sqrt{2\alpha} [I + \mathfrak{C}(\alpha I - \mathfrak{A}) \mathfrak{L}_c]^{-1} \mathfrak{CR}(\alpha, \mathfrak{A})(\cdot) \\ \mathfrak{D}_{d,o} &= [I + \mathfrak{C}(\alpha I - \mathfrak{A}) \mathfrak{L}_c]^{-1} \mathfrak{CR}(\alpha, \mathfrak{A}) \mathfrak{B} \\ \mathfrak{M}_{d,o} &= [I + \mathfrak{CR}(\alpha, \mathfrak{A}) \mathfrak{L}_c]^{-1} \mathfrak{CR}(\alpha, \mathfrak{A}) \mathfrak{L}_c \\ \mathfrak{L}_d &= \sqrt{2\alpha} \mathfrak{R}(\alpha, \mathfrak{A}) \mathfrak{L}_c\end{aligned}\tag{3.22}$$

It can be shown that using this approach, the discrete-time error dynamics will be stable if the continuous-time observer gain \mathfrak{L}_c is chosen such that \mathfrak{A}_o is

stable. It is also worth noting that the proposed methodology skips the need for model reduction associated with the discrete-time Luenberger observer, with no spatial approximation required as well [Ali2015Ali2015Review, 15, 33–35].

3.3.4 Model predictive control design, output feedback implementation

To enable real-time implementation under limited state access, the discrete-time model predictive controller is now augmented with the obtained discrete-time Luenberger observer. The reconstructed state $\hat{x}(\zeta, k)$ is substituted for the full state in the MPC formulation, yielding an observer-based output-feedback controller, as illustrated in Fig. 3.5.

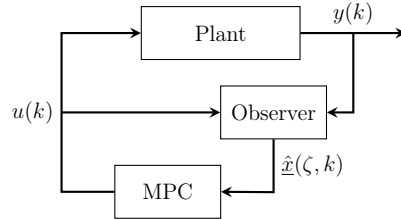


Figure 3.5: Block diagram representation of the observer-based MPC.

The cost function and terminal condition remain unchanged, but the predicted state trajectory is now driven by the estimated state:

$$\begin{aligned}
 \min_{\underline{U}} \quad & \sum_{l=0}^{N-1} \langle \hat{\underline{x}}(\zeta, k+l|k), \mathfrak{Q}\hat{\underline{x}}(\zeta, k+l|k) \rangle \\
 & + \langle u(k+l+1|k), \mathfrak{F}u(k+l+1|k) \rangle \\
 & + \langle \hat{\underline{x}}(\zeta, k+N|k), \mathfrak{P}\hat{\underline{x}}(\zeta, k+N|k) \rangle
 \end{aligned} \tag{3.23}$$

$$\text{s.t. } \hat{\underline{x}}(\zeta, k+l|k) = \mathfrak{A}_d \hat{\underline{x}}(\zeta, k+l-1|k) + \mathfrak{B}_d u(k+l|k)$$

$$u^{min} \leq u(k+l|k) \leq u^{max}$$

$$\langle \hat{\underline{x}}(\zeta, k+N|k), \underline{\phi}_u(\zeta) \rangle = 0$$

The observer provides $\hat{\underline{x}}(\zeta, k)$ at each time step by processing most recent output and control input. This reconstructed state initializes the prediction horizon and closes the loop in the absence of full-state access. The resulting control law inherits all properties of the full-state MPC while enabling output feedback implementation. The QP formulation follows analogously by substituting \underline{x} with $\hat{\underline{x}}$ in (4.46), and is detailed in (3.24).

$$\min_U J = U^\top \langle I, H \rangle U + 2U^\top \langle I, P \underline{x}(\zeta, k|k) \rangle$$

$$\text{s.t. } U^{min} \leq U \leq U^{max}$$

$$T_u \underline{x}(\zeta, k|k) + S_u U = 0$$

with $H =$

$$\begin{aligned} & \left[\begin{array}{cccc} \mathfrak{B}_d^* \mathfrak{P} \mathfrak{B}_d + \mathfrak{F} & \mathfrak{B}_d^* \mathfrak{A}_d^* \mathfrak{P} \mathfrak{B}_d & \dots & \mathfrak{B}_d^* \mathfrak{A}_d^{*N-1} \mathfrak{P} \mathfrak{B}_d \\ \mathfrak{B}_d^* \mathfrak{P} \mathfrak{A}_d \mathfrak{B}_d & \mathfrak{B}_d^* \mathfrak{P} \mathfrak{B}_d + \mathfrak{F} & \dots & \mathfrak{B}_d^* \mathfrak{A}_d^{*N-2} \mathfrak{P} \mathfrak{B}_d \\ \vdots & \vdots & \ddots & \vdots \\ \mathfrak{B}_d^* \mathfrak{P} \mathfrak{A}_d^{N-1} \mathfrak{B}_d & \mathfrak{B}_d^* \mathfrak{P} \mathfrak{A}_d^{N-2} \mathfrak{B}_d & \dots & \mathfrak{B}_d^* \mathfrak{P} \mathfrak{B}_d + \mathfrak{F} \end{array} \right] \\ & P = \left[\begin{array}{cccc} \mathfrak{B}_d^* \mathfrak{P} \mathfrak{A}_d & \mathfrak{B}_d^* \mathfrak{P} \mathfrak{A}_d^2 & \dots & \mathfrak{B}_d^* \mathfrak{P} \mathfrak{A}_d^N \end{array} \right]^\top \\ & T_u(\cdot) = \left[\begin{array}{c} \langle \mathfrak{A}_d^N(\cdot), \underline{\phi}_u \rangle \end{array} \right] \\ & S_u = \left[\begin{array}{cccc} \langle \mathfrak{A}_d^{N-1} \mathfrak{B}_d, \underline{\phi}_u \rangle & \langle \mathfrak{A}_d^{N-2} \mathfrak{B}_d, \underline{\phi}_u \rangle & \dots & \langle \mathfrak{B}_d, \underline{\phi}_u \rangle \end{array} \right] \\ & U = \left[\begin{array}{cccc} u(k+1|k) & u(k+2|k) & \dots & u(k+N|k) \end{array} \right]^\top \end{aligned} \tag{3.24}$$

3.4 Simulation Results

This section presents numerical simulations of the closed-loop system under both full-state feedback and output-feedback model predictive control schemes. The reactor model and all physical parameters follow those in Table 4.1, and the same control settings are used throughout: initial condition $c(\zeta, 0) = \sin^2(\pi\zeta)$, empty recycle stream, state and input penalty weights $Q = 0.04I$, $F = 27$, sampling time $\Delta t = 20$ s, control horizon $N = 9$, and input constraints $0 \leq u(t) \leq 0.15$. The control horizon corresponds to 180 s, which exceeds the recycle delay of 80 s. The subsections below compare the controller performance under full-state and output-feedback implementations.

3.4.1 Full-State Feedback MPC Performance

As the eigenvalue distribution obtained in Fig. 3.2 suggests, the open-loop system is unstable due to the presence of an eigenvalue with positive real part. The zero-input response of the system is shown in Fig. 3.6 where the initial condition for the reactor is set to $c(\zeta, 0) = \sin^2(\pi\zeta)$. The recycle stream is assumed to be empty at the beginning of the simulation.

An infinite-dimensional MPC is designed and applied to the unstable system. The closed-loop response of the system is shown in Fig. 3.7 and the control input as well as the measured output is shown in Fig. 3.8. It may be confirmed that the MPC successfully stabilizes the unstable system while satisfying the input constraints.

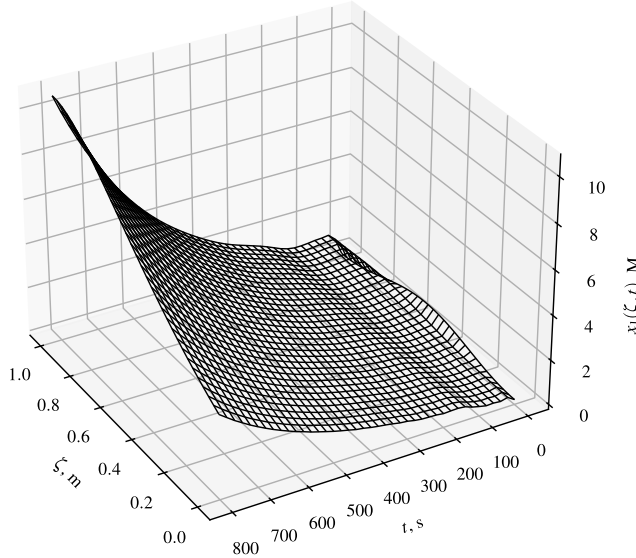


Figure 3.6: Open-loop concentration profile along the reactor.

One interesting aspect of considering a recycle stream is the oscillatory behavior of the system dynamics. While axial dispersion reactors show no

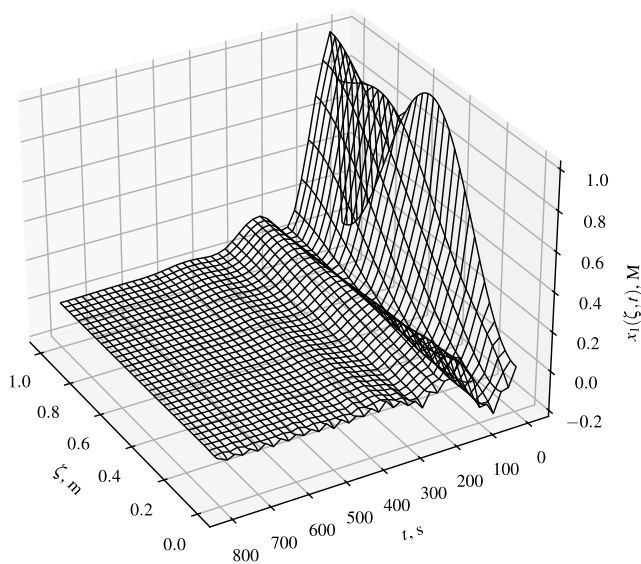


Figure 3.7: Stabilized reactor concentration profile under the proposed full-state MPC.

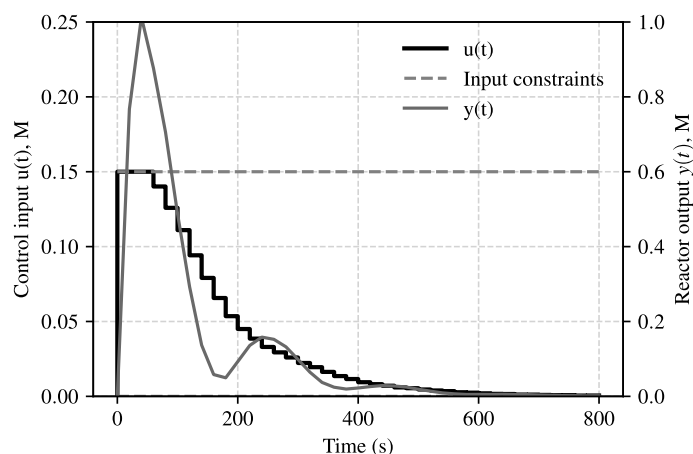


Figure 3.8: Input profile and reactor output under full-state MPC, subject to constraints.

oscillation in the absence of recycle, the nature of recycle streams can introduce such behavior. The choice of control horizon is another key factor. A short control horizon relative to the residence time of the recycle stream can lead to oscillatory input profiles due to the presence of delayed recycle stream. In this example, the control horizon, i.e., 180 s, is set to be considerably longer than the recycle delay, which is 80 s; resulting in a non-oscillatory input profile.

3.4.2 Observer-Based Output Feedback MPC

To evaluate the performance of the output-feedback controller, numerical simulations are conducted under the same conditions as in the full-state feedback case. This subsection presents the closed-loop behavior of the system when using the discrete-time Luenberger observer to reconstruct the states based on output measurements.

The eigenvalue distribution shown previously in Fig. 3.2 confirms that the open-loop system is unstable due to the presence of an eigenvalue with a positive real part. The observer gain is selected as a constant function $L_c = 1$, and the estimated state is initialized to zero across the domain.

The closed-loop reactor response under the proposed output-feedback controller is shown in Fig. 3.9, and the corresponding control input and measured output are shown in Fig. 3.10. The evolution of the state estimation error is depicted in Fig. 3.11. These results confirm that the observer-based MPC successfully stabilizes the unstable system while adhering to input constraints, using only output measurements.

An important aspect of the proposed observer-based controller is the relative speed of the observer error convergence compared to the system dynamics. As seen in Fig. 3.11, the observer error dynamics decay significantly faster than

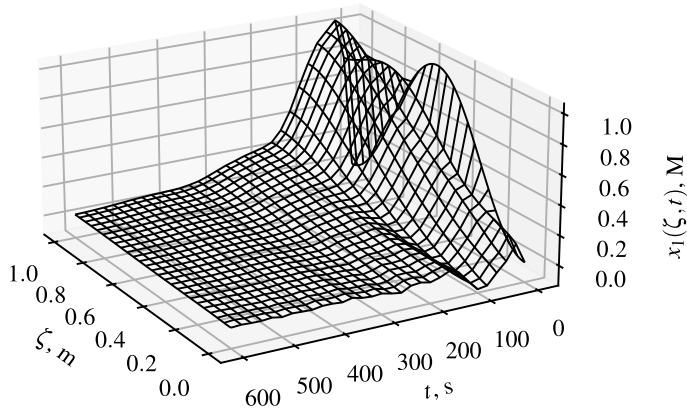


Figure 3.9: Stabilized reactor concentration profile under the proposed observer-based MPC.

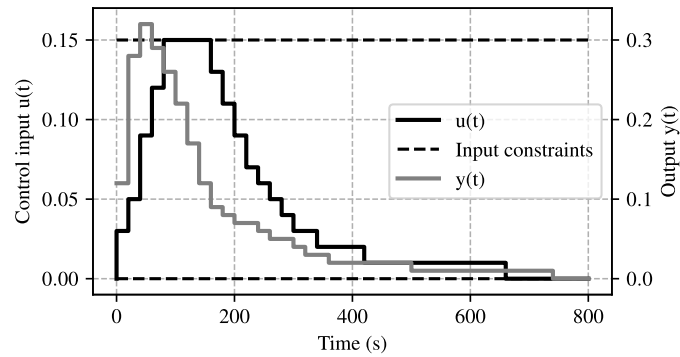


Figure 3.10: Input profile and reactor output under observer-based MPC.

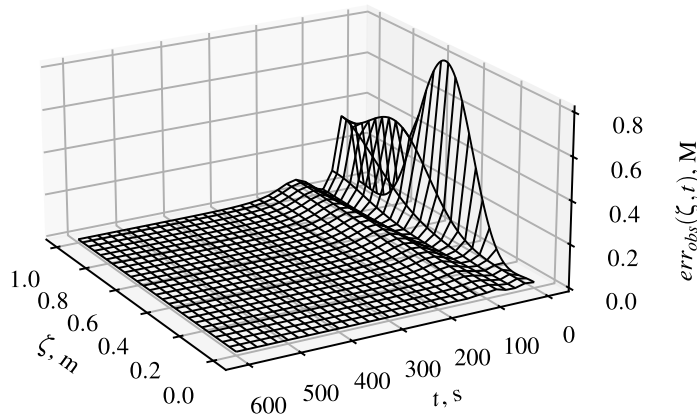


Figure 3.11: State reconstruction error profile along the reactor.

the closed-loop reactor response, helping prevent oscillations that may arise from poor state reconstruction.

Oscillatory behavior induced by the recycle stream is discussed at the end of the previous subsection. Since all simulation settings are shared, the same rationale applies here; the long control horizon relative to the recycle delay ensures a smooth input profile and stable closed-loop response.

3.5 Conclusion

In this work, model predictive control of an axial dispersion tubular reactor equipped with recycle is addressed, while considering the delay imposed by the recycle stream. This setup is common in industry but has received limited attention in the chemical engineering distributed parameter systems literature. The diffusion-convection-reaction dynamics of the reactor is modeled by a second-order parabolic PDE, while a notion of state delay is introduced to account for the delay imposed by the recycle stream. The state delay is addressed as a separate transport PDE, resulting in a boundary-controlled system governed by a coupled set of parabolic and hyperbolic PDEs under Danckwerts boundary conditions. Utilizing a late-lumping approach, the resolvent operator is obtained in a closed form in order to preserve the infinite-dimensional nature of the system without requiring spatial discretization. To implement MPC as a digital controller, the Cayley–Tustin transformation is used. This Crank–Nicolson type of discretization is chosen as it maintains important properties of the system such as stability and controllability when mapping the continuous-time system to a discrete-time one. Numerical simulations demonstrate the effectiveness of the proposed controller in stabilizing

an unstable system while satisfying input constraints under full-state feedback. Recognizing, however, that full-state information is often unavailable in practical implementations of distributed parameter systems, this work is further extended by designing and integrating a discrete-time Luenberger observer to reconstruct the state from output measurements alone, without any spatial approximation. A family of observer gains is examined, and spectral analysis is performed to select gains that ensure the state reconstruction error converges faster than the closed-loop system dynamics. This guarantees accurate state estimates during transients and prevents performance degradation due to estimation delay. The proposed approach can be further extended to incorporate the effects of temperature as well as disturbance rejection or set-point tracking in future work.

References

- [1] B. Moadeli, G. O. Cassol, and S. Dubljevic, “Optimal control of axial dispersion tubular reactors with recycle: Addressing state-delay through transport PDEs,” *The Canadian Journal of Chemical Engineering*, vol. 103, no. 8, pp. 3751–3766, 2025, ISSN: 0008-4034. DOI: [10.1002/cjce.25629](https://doi.org/10.1002/cjce.25629).
- [2] W. H. Ray, *Advanced process control*. McGraw-Hill: New York, NY, USA, 1981.
- [3] E. Davison, “The robust control of a servomechanism problem for linear time-invariant multivariable systems,” *IEEE transactions on Automatic Control*, vol. 21, no. 1, pp. 25–34, 1976, ISSN: 0018-9286. DOI: [10.1109/tac.1976.1101137](https://doi.org/10.1109/tac.1976.1101137).
- [5] A. A. Moghadam, I. Aksikas, S. Dubljevic, and J. F. Forbes, “Infinite-dimensional LQ optimal control of a dimethyl ether (DME) catalytic distillation column,” *Journal of Process Control*, vol. 22, no. 9, pp. 1655–1669, 2012, ISSN: 0959-1524. DOI: [10.1016/j.jprocont.2012.06.018](https://doi.org/10.1016/j.jprocont.2012.06.018).
- [6] P. D. Christofides, “Robust control of parabolic PDE systems,” *Chemical Engineering Science*, vol. 53, no. 16, pp. 2949–2965, 1998, ISSN: 2324-9749. DOI: [10.1007/978-1-4612-0185-4_5](https://doi.org/10.1007/978-1-4612-0185-4_5).

- [7] M. Krstic and A. Smyshlyaev, “Backstepping boundary control for first-order hyperbolic PDEs and application to systems with actuator and sensor delays,” *Systems & Control Letters*, vol. 57, no. 9, pp. 750–758, 2008, ISSN: 0167-6911. DOI: [10.1016/j.sysconle.2008.02.005](https://doi.org/10.1016/j.sysconle.2008.02.005).
- [8] X. Xu and S. Dubljevic, “The state feedback servo-regulator for counter-current heat-exchanger system modelled by system of hyperbolic PDEs,” *European Journal of Control*, vol. 29, pp. 51–61, 2016, ISSN: 0947-3580. DOI: [10.1016/j.ejcon.2016.02.002](https://doi.org/10.1016/j.ejcon.2016.02.002).
- [14] G. O. Cassol, D. Ni, and S. Dubljevic, “Heat exchanger system boundary regulation,” *AICHE Journal*, vol. 65, no. 8, e16623, 2019, ISSN: 0001-1541. DOI: [10.1002/aic.16623](https://doi.org/10.1002/aic.16623).
- [15] S. Khatibi, G. O. Cassol, and S. Dubljevic, “Model predictive control of a non-isothermal axial dispersion tubular reactor with recycle,” *Computers & Chemical Engineering*, vol. 145, p. 107159, 2021, ISSN: 0098-1354. DOI: [10.1016/j.compchemeng.2020.107159](https://doi.org/10.1016/j.compchemeng.2020.107159).
- [17] R. Curtain and H. Zwart. Springer Nature, 2020. DOI: [10.1007/978-1-0716-0590-5_1](https://doi.org/10.1007/978-1-0716-0590-5_1).
- [19] L. Mohammadi, I. Aksikas, S. Dubljevic, and J. F. Forbes, “LQ-boundary control of a diffusion-convection-reaction system,” *International Journal of Control*, vol. 85, no. 2, pp. 171–181, 2012, ISSN: 0959-1524. DOI: [10.1080/00207179.2011.642308](https://doi.org/10.1080/00207179.2011.642308).
- [21] M. Krstić (Systems & control). Birkhäuser, 2009.
- [22] G. O. Cassol and S. Dubljevic, “Discrete output regulator design for a mono-tubular reactor with recycle,” in *2019 American Control Conference (ACC)*, IEEE, 2019, pp. 1262–1267. DOI: [10.23919/acc.2019.8815250](https://doi.org/10.23919/acc.2019.8815250).
- [23] J. Qi, S. Dubljevic, and W. Kong, “Output feedback compensation to state and measurement delays for a first-order hyperbolic PIDE with recycle,” *Automatica*, vol. 128, p. 109565, 2021, ISSN: 0005-1098. DOI: [10.1016/j.automatica.2021.109565](https://doi.org/10.1016/j.automatica.2021.109565).
- [24] O. Levenspiel, *Chemical reaction engineering*. John Wiley & Sons, 1998.
- [25] K. F. Jensen and W. H. Ray, “The bifurcation behavior of tubular reactors,” *Chemical Engineering Science*, vol. 37, no. 2, pp. 199–222, 1982, ISSN: 0009-2509. DOI: [10.1016/0009-2509\(82\)80155-3](https://doi.org/10.1016/0009-2509(82)80155-3).
- [26] P. V. Danckwerts, “Continuous flow systems: Distribution of residence times,” *Chemical Engineering Science*, vol. 2, no. 1, pp. 1–13, 1953, ISSN: 0009-2509. DOI: [10.1016/0009-2509\(53\)80001-1](https://doi.org/10.1016/0009-2509(53)80001-1).

- [27] J. M. Ali, N. H. Hoang, M. A. Hussain, and D. Dochain, “Review and classification of recent observers applied in chemical process systems,” *Computers & Chemical Engineering*, vol. 76, pp. 27–41, 2015, ISSN: 0098-1354. DOI: [10.1016/j.compchemeng.2015.01.019](https://doi.org/10.1016/j.compchemeng.2015.01.019).
- [31] B. Moadeli and S. Dubljevic, “Model predictive control of axial dispersion tubular reactors with recycle: Addressing state-delay through transport PDEs,” in *2025 American Control Conference (ACC)*, 2025.
- [32] B. Moadeli and S. Dubljevic, “Observer-based MPC design of an axial dispersion tubular reactor: Addressing recycle delays through transport PDEs,” in *2025 European Control Conference (ECC)*, 2025.
- [33] D. Dochain, “State observers for tubular reactors with unknown kinetics,” *Journal of process control*, vol. 10, no. 2-3, pp. 259–268, 2000, ISSN: 0959-1524. DOI: [10.1016/s0959-1524\(99\)00020-7](https://doi.org/10.1016/s0959-1524(99)00020-7).
- [34] D. Dochain, “State observation and adaptive linearizing control for distributed parameter (bio) chemical reactors,” *International Journal of Adaptive Control and Signal Processing*, vol. 15, no. 6, pp. 633–653, 2001, ISSN: 0890-6327. DOI: [10.1002/acs.691](https://doi.org/10.1002/acs.691).
- [35] A. A. Alonso, I. G. Kevrekidis, J. R. Banga, and C. E. Frouzakis, “Optimal sensor location and reduced order observer design for distributed process systems,” *Computers & chemical engineering*, vol. 28, no. 1-2, pp. 27–35, 2004, ISSN: 0098-1354. DOI: [10.1016/s0098-1354\(03\)00175-3](https://doi.org/10.1016/s0098-1354(03)00175-3).
- [36] P. D. Christofides and P. Daoutidis, “Feedback control of hyperbolic PDE systems,” *AIChE Journal*, vol. 42, no. 11, pp. 3063–3086, 1996, ISSN: 0001-1541. DOI: [10.1002/aic.690421108](https://doi.org/10.1002/aic.690421108).
- [37] S. Dubljevic and P. D. Christofides, “Predictive control of parabolic PDEs with boundary control actuation,” *Chemical Engineering Science*, vol. 61, no. 18, pp. 6239–6248, 2006, ISSN: 0009-2509. DOI: [10.1016/j.ces.2006.05.041](https://doi.org/10.1016/j.ces.2006.05.041).
- [38] S. Hiratsuka and A. Ichikawa, “Optimal control of systems with transportation lags,” *IEEE Transactions on Automatic Control*, vol. 14, no. 3, pp. 237–247, 1969, ISSN: 0018-9286. DOI: [10.1109/TAC.1969.1099175](https://doi.org/10.1109/TAC.1969.1099175).
- [39] V. Havu and J. Malinen, “The Cayley transform as a time discretization scheme,” *Numerical Functional Analysis and Optimization*, vol. 28, no. 7-8, pp. 825–851, 2007, ISSN: 0163-0563. DOI: [10.1080/01630560701493321](https://doi.org/10.1080/01630560701493321).
- [40] Q. Xu and S. Dubljevic, “Linear model predictive control for transport-reaction processes,” *AIChE Journal*, vol. 63, no. 7, pp. 2644–2659, 2017, ISSN: 0001-1541. DOI: [10.1002/aic.15592](https://doi.org/10.1002/aic.15592).

- [41] E. Hairer, M. Hochbruck, A. Iserles, and C. Lubich, “Geometric numerical integration,” *Oberwolfach Reports*, vol. 3, no. 1, pp. 805–882, 2006, ISSN: 1660-8933. DOI: [10.4171/owr/2011/16](https://doi.org/10.4171/owr/2011/16).

Chapter 4

NON-ISOTHERMAL SYSTEM: MOVING HORIZON ESTIMATION AND MODEL PREDICTIVE CONTROL¹

4.1 Introduction

Distributed parameter systems (DPS), typically modeled by partial differential equations (PDEs), arise naturally in chemical engineering applications such as catalytic reactors, heat exchangers, and fluidized beds, where mass and energy transport processes are distributed over space and time [2, 3, 17]. Among these, axial dispersion tubular reactors with recycle represent an important class of industrial systems, characterized by strong coupling between reaction, convection, diffusion, and recirculation dynamics [25, 27, 43–46]. These reactors are often modeled using second-order parabolic PDEs under Danckwerts boundary conditions to reflect realistic inlet and outlet transport assumptions [26]. The inclusion of a recycle stream—commonly used to enhance conver-

¹This chapter has been submitted for review as B. Moadeli and S. Dubljevic, “Advanced control of non-isothermal axial dispersion tubular reactors with recycle-induced state delay,” *The Canadian Journal of Chemical Engineering*, 2025.

sion or efficiency—adds complexity, including dynamic instability and multiple steady states, under certain operating regimes [47, 48].

While numerous studies have investigated control of non-isothermal tubular reactors, most have either neglected the effect of recycle or, as in the work of Khatibi *et al.*, assumed it to be instantaneous—effectively disregarding the finite residence time of the returning stream [15]. This assumption, although mathematically convenient, limits the realism and applicability of the resulting control strategies. In contrast, recent advances have explored modeling recycle delay as a transport phenomenon. Moadeli *et al.* introduced a delay-aware framework for tubular reactors by modeling the recycle loop as a first-order hyperbolic PDE [1], a formulation that embeds the delay directly into the infinite-dimensional system. This approach is consistent with a well-established tradition in PDE control [49–53], commonly referred to as the late-lumping paradigm, where spatial dynamics are preserved throughout control synthesis to avoid distortions from premature discretization.

Modeling recycle-induced delay as a transport PDE, rather than as a delay differential equation (DDE), unifies and preserves the spatial-temporal structure of the system and enables analysis within an infinite-dimensional control framework [21]. Although rare in chemical engineering applications, such representations have been explored in general DPS literature as alternatives to lumped-delay models, particularly in systems with internal transport structures, giving rise to state delays [14, 23]. In Moadeli *et al.*'s work, the recycle-induced state delay was treated as a convective domain coupled to a parabolic PDE, leading to a Riesz-spectral generator and allowing for optimal control synthesis using operator Riccati equations [1]. However, that work assumed an

isothermal reactor, relied on non-optimal state reconstruction via a simple Luenberger observer, and did not address energy balances, process/measurement noises, or input/state constraints.

The present study unifies two previously disjoint modeling approaches. Moadeli *et al.* [1] introduced a delay-aware framework for tubular reactors by modeling the recycle stream as a transport PDE, capturing recycle-induced state delay within an infinite-dimensional formulation, but limited the model to isothermal dynamics. In contrast, Khatibi *et al.* [15] addressed non-isothermal reactor behavior but assumed an instantaneous recycle stream, neglecting the delay mechanism altogether. The current study integrates these two formulations by combining the transport-PDE representation of recycle delay with the full mass-energy dynamics of a non-isothermal reactor, resulting in a coupled four-equation PDE model. To prepare this infinite-dimensional system for implementation of digital estimation and control schemes, time discretization is performed using the Cayley-Tustin transformation; i.e. a structure-preserving midpoint integration technique that maintains Hamiltonian structure and improves robustness against sampling distortion[39, 40].

From a control and estimation perspective, each prior effort addressed only part of the broader challenge. Moadeli *et al.* formulated both full-state and output-based regulators using infinite-dimensional LQR theory in continuous time [1], but did not consider constraints or digital implementation. Khatibi *et al.*, by contrast, developed a constrained model predictive controller (MPC) in discrete time for a non-isothermal reactor, but employed a simple Luenberger observer for state estimation and neglected the recycle delay [15]. Recent discrete-time implementations based on the delay-aware model [31,

[32] extended the formulation to output-feedback MPC under constraints, yet continued to rely on Luenberger observers and did not incorporate temperature dynamics. In the current study, the observer is replaced with a moving horizon estimator (MHE), enabling output-based optimal state reconstruction under constraints and integrating it with constrained MPC within the same infinite-dimensional framework, while taking measurement noises as well as plant-model mismatch into account. The MHE formulation is inspired by recent developments in infinite-dimensional estimation for PDE systems [10, 54], and is adapted here to address the dynamics of a non-isothermal reactor with recycle-induced state delay.

This work represents the first MHE-MPC architecture to jointly incorporate non-isothermal reaction-diffusion-convection dynamics, recycle-induced state-delays, constrained MPC, and output-based estimation via MHE, all within a late-lumped infinite-dimensional setting. The rest of the paper is organized as follows: Section 2 presents the modeling and system formulation. Section 3 outlines the operator-theoretic representation. Section 4 details Cayley-Tustin discretization. Sections 5 and 6 present the MPC and MHE formulations, respectively. Section 7 illustrates closed-loop performance under realistic constraints and measurement noise.

4.2 Model Representation

4.2.1 Non-linear System Model with State Delays

A non-isothermal axial dispersion tubular reactor subject to first-order exothermic reaction and partial recycle is considered. The process configuration is shown in Figure 4.1. The governing equations describe the evolution of reac-

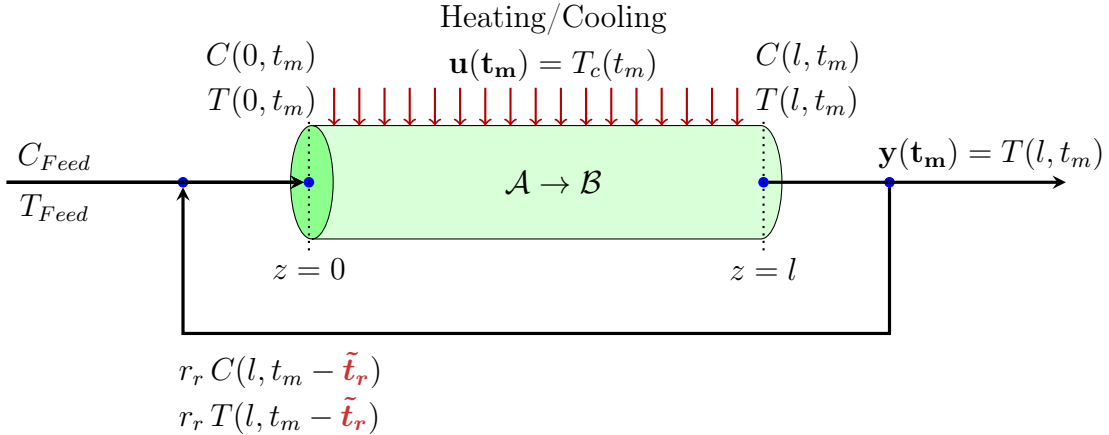


Figure 4.1: Non-isothermal axial dispersion tubular reactor with recycle stream.

tant concentration and temperature profiles along the reactor length, and are obtained by applying standard mass and energy balances over an infinitesimal axial segment [24], resulting in a coupled nonlinear convection–diffusion–reaction PDE system given in Equation (4.1). Here, $C(z, t_m)$ and $T(z, t_m)$ describe the concentration and temperature profiles along the reactor length $z \in [0, l]$ at time $t_m \in [0, \infty)$, respectively. All variables and parameters are defined in the nomenclature.

$$\left\{ \begin{array}{l} \partial_{t_m} C(z, t_m) = D \partial_{zz} C(z, t_m) - v \partial_z C(z, t_m) - k e^{\frac{-E}{RT(z, t_m)}} C(z, t_m) \\ \partial_{t_m} T(z, t_m) = \frac{\kappa}{\rho_f c_p} \partial_{zz} T(z, t_m) - v \partial_z T(z, t_m) - \frac{\Delta H}{\rho_f c_p} k e^{\frac{-E}{RT(z, t_m)}} C(z, t_m) \\ \quad + \frac{4h}{\rho_f c_p d_t} (T_c(t_m) - T(z, t_m)) \end{array} \right. \quad (4.1)$$

The boundary conditions adopt a Danckwerts-type formulation, which has become standard in the modeling of axial dispersion tubular reactors. Belong-

ing to the class of Robin boundaries, Danckwerts conditions preserve generality while remaining physically interpretable in the context of axial dispersion systems [26].

Except the delay-induced recycle, the present modeling assumptions leading to the governing equations and boundary structure follow Khatibi *et al.*'s contribution[15]. In this work, the effect of delay is incorporated into the same class of boundary conditions, giving rise to a recycle-induced delay term at the reactor inlet, as shown in Equation (4.2).

$$\begin{cases} \partial_z C(0, t_m) = \frac{v}{D} \left[C(0, t_m) - (1 - r_r)C_{Feed} - r_r C(l, t_m - \tilde{t}_r) \right] \\ \partial_z T(0, t_m) = \frac{\rho_f v c_p}{\kappa} \left[T(0, t_m) - (1 - r_r)T_{Feed} - r_r T(l, t_m - \tilde{t}_r) \right] \\ \partial_z C(l, t_m) = 0 \\ \partial_z T(l, t_m) = 0 \end{cases} \quad (4.2)$$

4.2.2 State Delays as Transport PDEs

As will be discussed in Section 4.3, the application of infinite-dimensional linear system theory relies on the existence of a strongly continuous semigroup generator acting on a Hilbert space. The delay term in Equation (4.2) introduces a dependence on past values of the system states—i.e., a state delay—which obstructs this formulation and prevents the system from being posed as a standard evolution problem [17]. To obtain a time-invariant representation suitable for operator-theoretic analysis, the delay terms are replaced by a set of first-order hyperbolic transport PDEs. This approach avoids direct use of delay differential equations by embedding the delay into the state space itself [21]. The resulting formulation follows the one originally developed for an isother-

mal recycle reactor configuration, and has since been reused in discrete-time controller and observer designs [1, 31, 32].

To eliminate the explicit delay terms from the reactor boundary conditions, two auxiliary states $C_r(z_r, t_m)$ and $T_r(z_r, t_m)$ are introduced to describe the convective transport through the recycle line. The state delay is thereby reformulated as a transport PDE evolving over the pseudo-spatial domain $z_r \in [0, l_r]$, governed by:

$$\begin{cases} \partial_{t_m} C_r(z_r, t_m) = -v_r \partial_{z_r} C_r(z_r, t_m) \\ \partial_{t_m} T_r(z_r, t_m) = -v_r \partial_{z_r} T_r(z_r, t_m) \end{cases} \quad (4.3)$$

with boundary conditions:

$$\begin{cases} C_r(l_r, t_m) = C(l, t_m) \\ T_r(l_r, t_m) = T(l, t_m) \end{cases} \quad (4.4)$$

Evaluating the transport states at the inlet, the delayed boundary terms in Equation (4.2) are equivalently expressed as:

$$\begin{cases} C_r(0, t_m) = C_r(l_r, t_m - \tilde{t}_r) = C(l, t_m - \tilde{t}_r) \\ T_r(0, t_m) = T_r(l_r, t_m - \tilde{t}_r) = T(l, t_m - \tilde{t}_r) \end{cases} \quad (4.5)$$

The substitution of Equations (4.3)-(4.5) into the original system in Equations (4.1) and (4.2) yields an equivalent formulation composed of four coupled nonlinear PDEs. This time-invariant representation, summarized in Equations (4.6) and (4.7), is a necessary step toward enabling the application of infinite-dimensional system theory via late-lumping, where the system must admit a well-posed Cauchy problem governed by a strongly continuous semi-group on a Hilbert space.

$$\left\{ \begin{array}{l} \partial_{t_m} C(z, t_m) = D \partial_{zz} C(z, t_m) - v \partial_z C(z, t_m) - k e^{\frac{-E}{RT(z, t_m)}} C(z, t_m) \\ \partial_{t_m} T(z, t_m) = \frac{\kappa}{\rho_f c_p} \partial_{zz} T(z, t_m) - v \partial_z T(z, t_m) - \frac{\Delta H}{\rho_f c_p} k e^{\frac{-E}{RT(z, t_m)}} C(z, t_m) \\ \quad + \frac{4h}{\rho_f c_p d_t} (T_c(t_m) - T(z, t_m)) \\ \partial_{t_m} C_r(z_r, t_m) = -v_r \partial_{z_r} C_r(z_r, t_m) \\ \partial_{t_m} T_r(z_r, t_m) = -v_r \partial_{z_r} T_r(z_r, t_m) \end{array} \right. \quad (4.6)$$

$$\left\{ \begin{array}{l} \partial_z C(0, t_m) = \frac{v}{D} [C(0, t_m) - (1 - r_r) C_{\text{Feed}} - r_r C_r(0, t_m)], \quad \partial_z C(l, t_m) = 0 \\ \partial_z T(0, t_m) = \frac{\rho_f v c_p}{\kappa} [T(0, t_m) - (1 - r_r) T_{\text{Feed}} - r_r T_r(0, t_m)], \quad \partial_z T(l, t_m) = 0 \\ C_r(l_r, t_m) = C(l, t_m) \\ T_r(l_r, t_m) = T(l, t_m) \end{array} \right. \quad (4.7)$$

For notational simplicity and to reveal the structure of the system more clearly, a dimensionless formulation is adopted using reference inlet values and characteristic length and time scales. The transformation is defined in Equation (4.8), leading to the introduction of normalized spatial and temporal coordinates, as well as dimensionless state variables.

$$\begin{cases} \zeta = \frac{z}{l} = \frac{z_r}{l_r}, & t = \frac{t_m}{\tilde{t}}, & \tau = \frac{\tilde{t}_r}{\tilde{t}}, \\ m_1(\zeta, t) = \frac{C_{\text{Feed}} - C(\zeta, t)}{C_{\text{Feed}}}, & m_2(\zeta, t) = \frac{T(\zeta, t) - T_{\text{Feed}}}{T_{\text{Feed}}}, \\ m_3(\zeta, t) = \frac{C_{\text{Feed}} - C_r(\zeta, t)}{C_{\text{Feed}}}, & m_4(\zeta, t) = \frac{T_r(\zeta, t) - T_{\text{Feed}}}{T_{\text{Feed}}}, \\ T_w(t) = \frac{T_c(t) - T_{\text{Feed}}}{T_{\text{Feed}}} \end{cases} \quad (4.8)$$

Substituting these variables into the nonlinear PDE system in Equations (4.6)-(4.7) yields the dimensionless representation of the system given in Equations (4.9) and (4.10).

$$\begin{cases} \partial_t m_1(\zeta, t) = \frac{1}{Pe_m} \partial_{\zeta\zeta} m_1(\zeta, t) - \partial_{\zeta} m_1(\zeta, t) + k_a (1 - m_1(\zeta, t)) e^{\frac{\eta m_2(\zeta, t)}{1+m_2(\zeta, t)}} \\ \partial_t m_2(\zeta, t) = \frac{1}{Pe_T} \partial_{\zeta\zeta} m_2(\zeta, t) - \partial_{\zeta} m_2(\zeta, t) + \alpha k_a (1 - m_1(\zeta, t)) e^{\frac{\eta m_2(\zeta, t)}{1+m_2(\zeta, t)}} \\ \quad + \sigma (T_w(t) - m_2(\zeta, t)) \\ \partial_t m_3(\zeta, t) = \frac{1}{\tau} \partial_{\zeta} m_3(\zeta, t) \\ \partial_t m_4(\zeta, t) = \frac{1}{\tau} \partial_{\zeta} m_4(\zeta, t) \end{cases} \quad (4.9)$$

$$\begin{cases} \partial_{\zeta} m_1(0, t) = Pe_m [m_1(0, t) - r_r m_3(0, t)], & \partial_{\zeta} m_1(l, t) = 0 \\ \partial_{\zeta} m_2(0, t) = Pe_T [m_2(0, t) - r_r m_4(0, t)], & \partial_{\zeta} m_2(l, t) = 0 \\ m_1(1, t) = m_3(1, t) \\ m_2(1, t) = m_4(1, t) \end{cases} \quad (4.10)$$

4.2.3 Steady-State Analysis

The steady-state configuration of the system is obtained by setting all time derivatives in Equation (4.6) to zero, yielding a system of four coupled nonlinear ODEs. The resulting boundary value problem is solved numerically using a collocation method with adaptive mesh refinement, as implemented in standard boundary value solvers. The solution process involves discretizing the spatial domain, minimizing the residual of the governing equations subject to nonlinear boundary conditions, and iteratively converging to a consistent steady-state profile.

Due to the nonlinear coupling in the reaction and energy terms, the system may exhibit multiple equilibrium profiles. This is well-established in the context of exothermic tubular reactors, where the interdependence between the concentration and temperature fields can generate both stable and unstable steady states [55, 56].

Similar to the results obtained in [15], one parameter configuration gives rise to multiple steady-state profiles, while a second set leads to a unique stable solution. These are shown in Figures 4.2 and 4.3, respectively. The two parameter sets are listed side-by-side in Table 4.1, and differ only in the temperature dependence of the reaction kinetics. The unstable equilibrium from the first case and the stable equilibrium from the second will serve as linearization points in the control and estimation developments that follow.

4.2.4 Linearized Model

To facilitate controller and observer design, the dimensionless nonlinear system in Equations (4.9)-(4.10) is linearized around a chosen steady-state profile.

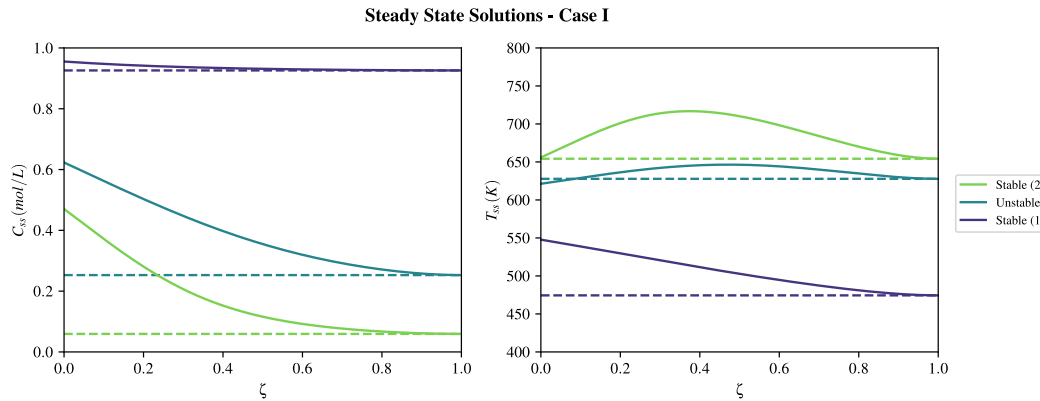


Figure 4.2: Steady-state solutions for Case I. Solid and dashed lines represent reactor and recycle stream profiles, respectively.

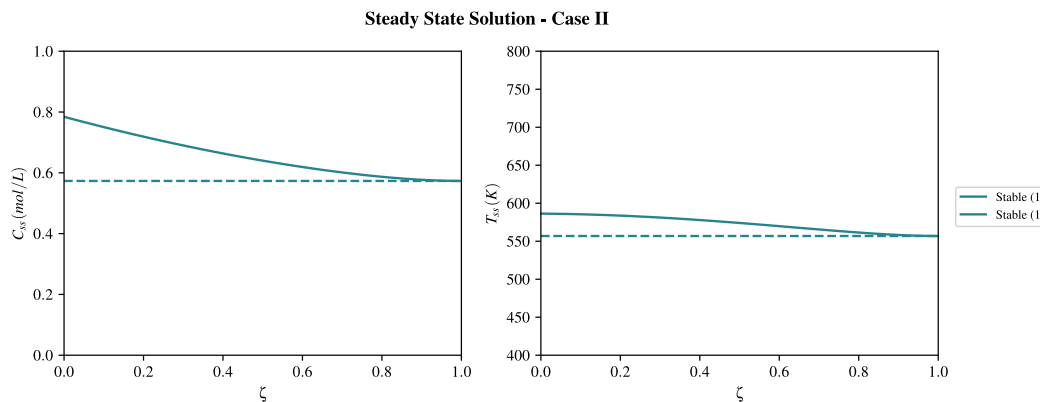


Figure 4.3: Steady-state solution for Case II. Solid and dashed lines represent reactor and recycle stream profiles, respectively.

Table 4.1: Parameters used in the steady-state analysis for Case I (Unstable) and Case II (Stable)

Parameter	Case I (Unstable)	Case II (Stable)
Pe_m	4	4
Pe_T	6	6
T_w^{ss}	-0.37	-0.37
T_{feed}	600 K	600 K
C_{feed}	1.0 M	1.0 M
k_a	0.6	0.6
r_r	0.3	0.3
α	0.8	0.8
η	14.0	6.0
σ	0.9	0.9
τ	0.5	0.5
R_1	-1.38	-0.45
R_2	6.48	1.95

Deviation variables are introduced as $x_i(\zeta, t) = m_i(\zeta, t) - m_i^{ss}(\zeta)$, where m_i^{ss} denotes the corresponding steady-state solution. These deviation variables form the state vector of the linearized system.

The jacket inlet temperature $T_w(t)$ is treated as the manipulated input and is similarly expressed in deviation form as $u(t) = T_w(t) - T_w^{ss}$. The measured output is taken to be the reactor outlet temperature deviation, defined as $y(t) = m_2(1, t) - m_2^{ss}(1)$.

The nonlinear reaction source terms, which depend on both concentration and temperature, are linearized with respect to the deviation variables:

$$\begin{cases} f_{\text{nl}}(m_1, m_2) = k_a(1 - m_1)e^{\frac{\eta m_2}{1+m_2}} \approx f_{\text{nl}}(m_1^{ss}, m_2^{ss}) + \tilde{R}_1(m_1 - m_1^{ss}) + \tilde{R}_2(m_2 - m_2^{ss}), \\ g_{\text{nl}}(m_1, m_2) = \alpha k_a(1 - m_1)e^{\frac{\eta m_2}{1+m_2}} \approx g_{\text{nl}}(m_1^{ss}, m_2^{ss}) + \alpha \tilde{R}_1(m_1 - m_1^{ss}) + \alpha \tilde{R}_2(m_2 - m_2^{ss}) \end{cases} \quad (4.11)$$

where the local Jacobian terms are given by:

$$\tilde{R}_1(\zeta) = -k_a e^{\frac{\eta m_2^{ss}(\zeta)}{1+m_2^{ss}(\zeta)}}, \quad \tilde{R}_2(\zeta) = \frac{\eta k_a (1 - m_1^{ss}(\zeta)) e^{\frac{\eta m_2^{ss}(\zeta)}{1+m_2^{ss}(\zeta)}}}{(1 + m_2^{ss}(\zeta))^2}. \quad (4.12)$$

To simplify the linearized system, spatially averaged coefficients are introduced:

$$R_1 = \int_0^1 \tilde{R}_1(\zeta) d\zeta, \quad R_2 = \int_0^1 \tilde{R}_2(\zeta) d\zeta. \quad (4.13)$$

The spatially averaged parameters R_1 and R_2 are calculated based on the steady-state profiles obtained in the previous section, with their values listed in Table 4.1 for each parameter configuration. These linearized reaction terms will be incorporated into the governing equations to obtain a spatially-invariant linear PDE model given in Equation (4.14). This approximation enables a

more tractable representation while preserving the system's infinite-dimensional character for operator-theoretic formulation.

$$\left\{ \begin{array}{l} \partial_t x_1(\zeta, t) = \frac{1}{Pe_m} \partial_{\zeta\zeta} x_1(\zeta, t) - \partial_\zeta x_1(\zeta, t) + R_1 x_1(\zeta, t) + R_2 x_2(\zeta, t) \\ \partial_t x_2(\zeta, t) = \frac{1}{Pe_T} \partial_{\zeta\zeta} x_2(\zeta, t) - \partial_\zeta x_2(\zeta, t) + \alpha R_1 x_1(\zeta, t) + \alpha R_2 x_2(\zeta, t) + \sigma [u(t) - x_2(\zeta, t)] \\ \partial_t x_3(\zeta, t) = \frac{1}{\tau} \partial_\zeta x_3(\zeta, t) \\ \partial_t x_4(\zeta, t) = \frac{1}{\tau} \partial_\zeta x_4(\zeta, t) \\ \partial_\zeta x_1(0, t) = Pe_m [x_1(0, t) - r_r x_3(0, t)], \quad \partial_\zeta x_1(1, t) = 0 \\ \partial_\zeta x_2(0, t) = Pe_T [x_2(0, t) - r_r x_4(0, t)], \quad \partial_\zeta x_2(1, t) = 0 \\ x_1(1, t) = x_3(1, t) \\ x_2(1, t) = x_4(1, t) \\ y(t) = x_2(1, t) \end{array} \right. \quad (4.14)$$

This linearized representation forms the foundation for the infinite-dimensional state-space modeling, estimation, and control design discussed in the next section.

4.3 Infinite-dimensional Representation

4.3.1 System Operators

The linearized dynamics of the coupled non-isothermal reactor and recycle system can be expressed as an infinite-dimensional linear time-invariant (LTI) system over a Hilbert space. Let the augmented state space be defined as $X := L^2([0, 1]; \mathbb{R}^4)$ and $X_{\mathbb{C}} := L^2([0, 1]; \mathbb{C}^4)$, where $X_{\mathbb{C}}$ denotes the complexification

of X , used later for spectral analysis. The system takes the abstract form given by Equation (4.15):

$$\begin{cases} \partial_t x(\zeta, t) &= Ax(\zeta, t) + Bu(t), \\ y(t) &= Cx(\zeta, t), \end{cases} \quad (4.15)$$

where $x(\zeta, t) \in X$, and $A : \mathcal{D}(A) \subset X \rightarrow X$ is an unbounded linear operator generating a C_0 -semigroup on X . The input and output operators are $B \in \mathcal{L}(\mathbb{R}, X)$ and $C \in \mathcal{L}(X, \mathbb{R})$, respectively. The structure of the operator A is given in Equation (4.16):

$$A(\cdot) = \begin{bmatrix} \frac{1}{Pe_m} \partial_{\zeta\zeta} - \partial_\zeta + R_1 & R_2 & 0 & 0 \\ \alpha R_1 & \frac{1}{Pe_T} \partial_{\zeta\zeta} - \partial_\zeta + \alpha R_2 - \sigma & 0 & 0 \\ 0 & 0 & \frac{1}{\tau} \partial_\zeta & 0 \\ 0 & 0 & 0 & \frac{1}{\tau} \partial_\zeta \end{bmatrix} \begin{bmatrix} (\cdot)_1 \\ (\cdot)_2 \\ (\cdot)_3 \\ (\cdot)_4 \end{bmatrix}, \quad (4.16)$$

with its domain, $\mathcal{D}(A)$ defined in Equation (4.17):

$$\begin{aligned} \mathcal{D}(A) := \Big\{ x = (x_1, x_2, x_3, x_4)^\top \in X : & x_1, x_2 \in H^2(0, 1), x_3, x_4 \in H^1(0, 1); \\ & \partial_\zeta x_1(1) = 0; \quad \partial_\zeta x_1(0) = Pe_m [x_1(0) - r_r x_3(0)]; \\ & \partial_\zeta x_2(1) = 0; \quad \partial_\zeta x_2(0) = Pe_T [x_2(0) - r_r x_4(0)]; \\ & x_1(1) = x_3(1); \quad x_2(1) = x_4(1) \Big\}. \end{aligned} \quad (4.17)$$

The definition of the input operator B is provided in Equation (4.18):

$$B(\cdot) = \begin{bmatrix} 0 \\ \sigma \\ 0 \\ 0 \end{bmatrix} (\cdot) \in \mathcal{L}(\mathbb{R}, X), \quad (4.18)$$

representing actuation on the inlet thermal condition of the reactor. The output operator corresponds to a pointwise measurement at the outlet of the reactor ($\zeta = 1$), and is defined in Equation (4.19), where $\delta(\zeta - 1)$ denotes the Dirac delta function:

$$C(\cdot) = \begin{bmatrix} 0 & \int_0^1 \delta(\zeta - 1)(\cdot)_2 d\zeta & 0 & 0 \end{bmatrix} \in \mathcal{L}(X, \mathbb{R}). \quad (4.19)$$

As the system delay has been reformulated as an auxiliary state governed by a transport PDE, the operator A is time-invariant, and the overall model assumes the structure of a linear time-invariant system in the sense of semigroup theory.

4.3.2 Spectral Analysis

The eigenvalues $\lambda_i \in \mathbb{C}$ and corresponding eigenfunctions $\phi_i \in \mathcal{D}(A) \subset X_{\mathbb{C}}$ of the generator A are determined by solving the spectral equation $A\phi_i = \lambda_i\phi_i$. This is achieved by constructing a first-order representation of the PDE system and enforcing boundary matching to globally satisfy the non-separated boundary conditions. Admissible eigenvalues are identified as those for which a non-trivial solution exists, and the associated eigenfunctions are then constructed by propagating these non-trivial profiles across the spatial domain using the solution operator derived from the lifted system.

The resulting eigenvalue distributions for two representative parameter sets

are shown in Figure 4.4. Case I exhibits instability, as evidenced by the presence of eigenvalues with positive real parts, whereas Case II is stable with all eigenvalues located in the left-half complex plane. Next step is to examine the spectral structure of A more closely, focusing on its adjoint properties in order to obtain an orthogonal basis for projection in the augmented state space X_C .

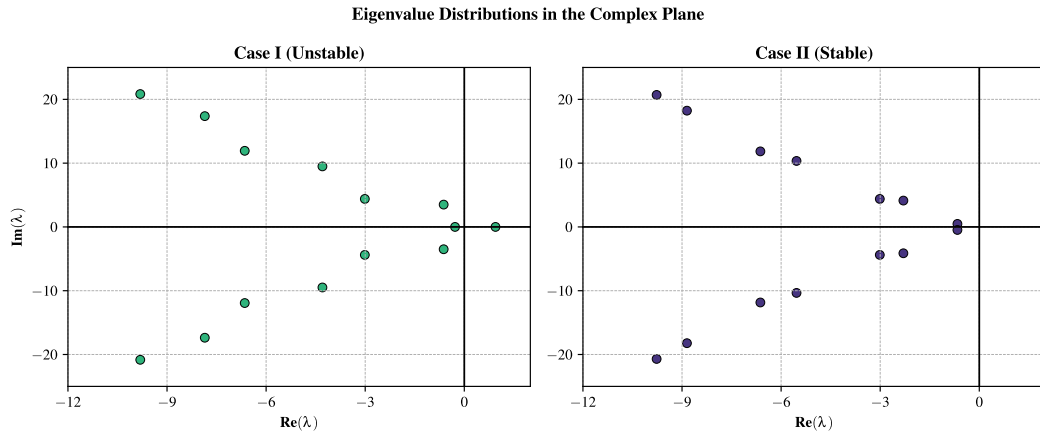


Figure 4.4: Eigenvalue distribution in the complex plane for Case I (Unstable) and Case II (Stable).

4.3.3 Adjoint System and Biorthogonal Basis

The presence of complex eigenvalues suggests that the generator A is not self-adjoint. This can be verified by evaluating the inner product relation $\langle Ax, x^\dagger \rangle_X = \langle x, A^*x^\dagger \rangle_X$ for all $x \in \mathcal{D}(A)$ and $x^\dagger \in \mathcal{D}(A^*)$, where the inner product on $X = L^2([0, 1]; \mathbb{C}^4)$ is defined by $\langle x, x^\dagger \rangle_X := \int_0^1 x(\zeta)^\top \overline{x^\dagger(\zeta)} d\zeta$. Performing integration by parts reveals the formal adjoint operator A^* , given in Equation (4.20), which differs structurally from A and confirms the lack of self-adjointness.

$$A^* = \begin{bmatrix} \frac{1}{Pe_m} \partial_{\zeta\zeta} + \partial_\zeta + R_1 & R_2 & 0 & 0 \\ \alpha R_1 & \frac{1}{Pe_T} \partial_{\zeta\zeta} + \partial_\zeta + \alpha R_2 - \sigma & 0 & 0 \\ 0 & 0 & -\frac{1}{\tau} \partial_\zeta & 0 \\ 0 & 0 & 0 & -\frac{1}{\tau} \partial_\zeta \end{bmatrix} \quad (4.20)$$

The corresponding domain $\mathcal{D}(A^*) \subset X$ is shown in Equation (4.21).

$$\begin{aligned} \mathcal{D}(A^*) := \Big\{ & x^\dagger = (x_1^\dagger, x_2^\dagger, x_3^\dagger, x_4^\dagger)^\top \in X : x_1^\dagger, x_2^\dagger \in H^2(0, 1), x_3^\dagger, x_4^\dagger \in H^1(0, 1); \\ & \partial_\zeta x_1^\dagger(0) = 0; \quad \partial_\zeta x_1^\dagger(1) = Pe_m \left[\frac{1}{\tau} x_3^\dagger(1) - x_1^\dagger(1) \right]; \\ & \partial_\zeta x_2^\dagger(0) = 0; \quad \partial_\zeta x_2^\dagger(1) = Pe_T \left[\frac{1}{\tau} x_4^\dagger(1) - x_2^\dagger(1) \right]; \\ & x_3^\dagger(0) = r_r \tau x_1^\dagger(0); \quad x_4^\dagger(0) = r_r \tau x_2^\dagger(0) \Big\}. \end{aligned} \quad (4.21)$$

Though not self-adjoint, the spectrum of A^* coincides with that of A , with each eigenvalue $\lambda_i \in \mathbb{C}$ admitting a complex-conjugate counterpart $\bar{\lambda}_i$ in the spectrum of A^* . Upon normalization, the associated eigenfunctions $\{\phi_i\}_{i \in \mathbb{Z}} \subset \mathcal{D}(A)$ and $\{\psi_i\}_{i \in \mathbb{Z}} \subset \mathcal{D}(A^*)$ form a biorthonormal system satisfying $\langle \phi_i, \psi_j \rangle_X = \delta_{ij}$, where δ_{ij} denotes the Kronecker delta. This biorthonormal structure enables modal projection of the infinite-dimensional system onto reduced-order subspaces. Specifically, it provides the analytical basis for solving the discrete-time Lyapunov equation used to compute the MPC terminal penalty, and the discrete algebraic filter Riccati equation used in MHE design [1, 15, 54].

Finally, the adjoint input and output operators are derived from the duality relations $\langle Bu, x \rangle_X = \langle u, B^*x \rangle_{\mathbb{R}}$ and $\langle Cx, y \rangle_{\mathbb{R}} = \langle x, C^*y \rangle_X$, and are expressed

in Equation (4.22). These operators are essential for constructing the discrete-time setting of the proposed estimation and control framework.

$$B^* = \begin{bmatrix} 0 & \sigma \int_0^1 (\cdot)_2 d\zeta & 0 & 0 \end{bmatrix}, \quad C^* = \begin{bmatrix} 0 \\ \delta(\zeta - 1) \\ 0 \\ 0 \end{bmatrix}. \quad (4.22)$$

4.4 Cayley–Tustin Time Discretization

To enable digital implementation of estimation and control algorithms, the continuous-time DPS model must be mapped into a discrete-time form. We follow the structure-preserving Cayley–Tustin time discretization method, as adopted in previous works on reactor control[15, 31, 32]. This approach is a Crank–Nicolson-type scheme belonging to the class of symplectic Runge–Kutta integrators, known for preserving key dynamical properties such as stability in the discrete-time setting[39, 41].

Assuming a piecewise constant (zero-order hold) input over each sampling interval of length Δt , the Cayley–Tustin method yields a discrete-time state-space model of the form represented in Equation (4.23). The discrete-time representation operators emerge naturally from the Cayley–Tustin framework by evaluating corresponding continuous-time operators through their resolvent form. In particular, the discrete-time dynamics are obtained by applying functions of the resolvent operator $\mathfrak{R}(s, A) := (sI - A)^{-1}$, evaluated at $s = \alpha$, where $\alpha = 2/\Delta t$.

$$\begin{cases} x(\zeta, k+1) = A_d x(\zeta, k) + B_d u(k) \\ y(k) = C_d x(\zeta, k) + D_d u(k) \end{cases} \quad (4.23)$$

Section 4.4.1 is therefore dedicated to deriving a closed-form expression for this resolvent that respects the infinite-dimensional structure of the original PDE model. The resulting operator will then serve as the foundation for constructing the discrete-time system operators A_d, B_d, C_d, D_d , as well as their adjoint counterparts in Section 4.4.2.

4.4.1 Resolvent Operator

As discussed previously, to evaluate the Cayley–Tustin mappings, one must first obtain the resolvent operator $\mathfrak{R}(s, A) := (sI - A)^{-1}$ for the system generator A . Rather than relying on modal decomposition and truncating the resulting infinite sum, we follow a direct Laplace-domain approach[15, 31], which yields a non-truncated expression that fully preserves the infinite-dimensional structure of the system. As shown in Equation (4.24), the resolvent $\mathfrak{R}(s, A)$ may be understood as the operator that maps either the initial condition $x_0(\zeta) := x(\zeta, t = 0)$ or the input $Bu(t)$ to the Laplace transform of the state, denoted by $X(\zeta, s) := \mathcal{L}\{x(\zeta, t)\}$.

$$\begin{aligned} \partial_t x(\zeta, t) &= Ax(\zeta, t) + Bu(t) \xrightarrow{\mathcal{L}} \\ sX(\zeta, s) - x_0(\zeta) &= AX(\zeta, s) + BU(s) \\ \Rightarrow \begin{cases} X(\zeta, s) &= \mathfrak{R}(s, A) x_0(\zeta) \quad (\text{if } u = 0), \\ X(\zeta, s) &= \mathfrak{R}(s, A) BU(s) \quad (\text{if } x_0(\zeta) = 0) \end{cases} \end{aligned} \quad (4.24)$$

To explicitly construct $\mathfrak{R}(s, A)$, we apply the Laplace transform to the original PDE system in Equation (4.14), and introduce auxiliary states to eliminate second-order spatial derivatives. This yields a lifted six-dimensional system

of first-order ODEs with respect to the spatial variable ζ . The resulting augmented state is denoted by $\tilde{X}(\zeta, s) := \begin{bmatrix} X_1 & \partial_\zeta X_1 & X_2 & \partial_\zeta X_2 & X_3 & X_4 \end{bmatrix}^\top$, and satisfies the differential equation given in Equation (4.25).

$$\partial_\zeta \tilde{X}(\zeta, s) = \tilde{A}(s) \tilde{X}(\zeta, s) + \tilde{Z}(\zeta, s) \quad (4.25)$$

Here, $\tilde{A}(s)$ is the lifted spatial generator, and $\tilde{Z}(\zeta, s)$ is the lifted inhomogeneity, which depends on whether we are analyzing the zero-input or zero-initial condition response. To ensure a linear operator structure with respect to the external signal, we construct $\tilde{Z}(\zeta, s)$ as in Equation (4.26), where the signal $\tilde{z}(\zeta, s)$ is either $x_0(\zeta)$ or $BU(s)$, and the lifting operator \mathcal{Q} is matrix-valued and depends on whether the problem involves an initial condition or an input. In particular, $\mathcal{Q} = \mathcal{Q}^x$ in the zero-input case, and $\mathcal{Q} = \mathcal{Q}^u$ in the zero-initial condition case. This ensures that the solution $\tilde{X}(\zeta, s)$ remains an explicit operator acting on \tilde{z} .

$$\tilde{Z}(\zeta, s) = \mathcal{Q} \tilde{z}(\zeta, s) \quad (4.26)$$

The variation-of-constants formula then yields the solution shown in Equation (4.27), where $\tilde{T}(\zeta, s) := e^{\tilde{A}(s)\zeta}$ denotes the state-transition matrix in space, and the integral operator $\mathcal{I}_\zeta[\tilde{z}(\xi, s)]$ captures the accumulated effect of the inhomogeneity.

$$\tilde{X}(\zeta, s) = \tilde{T}(\zeta, s) \tilde{X}(0, s) + \mathcal{I}_\zeta[\tilde{z}(\xi, s)], \quad \text{with } \mathcal{I}_\zeta(\cdot) := \int_0^\zeta \tilde{T}(\zeta - \xi, s) \mathcal{Q}(\cdot) d\xi \quad (4.27)$$

To eliminate the unknown value $\tilde{X}(0, s)$, we impose the Laplace-transformed boundary conditions in the algebraic form given in Equation (4.28).

$$M_0(s) \tilde{X}(0, s) + M_1(s) \tilde{X}(1, s) = 0 \quad (4.28)$$

Evaluating Equation (4.27) at $\zeta = 1$ and substituting the result $\tilde{X}(1, s) = \tilde{T}(1, s) \tilde{X}(0, s) + \mathcal{I}_1[\tilde{z}(\zeta, s)]$ into Equation (4.28) followed by solving for $\tilde{X}(0, s)$ yields the relation shown in Equation (4.29), where $\mathcal{M}(s)$ is the boundary matching operator.

$$\tilde{X}(0, s) = -\mathcal{M}(s) \mathcal{I}_1[\tilde{z}(\zeta, s)], \quad \text{with } \mathcal{M}(s) := \left(M_0(s) + M_1(s) \tilde{T}(1, s) \right)^{-1} M_1(s) \quad (4.29)$$

Substituting Equation (4.29) back into Equation (4.27) gives the final expression for the augmented solution, shown in Equation (4.30).

$$\tilde{X}(\zeta, s) = -\tilde{T}(\zeta, s) \mathcal{M}(s) \mathcal{I}_1[\tilde{z}(\zeta, s)] + \mathcal{I}_\zeta[\tilde{z}(\zeta, s)] \quad (4.30)$$

The Laplace-domain solution $X(\zeta, s)$ is then recovered as shown in Equation (4.31), where the projection operator \mathcal{Q}^X is a matrix-valued operator that simply extracts the physical state variables from the augmented state.

$$X(\zeta, s) = \mathcal{Q}^X \tilde{X}(\zeta, s) \quad (4.31)$$

Putting these steps together, the resolvent operator $\mathfrak{R}(s, A)$ admits the explicit operator-valued form given in Equation (4.32). This representation maintains a structured dependence on the external signal—either the initial condition $x_0(\zeta)$ or the input $BU(s)$ —which appears solely as the operand of a linear operator expression.

$$\mathfrak{R}(s, A)(\cdot) = \mathcal{Q}^X \left[\mathcal{I}_\zeta(\cdot) - \tilde{T}(\zeta, s) \mathcal{M}(s) \mathcal{I}_1(\cdot) \right] \quad (4.32)$$

This formulation will be used in Section 4.4.2 to evaluate the discrete-time operators A_d , B_d , C_d , and D_d via Cayley–Tustin discretization. It is worth mentioning that by implementing the generator and the boundary matching constraints of the adjoint system into the framework obtained at this stage, the resolvent-based mappings may also be derived for the discrete-time adjoint operators.

Example. To illustrate the concrete realization of the abstract operators introduced in this section, we present the lifted system representation for the non-isothermal reactor model described in Section 4.2. The original and augmented state vectors are defined in Equation (4.33).

$$x(\zeta, t) = \begin{bmatrix} x_1(\zeta, t) \\ x_2(\zeta, t) \\ x_3(\zeta, t) \\ x_4(\zeta, t) \end{bmatrix}, \quad \tilde{X}(\zeta, s) = \begin{bmatrix} X_1(\zeta, s) \\ \partial_\zeta X_1(\zeta, s) \\ X_2(\zeta, s) \\ \partial_\zeta X_2(\zeta, s) \\ X_3(\zeta, s) \\ X_4(\zeta, s) \end{bmatrix} \quad (4.33)$$

Applying the Laplace transform to the PDE system in Equation (4.14) and lifting the second-order structure to first order yields the spatial ODE system given in Equation (4.34).

$$\partial_\zeta \tilde{X}(\zeta, s) = \tilde{A}(s) \tilde{X}(\zeta, s) + \tilde{Z}(\zeta, s) \quad (4.34)$$

The lifted operator $\tilde{A}(s) \in \mathbb{R}^{6 \times 6}$ appearing in Equation (4.34) is provided in Equation (4.35).

$$\tilde{A}(s) = \begin{bmatrix} 0 & 1 & 0 & 0 & 0 & 0 \\ \text{Pe}_m(s - R_1) & \text{Pe}_m & -\text{Pe}_m R_2 & 0 & 0 & 0 \\ 0 & 0 & 0 & 1 & 0 & 0 \\ -\text{Pe}_T \alpha R_1 & 0 & \text{Pe}_T(s + \sigma - \alpha R_2) & \text{Pe}_T & 0 & 0 \\ 0 & 0 & 0 & 0 & \tau s & 0 \\ 0 & 0 & 0 & 0 & 0 & \tau s \end{bmatrix} \quad (4.35)$$

The inhomogeneity term $\tilde{Z}(\zeta, s)$ captures the effect of both the initial condition and the boundary input and is given in Equation (4.36).

$$\tilde{Z}(\zeta, s) = \begin{bmatrix} 0 \\ -\text{Pe}_m x_1(\zeta) \\ 0 \\ -\text{Pe}_T [x_2(\zeta) + \sigma U(s)] \\ -\tau x_3(\zeta) \\ -\tau x_4(\zeta) \end{bmatrix} \quad (4.36)$$

This expression can be decomposed into a sum of lifted operator terms acting on the initial condition and input, as shown in Equation (4.37).

$$\tilde{Z}(\zeta, s) = \mathcal{Q}^x x_0(\zeta) + \mathcal{Q}^u B U(s) \quad (4.37)$$

Here, the initial condition is denoted by $x_0(\zeta) = [x_1(\zeta, 0) \ x_2(\zeta, 0) \ x_3(\zeta, 0) \ x_4(\zeta, 0)]^\top$, and the input operator is given by $B = [0 \ \sigma \ 0 \ 0]^\top$. The lifting matrices \mathcal{Q}^x and \mathcal{Q}^u appearing in Equation (4.37) are defined in Equation (4.38).

$$\mathcal{Q}^x = \begin{bmatrix} 0 & 0 & 0 & 0 \\ -\text{Pe}_m & 0 & 0 & 0 \\ 0 & 0 & 0 & 0 \\ 0 & -\text{Pe}_T & 0 & 0 \\ 0 & 0 & -\tau & 0 \\ 0 & 0 & 0 & -\tau \end{bmatrix}, \quad \mathcal{Q}^u = \begin{bmatrix} 0 & 0 & 0 & 0 \\ 0 & 0 & 0 & 0 \\ 0 & 0 & 0 & 0 \\ 0 & -\text{Pe}_T & 0 & 0 \\ 0 & 0 & 0 & 0 \\ 0 & 0 & 0 & 0 \end{bmatrix} \quad (4.38)$$

This corresponds to the abstract structure $\tilde{Z}(\zeta, s) = \mathcal{Q}\tilde{z}(\zeta, s)$ used in Equation 4.26, where $\mathcal{Q} := \mathcal{Q}^x$ and $\tilde{z} := x_0$ in the zero-input case, and $\mathcal{Q} := \mathcal{Q}^u$ and $\tilde{z} := BU(s)$ in the zero-initial condition case.

The projection operator \mathcal{Q}^X used to recover the physical state $X(\zeta, s)$ from the augmented state $\tilde{X}(\zeta, s)$ is given in Equation (4.39).

$$\mathcal{Q}^X = \begin{bmatrix} 1 & 0 & 0 & 0 & 0 & 0 \\ 0 & 0 & 1 & 0 & 0 & 0 \\ 0 & 0 & 0 & 0 & 1 & 0 \\ 0 & 0 & 0 & 0 & 0 & 1 \end{bmatrix} \quad (4.39)$$

Finally, the boundary condition matrices M_0 and M_1 , used in Equation (4.28), are given in Equation (4.40). These matrices implement the Danckwerts-type inflow conditions and the algebraic recycle coupling at the reactor outlet.

$$M_0 = \begin{bmatrix} -\text{Pe}_m & 1 & 0 & 0 & \text{Pe}_m r_r & 0 \\ 0 & 0 & -\text{Pe}_T & 1 & 0 & \text{Pe}_T r_r \\ 0 & 0 & 0 & 0 & 0 & 0 \\ 0 & 0 & 0 & 0 & 0 & 0 \\ 0 & 0 & 0 & 0 & 0 & 0 \\ 0 & 0 & 0 & 0 & 0 & 0 \end{bmatrix}, \quad M_1 = \begin{bmatrix} 0 & 0 & 0 & 0 & 0 & 0 \\ 0 & 0 & 0 & 0 & 0 & 0 \\ 0 & 1 & 0 & 0 & 0 & 0 \\ 0 & 0 & 0 & 1 & 0 & 0 \\ 1 & 0 & 0 & 0 & -1 & 0 \\ 0 & 0 & 1 & 0 & 0 & -1 \end{bmatrix} \quad (4.40)$$

These matrices form the core components in the numerical implementation of the resolvent via the expression in Equation (4.32), and illustrate how the general operator-theoretic framework developed in this section reduces to a concrete matrix-based realization for the reactor system. This formulation is directly usable in numerical evaluations of $\mathfrak{R}(s, A)(\cdot)$, eliminating the need for early lumping.

4.4.2 Operator Mapping

With the resolvent operator $\mathfrak{R}(s, A)$ now available in the explicit form derived in Section 4.4.1, we may proceed to construct the discrete-time operators required for digital implementation. Under the Cayley–Tustin scheme, and for a fixed time step Δt , the discrete-time system operators are obtained by evaluating $\mathfrak{R}(s, A)$ at $s = \alpha := 2/\Delta t$. The mapping is defined formally as:

$$\begin{bmatrix} A_d & B_d \\ C_d & D_d \end{bmatrix} = \begin{bmatrix} -I + 2\alpha\mathfrak{R}(\alpha, A) & \sqrt{2\alpha}\mathfrak{R}(\alpha, A)B \\ \sqrt{2\alpha}C\mathfrak{R}(\alpha, A) & C\mathfrak{R}(\alpha, A)B \end{bmatrix} \quad (4.41)$$

State and input evolution operators. The operator A_d follows directly from Equation (4.41) by applying the resolvent $\mathfrak{R}(\alpha, A)$ to the initial condition x_0 . In this context, the lifted inhomogeneity uses \mathcal{Q}^x as defined in

Equation (4.38). Similarly, the input operator B_d is obtained by evaluating the same resolvent with \mathcal{Q}^u used instead, corresponding to the zero-state case. Both constructions rely on the same numerical machinery introduced earlier.

Output and feedthrough operators. The output operator C_d may be constructed explicitly from the definition of the original output operator C , which measures the physical state at the reactor outlet. Formally, C corresponds to a Dirac-point evaluation functional acting at $\zeta = 1$, and can be represented as

$$C x = \begin{bmatrix} 0 & \int_0^1 \delta(\zeta - 1) (\cdot)_2 d\zeta & 0 & 0 \end{bmatrix} \quad (4.42)$$

when applied to $x(\zeta) \in L^2([0, 1]; \mathbb{R}^4)$. Composing C with $\mathfrak{R}(\alpha, A)$ therefore involves evaluating the second component of $X(\zeta, s)$ at $\zeta = 1$, where $X = \mathfrak{R}(\alpha, A)x_0$ and $\mathcal{Q} = \mathcal{Q}^x$. For the feedthrough operator D_d , the same process applies, but the resolvent acts on $B U(s)$ and uses \mathcal{Q}^u instead.

Adjoint operator mapping. The discrete-time adjoint operators $(A_d^*, B_d^*, C_d^*, D_d^*)$ may be obtained in a structurally identical manner by replacing the original generator A with its adjoint A^* and applying the Cayley–Tustin scheme to the adjoint dynamics. The corresponding resolvent $\mathfrak{R}^*(\alpha, A^*)$ is applied to the adjoint generator and measurement structure. The discrete-time mappings then follow as:

$$\begin{bmatrix} A_d^* & C_d^* \\ B_d^* & D_d^* \end{bmatrix} = \begin{bmatrix} -I + 2\alpha \mathfrak{R}^*(\alpha, A^*) & \sqrt{2\alpha} \mathfrak{R}^*(\alpha, A^*) C^* \\ \sqrt{2\alpha} B^* \mathfrak{R}^*(\alpha, A^*) & B^* \mathfrak{R}^*(\alpha, A^*) C^* \end{bmatrix} \quad (4.43)$$

Since the adjoint operators A^*, B^*, C^* have already been introduced in Section 4.3.3, the computation of their discrete-time counterparts proceeds without additional derivations.

This completes the transition from continuous- to discrete-time representation under the Cayley–Tustin framework. The resulting operators (A_d, B_d, C_d, D_d) and their adjoints are now suitable for direct use in the implementation of constrained state estimation and control algorithms, as developed in the next section.

4.5 Control and Estimation

4.5.1 Model Predictive Control

This subsection outlines the discrete-time full-state Model Predictive Control (MPC) formulation used in this work. The controller is designed to stabilize the linearized infinite-dimensional system under input and state constraints and is implemented in discrete time based on the Cayley–Tustin mapping developed in Section 4.4. Since this control formulation has been established in previous work[31], it is briefly reviewed here for completeness.

The standard finite-horizon infinite-dimensional MPC problem is formulated in Equation 4.44, where $Q_{\text{MPC}}, R_{\text{MPC}}$ are coercive operators that penalize the state and control input, respectively. At each sampling instant k , the control input is computed by solving a constrained quadratic optimization problem over a finite prediction horizon N_{MPC} with the goal of minimizing the weighted sum of the state and control input costs. Terminal costs are also included to ensure stability in the finite-horizon setting.

$$\begin{aligned}
 \min_U & \sum_{l=0}^{N_{\text{MPC}}-1} \langle x_{k+l|k}, x_{k+l|k} \rangle_{Q_{\text{MPC}}} + \langle u_{k+l+1|k}, u_{k+l+1|k} \rangle_{R_{\text{MPC}}} \\
 & + \langle x_{k+N_{\text{MPC}}|k}, x_{k+N_{\text{MPC}}|k} \rangle_{P_{\text{MPC}}} \\
 \text{s.t. } & x_{k+l+1|k} = A_d x_{k+l|k} + B_d u_{k+l|k} \\
 & u^{\min} \leq u_{k+l|k} \leq u^{\max} \\
 & \langle x_{k+N_{\text{MPC}}|k}, \phi_u \rangle = 0
 \end{aligned} \tag{4.44}$$

Here, $\{\phi_u\}$ denotes the set of unstable eigenfunctions of the system operator A , associated with eigenvalues λ_u satisfying $\text{Re}(\lambda_u) \geq 0$. The terminal cost operator P_{MPC} encodes the long-term impact of future states and is computed as the unique solution to the discrete Lyapunov equation, which is equivalent under Cayley–Tustin discretization to the continuous-time operator Lyapunov equation[15, 17]. The closed-form expression for P_{MPC} is therefore obtained as the infinite series given in Equation 4.45 over the eigenfunctions $\{\phi_m\}$ and adjoint eigenfunctions $\{\psi_n\}$ of the operator A .

$$P_{\text{MPC}}(\cdot) = \sum_{m=0}^{\infty} \sum_{n=0}^{\infty} -\frac{\langle \phi_m, \psi_n \rangle_{Q_{\text{MPC}}}}{\lambda_m + \bar{\lambda}_n} \langle (\cdot), \psi_n \rangle \phi_m \tag{4.45}$$

When all eigenvalues satisfy $\text{Re}(\lambda) < 0$, the operator P_{MPC} becomes coercive automatically. In the presence of unstable modes, however, this property no longer holds unless the contribution of those modes is explicitly removed. The terminal constraint in the MPC problem serves this exact purpose: it eliminates the unstable components of the terminal state, ensuring that P_{MPC} is evaluated only over the stable subspace. As such, it guarantees that the cost function remains convex and the optimization problem is well-posed[17, 40].

To express the finite-horizon MPC problem in a quadratic programming (QP) form, the future states are recursively substituted in terms of the current

state and future inputs using the system dynamics. The result is the standard QP formulation given in Equation 4.46.

$$\min_U J_{\text{MPC}} = U^T \langle I_{N_{\text{MPC}}}, H \rangle U + 2U^T \langle I_{N_{\text{MPC}}}, Px(\zeta)_{k|k} \rangle$$

$$\text{s.t. } U^{min} \leq U \leq U^{max}$$

$$T_u x(\zeta)_{k|k} + S_u U = 0$$

with $H =$

$$\begin{aligned} H &= \begin{bmatrix} B_d^* P_{\text{MPC}} B_d + R_{\text{MPC}} & B_d^* A_d^* P_{\text{MPC}} B_d & \dots & B_d^* A_d^{*N_{\text{MPC}}-1} P_{\text{MPC}} B_d \\ B_d^* P_{\text{MPC}} A_d B_d & B_d^* P_{\text{MPC}} B_d + R_{\text{MPC}} & \dots & B_d^* A_d^{*N_{\text{MPC}}-2} P_{\text{MPC}} B_d \\ \vdots & \vdots & \ddots & \vdots \\ B_d^* P_{\text{MPC}} A_d^{N_{\text{MPC}}-1} B_d & B_d^* P_{\text{MPC}} A_d^{N_{\text{MPC}}-2} B_d & \dots & B_d^* P_{\text{MPC}} B_d + R_{\text{MPC}} \end{bmatrix} \\ P &= \begin{bmatrix} B_d^* P_{\text{MPC}} A_d & B_d^* P_{\text{MPC}} A_d^2 & \dots & B_d^* P_{\text{MPC}} A_d^{N_{\text{MPC}}} \end{bmatrix}^T \\ T_u(\cdot) &= \begin{bmatrix} \langle A_d^{N_{\text{MPC}}}(\cdot), \phi_u \rangle \end{bmatrix} \\ S_u &= \begin{bmatrix} \langle A_d^{N_{\text{MPC}}-1} B_d, \phi_u \rangle & \langle A_d^{N_{\text{MPC}}-2} B_d, \phi_u \rangle & \dots & \langle B_d, \phi_u \rangle \end{bmatrix} \\ U &= \begin{bmatrix} u_{(k+1)|k} & u_{(k+2)|k} & \dots & u_{(k+N_{\text{MPC}})|k} \end{bmatrix}^T \end{aligned} \tag{4.46}$$

Once the obtained QP is solved at each time step, only the first element of the optimal control sequence, $u_{k+1|k}$, is applied to the system. At the next sampling instant, the process is repeated with updated measurements, resulting in a receding horizon control strategy.

It is important to note that up to this point, all operators used in the QP are derived with no need for any spatial discretization. This preserves the underlying infinite-dimensional structure of the dynamics throughout the design. Spatial discretization is introduced only at the final stage, when evaluating inner products and solving the quadratic program numerically to compute the

optimal input. This separation between modeling and numerical implementation motivates the term *late-lumping*, as it allows control design to remain consistent with the distributed nature of the plant.

4.5.2 Moving Horizon Estimation

The full-state availability assumption made in the MPC formulation is rarely justifiable for distributed parameter systems, where the state is infinite-dimensional and cannot be fully observed. To enable output-based feedback, we now introduce a moving horizon estimation (MHE) framework—a finite-horizon, optimization-based estimator—for state reconstruction from partial, noisy measurements. In addition to optimally reconstructing the states, MHE naturally accommodates constraints and disturbances within its optimization framework, making it well-suited for control-integrated estimation.

Following the structure introduced in Section 4.4, the discrete-time model is extended with additive disturbance terms, as shown in equation (4.47), where $w_k \in W \subset \mathbb{R}^{n_w}$ and $v_k \in V \subset \mathbb{R}^{n_y}$ denote the process and measurement noise, respectively. The operator $\mathcal{N}_d \in \mathcal{L}(W, X)$ maps process disturbances into the state space. All other operators and variables are as defined in the previous sections.

$$\begin{cases} x(\zeta, k+1) &= A_d x(\zeta, k) + B_d u(k) + \mathcal{N}_d w(k), \\ y(k) &= C_d x(\zeta, k) + D_d u(k) + v(k) \end{cases} \quad (4.47)$$

As mentioned earlier, the state space $X \subset L^2([0, 1]; \mathbb{R}^4)$ is infinite-dimensional, and the discrete-time operators A_d, B_d, C_d, D_d are those derived via the Cayley–Tustin discretization of the continuous-time system in equation (4.23). Building on top of the estimation model in Xie *et al.*'s work[54], the key difference

here is the presence of the input term $B_d u_k$, which is essential in the control-integrated setting of our application. In Xie's formulation, the term $B_d w_k$ corresponds to what is denoted as $\mathcal{N}_d w_k$ in our model.

Similar to the input operator B_d , the discrete-time process noise operator \mathcal{N}_d is constructed from its continuous-time counterpart \mathcal{N} using the same resolvent-based mapping framework described in Section 4.4.2, with $\mathcal{Q} = \mathcal{Q}^w$ serving as the lifting operator that maps $\mathcal{N}_d W(s)$ from the Laplace-transformed state-space into the Laplace transform of the lifted state-space, enabling consistent application of the noise operator in the lifted setting. The continuous and discrete-time forms of the process noise operator are given in equation (4.48), where $\delta(\zeta)$ denotes the Dirac delta function. Corresponding adjoint noise operators \mathcal{N}^* and \mathcal{N}_d^* can also be derived analogously to B^* and B_d^* , but are omitted here for brevity.

$$\mathcal{N}(\cdot) = \begin{bmatrix} 0 \\ \delta(\zeta) \\ 0 \\ 0 \end{bmatrix} (\cdot), \quad \mathcal{N}_d(\cdot) = \sqrt{2\alpha} \Re(\alpha, A) \mathcal{N}(\cdot) \quad (4.48)$$

To proceed with the estimator design, we adopt the infinite-dimensional output feedback structures introduced in Xie *et al.* and Zhang *et al.*'s contributions[10, 54]. This approach formulates a constrained optimization problem over a sliding window of the most recent N_{MHE} output measurements. The objective is to reconstruct the most plausible state and disturbance trajectory that explains the observed outputs, subject to system dynamics and noise bounds. A finite-dimensional projection is introduced only at the numerical solution stage, consistent with the late-lumping framework developed through-

out this work.

The finite-horizon MHE problem is formulated in equation (4.49), following the structure established in Xie *et al.*'s work [54]. At each time step T , the optimization seeks to reconstruct the most likely state and disturbance trajectory over the past N_{MHE} steps, using all available measurements and inputs, while accounting for process and output noise constraints. The optimization variable is defined as $\omega_T := \begin{bmatrix} \hat{x}_{T-N_{\text{MHE}}|T} & | & \hat{w}_{T-N_{\text{MHE}}|T} & \cdots & \hat{w}_{T-1|T} \end{bmatrix}^\top$, which belongs to the hybrid space $\Omega := X \times W^{N_{\text{MHE}}}$.

$$\begin{aligned}
 \min_{\omega_T} \quad & \sum_{k=T-N_{\text{MHE}}}^{T-1} \left(\langle \hat{w}_{k|T}, \hat{w}_{k|T} \rangle_{Q_{\text{MHE}}^{-1}} + \langle \hat{v}_{k|T}, \hat{v}_{k|T} \rangle_{R_{\text{MHE}}^{-1}} \right) \\
 & + \langle (\hat{x}_{T-N_{\text{MHE}}|T} - \hat{x}_{T-N_{\text{MHE}}|T-1}), (\hat{x}_{T-N_{\text{MHE}}|T} - \hat{x}_{T-N_{\text{MHE}}|T-1}) \rangle_{P_{\text{MHE}}^{-1}} \\
 \text{s.t.} \quad & x_{k+1} = A_d x_k + B_d u_k + \mathcal{N}_d w_k \\
 & y_k = C_d x_k + D_d u_k + v_k \\
 & w_k \in [w^{\min}, w^{\max}], \quad \hat{y}_k \in [y_k - v^{\max}, y_k - v^{\min}]
 \end{aligned} \tag{4.49}$$

Here, $\hat{x}_{T-N_{\text{MHE}}|T-N_{\text{MHE}}-1}$ is the prior state estimate, and the terms $\hat{v}_{k|T}$ are computed via model consistency with the measurements. The penalty operator P_{MHE} accounts for the arrival cost and is computed as the minimal nonnegative self-adjoint solution to the discrete-time algebraic Riccati filter equation[54], which guarantees well-posedness of the estimation problem under mild detectability conditions.

To express the finite-horizon MHE problem in a quadratic programming (QP) form, the predicted outputs and state trajectory are recursively substituted in terms of the initial state and noise sequence using the system dynamics. The result is the standard QP formulation given in Equation 4.50.

$$\begin{aligned} \min_{\omega_T} \quad & J_{\text{MHE}} = \omega_T^\top \langle I_{N_{\text{MHE}}}, G \rangle \omega_T + 2\omega_T^\top \langle I_{N_{\text{MHE}}}, f_{\text{MHE}} \rangle \\ \text{s.t.} \quad & \begin{bmatrix} [0, I_{N_{\text{MHE}}}] \\ -[0, I_{N_{\text{MHE}}}] \\ -S_y \\ S_y \end{bmatrix} \omega_T \leq \begin{bmatrix} w_{N_{\text{MHE}} \times 1}^{\max} \\ -w_{N_{\text{MHE}} \times 1}^{\min} \\ v_{N_{\text{MHE}} \times 1}^{\max} - Y_T \\ Y_T - v_{N_{\text{MHE}} \times 1}^{\min} \end{bmatrix} \end{aligned}$$

with $G = S_y^*(I_{N_{\text{MHE}}} \otimes R_{\text{MHE}}^{-1})S_y + \text{blkdiag}(P_{\text{MHE}}^{-1}, I_{N_{\text{MHE}}} \otimes Q_{\text{MHE}}^{-1}) \in \mathcal{L}(\Omega, \Omega)$,

$$\begin{aligned} f_{\text{MHE}} = & -S_y^*(I_{N_{\text{MHE}}} \otimes R_{\text{MHE}}^{-1})(Y_T - U_y U_T) + \begin{bmatrix} -P_{\text{MHE}}^{-1} \hat{x}_{T-N_{\text{MHE}}|T-N_{\text{MHE}}-1} \\ 0_{N_{\text{MHE}} \times 1} \end{bmatrix}, \\ S_y = & [\mathcal{O}, T_y], \quad \mathcal{O} = \begin{bmatrix} C_d & C_d A_d & \dots & C_d A_d^{N_{\text{MHE}}-1} \end{bmatrix}^\top, \\ T_y = & \begin{bmatrix} 0 & 0 & \dots & 0 \\ C_d \mathcal{N}_d & 0 & \dots & 0 \\ \vdots & \vdots & \ddots & \vdots \\ C_d A_d^{N_{\text{MHE}}-2} \mathcal{N}_d & \dots & C_d \mathcal{N}_d & 0 \end{bmatrix}, \quad U_y = \begin{bmatrix} D_d & 0 & \dots & 0 \\ C_d B_d & D_d & \dots & 0 \\ \vdots & \vdots & \ddots & \vdots \\ C_d A_d^{N_{\text{MHE}}-2} B_d & \dots & C_d B_d & D_d \end{bmatrix}, \\ \omega_T = & \begin{bmatrix} \hat{x}_{T-N_{\text{MHE}}|T} \\ \hat{w}_{T-N_{\text{MHE}}|T} \\ \vdots \\ \hat{w}_{T-1|T} \end{bmatrix}, \quad Y_T = \begin{bmatrix} y_{T-N_{\text{MHE}}} \\ y_{T-N_{\text{MHE}}+1} \\ \vdots \\ y_{T-1} \end{bmatrix}, \quad U_T = \begin{bmatrix} u_{T-N_{\text{MHE}}} \\ u_{T-N_{\text{MHE}}+1} \\ \vdots \\ u_{T-1} \end{bmatrix} \end{aligned} \tag{4.50}$$

All system operators $A_d, B_d, C_d, D_d, \mathcal{N}_d$, and P_{MHE} are derived in closed form from the continuous-time model using Cayley–Tustin discretization, without the need for spatial approximation. As with the MPC formulation, discretization is introduced only at the numerical stage when evaluating inner products and solving the resulting quadratic program, in line with the late-lumping

philosophy adopted throughout this work.

4.5.3 Closed Loop MHE-MPC Implementation

The integrated MHE-MPC framework is executed as a closed-loop system in which the estimator and controller interact at each sampling instant. The estimation problem is solved over a backward-moving window using the latest available measurements, while the MPC problem is solved over a forward-moving prediction horizon using the most recent state estimate. Both optimization problems are formulated entirely in operator terms and evaluated numerically only at the final stage, consistent with the late-lumping strategy adopted throughout this work. The complete online procedure is summarized in Table 4.2, outlining the initialization, estimation, and control steps performed at each iteration.

The formulated MHE–MPC scheme provides a practical pathway for output-feedback control in distributed parameter systems. Its numerical implementation and interaction with the plant are demonstrated through simulations in Section 4.6.

4.6 Simulation Results

To evaluate the performance and limitations of the proposed control and estimation framework, we simulate two representative scenarios. Case I considers a full-state MPC applied to an inherently unstable system, while Case II investigates the closed-loop integration of MHE and MPC under nominally stable dynamics.

Despite its practical and structural advantages, the MHE–MPC combi-

Table 4.2: Proposed MHE–MPC Algorithm

-
- 0). Assume plant dynamics $\{w_k, v_k\}_{k=0}^{k_{\text{end}}}$ and initial condition x_0 are known.
Let $N = N_{\text{MHE}}$.

Initialization window ($T < N$):

- 1). Assign desired values to the input sequence $\{u_k\}_{k=0}^{N-1}$.

2). Run the plant model:
$$\left\{ \begin{array}{l} x_{k+1} = A_d x_k + B_d u_k + \mathcal{N}_d w_k \\ y_k = C_d x_k + D_d u_k + v_k \end{array} \right\}_{k=0}^{N-1}$$
 to obtain $\{y_k\}_{k=0}^{N-1}$.

- 3). Provide an initial guess for $\hat{x}_{0|N-1}$.
-

Control–Estimation window ($T \geq N$):

- 4). Collect $\{u_k, y_k\}_{k=T-N}^{T-1}$ and prior estimate $\hat{x}_{T-N|T-1}$. Solve $\min_{\omega_T} J_{\text{MHE}}$ to obtain $\omega_T = [\hat{x}_{T-N|T} | \{\hat{w}_{k|T}\}_{k=T-N}^{T-1}]$

- 5). Simulate the model: $\{\hat{x}_{k+1|T} = A_d \hat{x}_{k|T} + B_d u_k + \mathcal{N}_d \hat{w}_{k|T}\}_{k=0}^{N-1}$ to compute $\hat{x}_{T-N+1|T}$ and $\hat{x}_{T|T}$.

- 6). Use $\hat{x}_{T|T}$ to solve $\min_U J_{\text{MPC}}$ and obtain u_T .

7). Apply u_T to the plant:
$$\left\{ \begin{array}{l} x_{T+1} = A_d x_T + B_d u_T + \mathcal{N}_d w_T \\ y_T = C_d x_T + D_d u_T + v_T \end{array} \right.$$
 to obtain y_T .

- 8). Update $T \leftarrow T + 1$ and repeat steps 4-8.
-

nation does not inherently guarantee closed-loop stability. Unlike infinite-dimensional Luenberger observers, which enable direct spectral shaping of the estimation error dynamics, MHE lacks explicit control over estimator convergence speed. Its performance depends implicitly on the formulation and weights of the MHE optimization problem. Therefore, we apply the MHE-MPC architecture only to the stable Case II system, where estimation and control operate over a stable baseline. In contrast, Case I illustrates the stabilizing role of full-state MPC when state measurements are fully available. Output-feedback MPC based on infinite-dimensional observers remains a viable path for future stabilization of unstable systems without full-state access[15, 32].

Numerical simulations are conducted for both cases over the dimensionless time interval $t \in [0, 10]$, using a time step of $\Delta t = 0.2$ and a spatial discretization of $N_\zeta = 100$ points over the dimensionless space $\zeta \in [0, 1]$. Following the late-lumping approach, spatial discretization is performed only at the final implementation stage to enable numerical operations such as integration on the infinite-dimensional system, as well as numerical evaluation of controller and estimator performance.

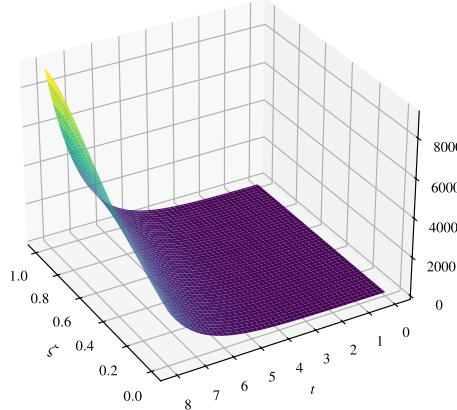
All simulations are initialized from the same nontrivial state, where the reactor states are assigned smooth spatial profiles and applied to the deviation variables around the dimensionless steady states shown in Figures 4.2–4.3. Specifically, $x_1(\zeta, 0) = \sin(1.5\pi\zeta) + c_1$ and $x_2(\zeta, 0) = \sin(0.5\pi\zeta) + c_2$, with constants c_1 and c_2 computed from model parameters to ensure compatibility with the boundary conditions. The recycle states x_3 and x_4 are initialized as uniform offsets matching their respective inlet boundary values. Among state

profiles throughout this section, only the first two state variables, $x_1(\zeta, t)$ and $x_2(\zeta, t)$, are shown, representing deviations in concentration and temperature within the reactor. State profiles along the recycle stream are omitted for brevity. Lastly, the parameters used in the simulations can be found in Table 4.1.

4.6.1 Full-State MPC (Case I)

To validate the stabilizing performance of the model predictive controller, an open-loop simulation is first carried out under zero input. As shown in Figure 4.5, the system exhibits clear instability, confirming the presence of unstable dynamics due to the eigenvalue spectrum displayed for Case I in Figure 4.4. This behavior motivates the design of an MPC scheme capable of stabilizing the system while enforcing constraints.

Zero-Input Response: $x_1(\zeta, t)$



Zero-Input Response: $x_2(\zeta, t)$

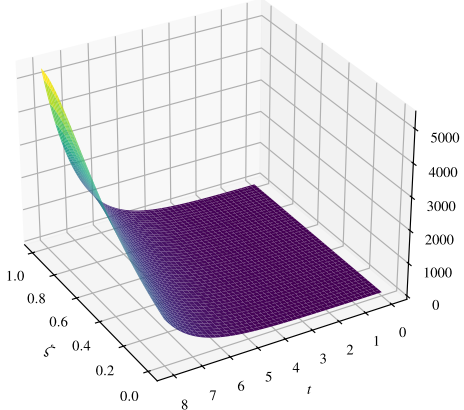


Figure 4.5: 3D profile of the state $x(\zeta, t)$ evolution over space and time (ζ, t) for Case I system with zero input.

A finite-horizon discrete-time MPC is applied using a control horizon of $N_{\text{MPC}} = 9$ and a terminal cost operator constructed from 4 dominant eigen-

modes. The cost weights are set as $Q_{\text{MPC}} = 10$ and $R_{\text{MPC}} = 1$. Input constraints are imposed as $u \in [-0.8, 0.05]$, and both bounds become active during the simulation. No output constraints are enforced. Since the open-loop system possesses one unstable eigenmode, a single equality constraint is included at the terminal step to ensure the terminal state lies entirely within the stable subspace. This terminal constraint guarantees that the resulting quadratic program remains convex, ensuring well-posedness under feasible conditions.

Figure 4.7 confirms that the closed-loop system is successfully stabilized under this controller. The control input and corresponding plant output, shown in Figure 4.6, further verify the effectiveness of the proposed strategy in maintaining output regulation while satisfying all input constraints.

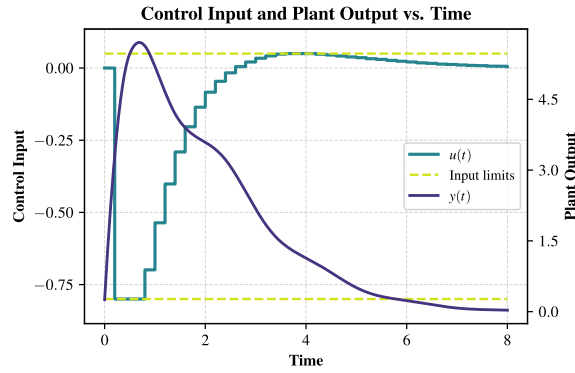


Figure 4.6: Profiles of plant output $y(t)$ and control input $u(t)$ over time for Case I system with full-state feedback MPC.

4.6.2 Output Feedback MHE–MPC (Case II)

To demonstrate output-based stabilization under partial state information, the full-state assumption is relaxed and an MHE–MPC structure is deployed.

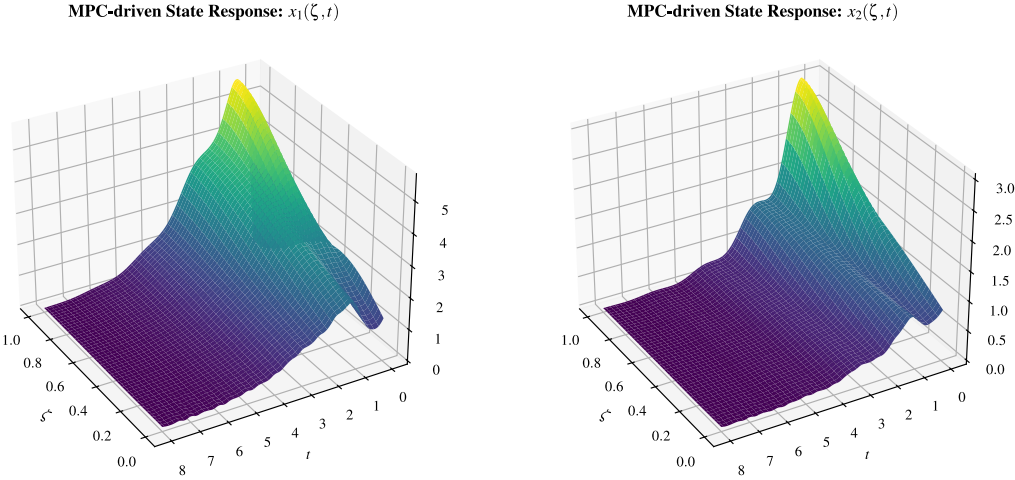


Figure 4.7: 3D profile of the state $x(\zeta, t)$ evolution over space and time (ζ, t) for Case I system with full-state feedback MPC.

The underlying system in this case is already stable but subject to persistent process and measurement noise added respectively as $w_k = 0.05 \sin(t_k)$ and v_k sampled from a zero-mean Gaussian distribution with standard deviation 0.1. The initial guess for the state estimate is generated by perturbing the true initial state with zero-mean Gaussian noise of standard deviation 0.1.

Estimation is performed using a moving horizon estimator with window length $N_{\text{MHE}} = 3$, 4 dominant eigenmodes picked for Riccati projection, and filter weights $Q_{\text{MHE}} = 10$, $R_{\text{MHE}} = 1$. At each iteration, process and measurement noise constraints are imposed as $w_k \in [-0.1, 0.1]$, $v_k \in [-0.25, 0.25]$; these constraints become active throughout the simulation, though not separately plotted to avoid clutter.

The MPC in this scenario is designed with a shorter control horizon of $N_{\text{MPC}} = 5$, a terminal cost operator based on 4 dominant modes, and cost weights $Q_{\text{MPC}} = 1$, $R_{\text{MPC}} = 1$. Since all modes of the plant are stable, no terminal constraint is applied and the problem remains convex with $m_{\text{eq}} = 0$.

The input is constrained within $u \in [-0.5, 0.1]$, with both limits reached during the control horizon.

Figure 4.8 shows the output tracking performance alongside the applied input. Note that MHE requires N_{MHE} steps before estimation begins, during which the system evolves in open loop. To force the stable system further away from the initial condition, a constant input sequence of $u_k = 0.5$ is applied during this period. True states $x(\zeta, t)$ and estimated states $\hat{x}(\zeta, t)$ are shown in Figures 4.9 - 4.10, with state estimation error squared illustrated in Figure 4.11. Despite ongoing process and measurement noise, the estimation error quickly converges to near zero and remains bounded throughout the simulation. The reconstructed state provides sufficiently accurate feedback for the MPC to maintain closed-loop stability, as evidenced by the regulated output and spatial state evolution.

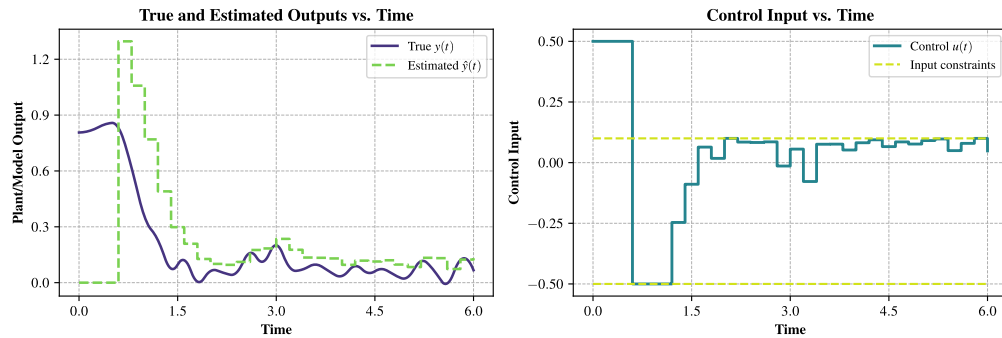


Figure 4.8: Profiles of plant output $y(t)$ and estimated output $\hat{y}(t)$ (left), and control input $u(t)$ (right) over time for Case II system with output feedback MHE-MPC.

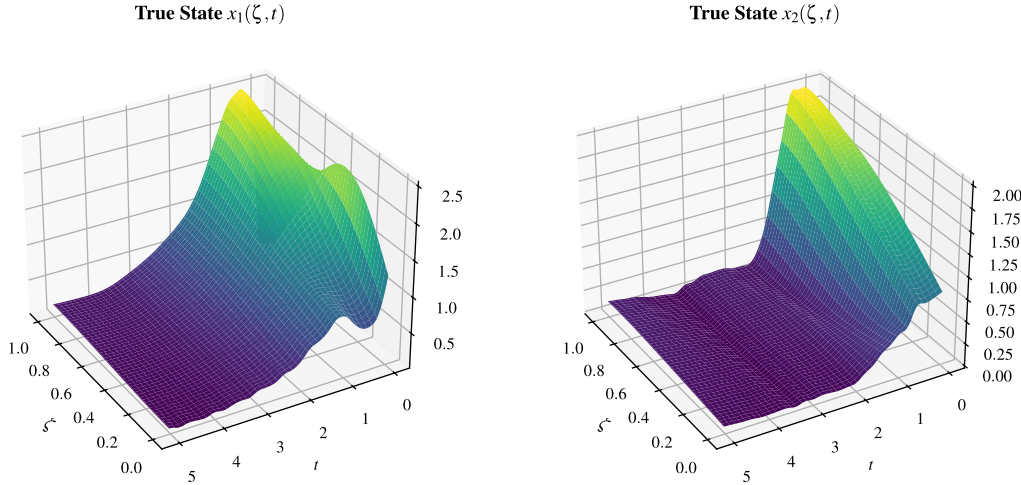


Figure 4.9: 3D profile of the true state $x(\zeta, t)$ over time for Case II system with output feedback MHE-MPC.

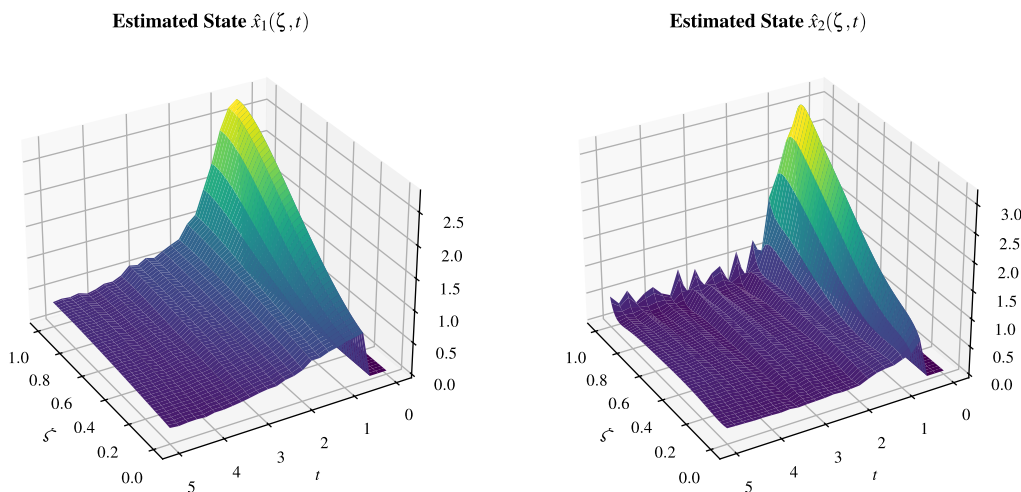


Figure 4.10: 3D profile of the estimated state $\hat{x}(\zeta, t)$ over time for Case II system with output feedback MHE-MPC.

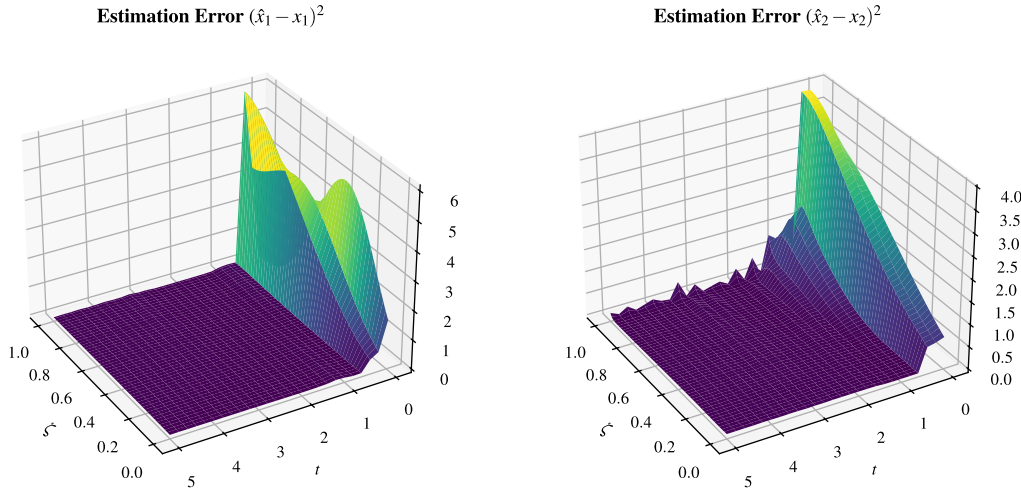


Figure 4.11: 3D profile of the state estimation error $e(\zeta, t) = x(\zeta, t) - \hat{x}(\zeta, t)$ over time for Case II system with output feedback MHE-MPC.

4.7 Conclusion

This work establishes a delay-aware, late-lumped framework for output-based estimation and constrained control of a non-isothermal axial dispersion tubular reactor with recycle. By modeling the state delay as a transport PDE, the recycle stream is incorporated into the system without approximation, preserving the infinite-dimensional structure of the coupled mass–energy dynamics. The proposed Cayley–Tustin discretization enables structure-preserving transition to a discrete-time setting, while the use of closed-form resolvent operators eliminates the need for spatial discretization or model reduction.

Full-state MPC is shown to effectively stabilize an unstable setup while enforcing input constraints, confirming its viability for delay-affected infinite-dimensional systems. The MHE–MPC framework enables constrained output feedback control using only partial measurements; i.e. essential for infinite-dimensional systems where full-state information is generally inaccessible. The

optimization-based structure of the integrated MHE–MPC framework naturally accommodates constraints while the fact that it operates in discrete-time setting makes it well suited for digital implementation, especially in the presence of measurement noise or model inaccuracies. However, unlike observer-based designs that allow explicit pole placement, MHE does not permit direct shaping of the estimation error dynamics. As a result, there is no guarantee that the estimator converges faster than the controller acts—a requirement for closed-loop stability in output-feedback settings. To avoid this limitation, the integrated MHE–MPC strategy is applied to a nominally stable system, where it reconstructs distributed states under process and measurement noise and stabilizes the system within an optimal framework, while successfully accommodating constraints throughout closed-loop operation.

To conclude, the obtained modeling framework along with the proposed MHE–MPC architecture provide a modular foundation for infinite-dimensional estimation and control of diffusion–convection–reaction systems with state delays, as encountered in advanced chemical engineering applications.

References

- [1] B. Moadeli, G. O. Cassol, and S. Dubljevic, “Optimal control of axial dispersion tubular reactors with recycle: Addressing state-delay through transport PDEs,” *The Canadian Journal of Chemical Engineering*, vol. 103, no. 8, pp. 3751–3766, 2025, ISSN: 0008-4034. DOI: [10.1002/cjce.25629](https://doi.org/10.1002/cjce.25629).
- [2] W. H. Ray, *Advanced process control*. McGraw-Hill: New York, NY, USA, 1981.
- [3] E. Davison, “The robust control of a servomechanism problem for linear time-invariant multivariable systems,” *IEEE transactions on Automatic Control*, vol. 21, no. 1, pp. 25–34, 1976, ISSN: 0018-9286. DOI: [10.1109/tac.1976.1101137](https://doi.org/10.1109/tac.1976.1101137).

- [10] L. Zhang, J. Xie, and S. Dubljevic, “Tracking model predictive control and moving horizon estimation design of distributed parameter pipeline systems,” *Computers & Chemical Engineering*, vol. 178, p. 108381, 2023, ISSN: 0098-1354. DOI: [10.1016/j.compchemeng.2023.108381](https://doi.org/10.1016/j.compchemeng.2023.108381).
- [14] G. O. Cassol, D. Ni, and S. Dubljevic, “Heat exchanger system boundary regulation,” *AICHE Journal*, vol. 65, no. 8, e16623, 2019, ISSN: 0001-1541. DOI: [10.1002/aic.16623](https://doi.org/10.1002/aic.16623).
- [15] S. Khatibi, G. O. Cassol, and S. Dubljevic, “Model predictive control of a non-isothermal axial dispersion tubular reactor with recycle,” *Computers & Chemical Engineering*, vol. 145, p. 107159, 2021, ISSN: 0098-1354. DOI: [10.1016/j.compchemeng.2020.107159](https://doi.org/10.1016/j.compchemeng.2020.107159).
- [17] R. Curtain and H. Zwart. Springer Nature, 2020. DOI: [10.1007/978-1-0716-0590-5_1](https://doi.org/10.1007/978-1-0716-0590-5_1).
- [21] M. Krstić (Systems & control). Birkhäuser, 2009.
- [23] J. Qi, S. Dubljevic, and W. Kong, “Output feedback compensation to state and measurement delays for a first-order hyperbolic PIDE with recycle,” *Automatica*, vol. 128, p. 109565, 2021, ISSN: 0005-1098. DOI: [10.1016/j.automatica.2021.109565](https://doi.org/10.1016/j.automatica.2021.109565).
- [24] O. Levenspiel, *Chemical reaction engineering*. John Wiley & Sons, 1998.
- [25] K. F. Jensen and W. H. Ray, “The bifurcation behavior of tubular reactors,” *Chemical Engineering Science*, vol. 37, no. 2, pp. 199–222, 1982, ISSN: 0009-2509. DOI: [10.1016/0009-2509\(82\)80155-3](https://doi.org/10.1016/0009-2509(82)80155-3).
- [26] P. V. Danckwerts, “Continuous flow systems: Distribution of residence times,” *Chemical Engineering Science*, vol. 2, no. 1, pp. 1–13, 1953, ISSN: 0009-2509. DOI: [10.1016/0009-2509\(53\)80001-1](https://doi.org/10.1016/0009-2509(53)80001-1).
- [27] J. M. Ali, N. H. Hoang, M. A. Hussain, and D. Dochain, “Review and classification of recent observers applied in chemical process systems,” *Computers & Chemical Engineering*, vol. 76, pp. 27–41, 2015, ISSN: 0098-1354. DOI: [10.1016/j.compchemeng.2015.01.019](https://doi.org/10.1016/j.compchemeng.2015.01.019).
- [31] B. Moadeli and S. Dubljevic, “Model predictive control of axial dispersion tubular reactors with recycle: Addressing state-delay through transport PDEs,” in *2025 American Control Conference (ACC)*, 2025.
- [32] B. Moadeli and S. Dubljevic, “Observer-based MPC design of an axial dispersion tubular reactor: Addressing recycle delays through transport PDEs,” in *2025 European Control Conference (ECC)*, 2025.

- [39] V. Havu and J. Malinen, “The Cayley transform as a time discretization scheme,” *Numerical Functional Analysis and Optimization*, vol. 28, no. 7-8, pp. 825–851, 2007, ISSN: 0163-0563. DOI: [10.1080/01630560701493321](https://doi.org/10.1080/01630560701493321).
- [40] Q. Xu and S. Dubljevic, “Linear model predictive control for transport-reaction processes,” *AIChE Journal*, vol. 63, no. 7, pp. 2644–2659, 2017, ISSN: 0001-1541. DOI: [10.1002/aic.15592](https://doi.org/10.1002/aic.15592).
- [41] E. Hairer, M. Hochbruck, A. Iserles, and C. Lubich, “Geometric numerical integration,” *Oberwolfach Reports*, vol. 3, no. 1, pp. 805–882, 2006, ISSN: 1660-8933. DOI: [10.4171/owr/2011/16](https://doi.org/10.4171/owr/2011/16).
- [42] B. Moadeli and S. Dubljevic, “Advanced control of non-isothermal axial dispersion tubular reactors with recycle-induced state delay,” *The Canadian Journal of Chemical Engineering*, 2025.
- [43] V. Hlaváček and H. Hofmann, “Modeling of chemical reactors—XVII steady state axial heat and mass transfer in tubular reactors numerical investigation of multiplicity,” *Chemical Engineering Science*, vol. 25, no. 1, pp. 187–199, 1970, ISSN: 0009-2509. DOI: [10.1016/0009-2509\(70\)85031-x](https://doi.org/10.1016/0009-2509(70)85031-x).
- [44] V. Hlaváček and H. Hofmann, “Modeling of chemical reactors—XVI steady state axial heat and mass transfer in tubular reactors an analysis of the uniqueness of solutions,” *Chemical Engineering Science*, vol. 25, no. 1, pp. 173–185, 1970, ISSN: 0009-2509. DOI: [10.1016/0009-2509\(70\)85030-8](https://doi.org/10.1016/0009-2509(70)85030-8).
- [45] D. S. Cohen and A. B. Poore, “Tubular chemical reactors: The ‘lumping approximation’ and bifurcation of oscillatory states,” *SIAM Journal on Applied Mathematics*, vol. 27, no. 3, pp. 416–429, 1974, ISSN: 0036-1399. DOI: [10.1137/0127032](https://doi.org/10.1137/0127032).
- [46] C. Georgakis, R. Aris, and N. R. Amundson, “Studies in the control of tubular reactors-I general considerations,” *Chemical Engineering Science*, vol. 32, no. 11, pp. 1359–1369, 1977, ISSN: 0009-2509. DOI: [10.1016/0009-2509\(77\)85032-x](https://doi.org/10.1016/0009-2509(77)85032-x).
- [47] D. Luss and N. R. Amundson, “Stability of loop reactors,” *AIChE Journal*, vol. 13, no. 2, pp. 279–290, 1967, ISSN: 0001-1541. DOI: [10.1002/aic.690130218](https://doi.org/10.1002/aic.690130218).
- [48] C. S. Bildea, A. C. Dimian, S. C. Cruz, and P. D. Iedema, “Design of tubular reactors in recycle systems,” *Computers & chemical engineering*, vol. 28, no. 1-2, pp. 63–72, 2004, ISSN: 0098-1354. DOI: [10.1016/s0098-1354\(03\)00170-4](https://doi.org/10.1016/s0098-1354(03)00170-4).

- [49] P. D. Christofides and P. Daoutidis, “Finite-dimensional control of parabolic PDE systems using approximate inertial manifolds,” *Journal of Mathematical Analysis and Applications*, vol. 216, no. 2, pp. 398–420, 1997, ISSN: 0022-247X. DOI: [10.1006/jmaa.1997.5649](https://doi.org/10.1006/jmaa.1997.5649).
- [50] A. Armaou and P. D. Christofides, “Dynamic optimization of dissipative PDE systems using nonlinear order reduction,” *Chemical Engineering Science*, vol. 57, no. 24, pp. 5083–5114, 2002, ISSN: 0009-2509. DOI: [10.1016/s0009-2509\(02\)00419-0](https://doi.org/10.1016/s0009-2509(02)00419-0).
- [51] I. Aksikas, A. A. Moghadam, and F. Forbes, “Optimal linear–quadratic control of coupled parabolic–hyperbolic PDEs,” *International Journal of Control*, vol. 90, no. 10, pp. 2152–2164, 2017. DOI: [10.1109/icca.2017.8003083](https://doi.org/10.1109/icca.2017.8003083).
- [52] M. J. Balas, “Feedback control of linear diffusion processes,” *International Journal of Control*, vol. 29, no. 3, pp. 523–534, 1979. DOI: [10.1016/b978-0-12-734250-4.50041-2](https://doi.org/10.1016/b978-0-12-734250-4.50041-2).
- [53] R. Curtain, “Finite-dimensional compensator design for parabolic distributed systems with point sensors and boundary input,” *IEEE Transactions on Automatic Control*, vol. 27, no. 1, pp. 98–104, 1982, ISSN: 0018-9286. DOI: [10.1109/tac.1982.1102875](https://doi.org/10.1109/tac.1982.1102875).
- [54] J. Xie, J.-P. Humaloja, C. R. Koch, and S. Dubljevic, “Constrained receding horizon output estimation of linear distributed parameter systems,” *IEEE Transactions on Automatic Control*, vol. 68, no. 8, pp. 5103–5110, 2022, ISSN: 0018-9286. DOI: [10.1109/tac.2022.3217111](https://doi.org/10.1109/tac.2022.3217111).
- [55] R. F. Heinemann and A. B. Poore, “The effect of activation energy on tubular reactor multiplicity,” *Chemical Engineering Science*, vol. 37, no. 1, pp. 128–131, 1982, ISSN: 0009-2509. DOI: [10.1016/0009-2509\(82\)80079-1](https://doi.org/10.1016/0009-2509(82)80079-1).
- [56] A. Hastir, F. Lamoline, J. J. Winkin, and D. Dochain, “Analysis of the existence of equilibrium profiles in nonisothermal axial dispersion tubular reactors,” *IEEE Transactions on Automatic Control*, vol. 65, no. 4, pp. 1525–1536, 2020, ISSN: 0018-9286. DOI: [10.1109/tac.2019.2921675](https://doi.org/10.1109/tac.2019.2921675).

Chapter 5

Concluding Remarks

5.1 Introduction

Figures and Tables play a crucial role in conveying information effectively in academic documents. This chapter will delve into the intricacies of incorporating figures and tables in your L^AT_EX document, exploring various features and advanced techniques to enhance the visual appeal and clarity of your content. While there are many types of figures that one might have in their document, this Chapter more specifically focuses on the inclusion of graphic figures (pictures), as well as how to lay out multi figures (sub-figures).

⚠ WARNING Throughout this Chapter there will be code listings that include lines that show the required packages. These lines should be included in your L^AT_EX preamble, not in the body of your document. To make this easy I have actually included a document specifically to add your packages too. This can be found in the `includePackages.tex` file found in the `00_LaTeX_Files` folder.

💡 `./00_LaTeX_Files/includePackages.tex` includes all the packages required for creating all the examples in this document, some of these will not be necessary for your own thesis, however, I have included comments on all packages for what they are used for. This allows you to make a decision on if you will need them as well. If you are unsure, you may just comment out the line so as to not forget the packages that were originally included.

5.2 Inserting Figures

In L^AT_EX, figures are included using the `graphicx` package. The `\includegraphics` command is used to insert an image. Let's consider an example:

Listing 5.1: A Basic Example of Including a Figure.

```
\usepackage{graphicx}

\begin{figure}[htb]
    \centering
    \includegraphics[width=0.7\linewidth]{example-image}
    \caption{Example Figure}
    \label{fig:example}
\end{figure}
```

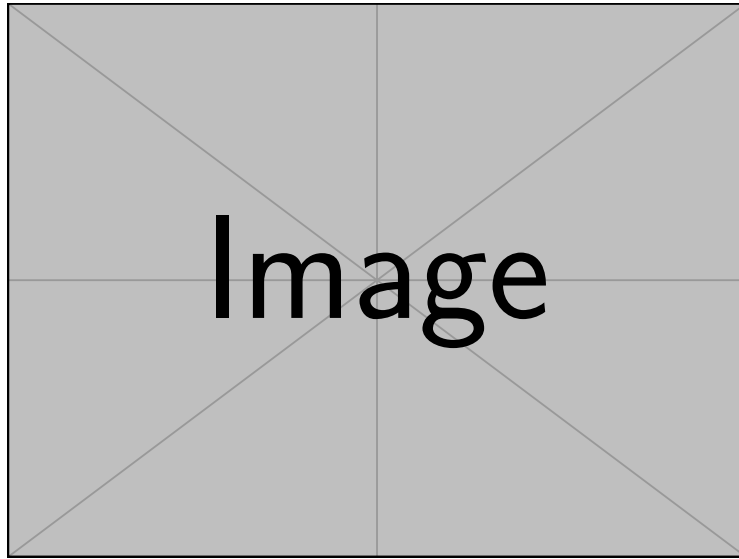


Figure 5.1: This is an example of a single figure similar to that produced by Listing 5.1.

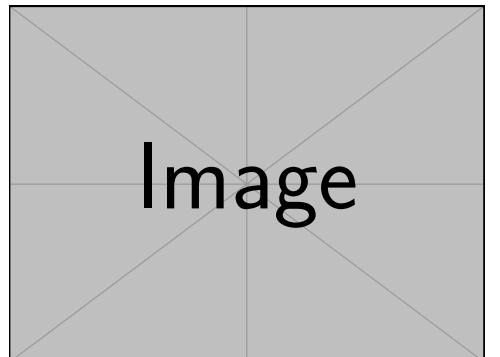
In this example, the `figure` environment is used to contain the image. The `\centering` command ensures the image is centred horizontally. The `width` parameter is used to control the size of the image; in this case, it has been set to `0.45\cmd{linewidth}` which will make it fill a space that is 0.45 times the width of the current line. The `\caption` and `\label` commands provide a caption and label for referencing, respectively.

Figures can be formatted to meet specific requirements. The `\subfigure` command from the `subcaption` package can be used for side-by-side figures:

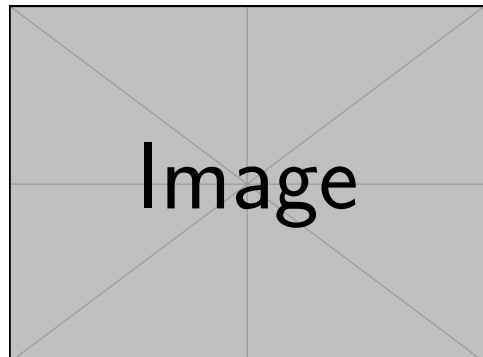
This example uses the `subfigure` environment to create subfigures within a larger figure (as shown in Figure 5.2). The `\hfill` command adds horizontal space between the subfigures.

```
\usepackage{subcaption}

\begin{figure}[htb]
    \begin{subfigure}{0.45\linewidth}
        \centering
        \includegraphics[width=\linewidth]{example-image-a}
    }
    \caption{Subfigure A} % Leave blank for just
    letter
    \label{subfig:a}
\end{subfigure}
\hfill
\begin{subfigure}{0.45\linewidth}
    \centering
    \includegraphics[width=\linewidth]{example-image-b}
}
    \caption{Subfigure B} % Leave blank for just
    letter
    \label{subfig:b}
\end{subfigure}
\caption{Example with Subfigures}
\label{fig:subfigures}
\end{figure}
```



(a)



(b)

Figure 5.2: This is an example of a double image figure similar to that produced by [Section 5.2](#).

While this section provided a few examples on how to make some figures and subfigures, I would strongly recommend checking out some of the more

complex examples of figures shown in [Appendix A](#). This will provide the code and examples for how to create more intricate subfigures and layouts.

5.3 Tables and Tabularx

Tables in L^AT_EX are created using the `tabular` environment. The `tabularx` package is particularly useful when you want the table to automatically adjust its width. Let's define some custom column types for convenience:

```
\usepackage{tabularx}
\newcolumntype{C}{>{\centering\arraybackslash}X}
\newcolumntype{L}{>{\raggedright\arraybackslash}X}
\newcolumntype{R}{>{\raggedleft\arraybackslash}X}
```

Now, let's create a table using tabularx:

```
\begin{table}[htb]
    \centering
    \begin{tabularx}{\linewidth}{|C|L|R|}
        \hline
        \textbf{Centered} & \textbf{Left Justified} & \
        \textbf{Right Justified} \\
        \hline
        Content & More content & Additional content \\
        \hline
    \end{tabularx}
    \caption{Example Table with Tabularx}
    \label{tab:example}
\end{table}
```

In this example, the `tabularx` environment is used, and the custom column types `C`, `L`, and `R` are applied to the columns. This ensures the content is centered, left-justified, and right-justified, respectively.

5.4 Advanced Table Features

To create professional-looking tables, the `booktabs` package can be employed.

It provides commands for better spacing and styling of tables:

```
\usepackage{booktabs}

\begin{table}[htb]
    \centering
    \begin{tabular}{ccc}
        \toprule
        \textbf{Header 1} & \textbf{Header 2} & \textbf{Header 3} \\
        Content 1 & Content 2 & Content 3 \\
        Content 4 & Content 5 & Content 6 \\
        \bottomrule
    \end{tabular}
    \caption{Example Table with Booktabs}
    \label{tab:booktabs_example}
\end{table}
```

The `\toprule`, `\midrule`, and `\bottomrule` commands create horizontal rules with appropriate spacing.

5.5 Additional Packages for Enhanced Table Functionality

Several other packages can be employed to enhance table functionality:

The `longtable` package allows tables to span multiple pages, which is useful for large datasets. The `multirow` and `multicolumn` packages provide commands for cells that span multiple rows or columns, respectively. The `makecell` package enables more complex table layouts. Each of these packages comes with its set of commands and options. Let's briefly explore the

usage of `longtable`, `multirow`, and `multicolumn`:

In these examples, the `longtable` environment is used for tables that span multiple pages. The `\multirow` command is employed to create cells that span multiple rows, while `\multicolumn` is used for cells that span multiple columns.

5.6 Conclusion

This Chapter provided a comprehensive overview of including figures and tables in your L^AT_EX document. From basic insertion of figures to advanced table formatting using packages like `tabularx`, `booktabs`, and others, you now have a solid foundation to include tables and figures in your thesis. While this provides a lot of details on how to add figures that have already been pre-generated, one might want to generate figures on the spot potentially even using data generated from other programs (such as MatLab[®], Python, *etc.*). For this ?? provides in-depth workings of the `pgfplots` package and how to generate consistent and professional looking plots and graphs.

```
\usepackage{longtable}
\usepackage{multirow}
\usepackage{multicolumn}

% Example Longtable
\begin{longtable}{|c|c|}%
  \caption{Longtable Example} \label{tab:longtable} \\
  \hline
  \textbf{Header 1} & \textbf{Header 2} \\
  \hline
  \endfirsthead
  \hline
  \textbf{Header 1} & \textbf{Header 2} \\
  \hline
  \endhead
  Content 1 & Content 2 \\
  Content 3 & Content 4 \\
  \hline
\end{longtable}

% Example Multirow and Multicolumn
\begin{table}[htb]
  \centering
  \begin{tabular}{|c|c|c|}%
    \hline
    \multicolumn{2}{*}{\textbf{Multirow-Col1}} & \multicolumn{2}{c|}{\textbf{Multicolumn-Col2-3}} \\
    \hline
    \cline{2-3}
    & \textbf{Column 2} & \textbf{Column 3} \\
    \hline
    Content 1 & Content 2 & Content 3 \\
    \hline
  \end{tabular}
  \caption{Example Table with Multirow and Multicolumn}
  \label{tab:multirow_multicolumn}
\end{table}
```

Bibliography

- [1] B. Moadeli, G. O. Cassol, and S. Dubljevic, “Optimal control of axial dispersion tubular reactors with recycle: Addressing state-delay through transport PDEs,” *The Canadian Journal of Chemical Engineering*, vol. 103, no. 8, pp. 3751–3766, 2025, ISSN: 0008-4034. DOI: [10.1002/cjce.25629](https://doi.org/10.1002/cjce.25629).
- [2] W. H. Ray, *Advanced process control*. McGraw-Hill: New York, NY, USA, 1981.
- [3] E. Davison, “The robust control of a servomechanism problem for linear time-invariant multivariable systems,” *IEEE transactions on Automatic Control*, vol. 21, no. 1, pp. 25–34, 1976, ISSN: 0018-9286. DOI: [10.1109/tac.1976.1101137](https://doi.org/10.1109/tac.1976.1101137).
- [4] B. A. Francis, “The linear multivariable regulator problem,” *SIAM Journal on Control and Optimization*, vol. 15, no. 3, pp. 486–505, 1977, ISSN: 0363-0129. DOI: [10.1137/0315033](https://doi.org/10.1137/0315033).
- [5] A. A. Moghadam, I. Aksikas, S. Dubljevic, and J. F. Forbes, “Infinite-dimensional LQ optimal control of a dimethyl ether (DME) catalytic distillation column,” *Journal of Process Control*, vol. 22, no. 9, pp. 1655–1669, 2012, ISSN: 0959-1524. DOI: [10.1016/j.jprocont.2012.06.018](https://doi.org/10.1016/j.jprocont.2012.06.018).
- [6] P. D. Christofides, “Robust control of parabolic PDE systems,” *Chemical Engineering Science*, vol. 53, no. 16, pp. 2949–2965, 1998, ISSN: 2324-9749. DOI: [10.1007/978-1-4612-0185-4_5](https://doi.org/10.1007/978-1-4612-0185-4_5).
- [7] M. Krstic and A. Smyshlyaev, “Backstepping boundary control for first-order hyperbolic PDEs and application to systems with actuator and sensor delays,” *Systems & Control Letters*, vol. 57, no. 9, pp. 750–758, 2008, ISSN: 0167-6911. DOI: [10.1016/j.sysconle.2008.02.005](https://doi.org/10.1016/j.sysconle.2008.02.005).
- [8] X. Xu and S. Dubljevic, “The state feedback servo-regulator for counter-current heat-exchanger system modelled by system of hyperbolic PDEs,” *European Journal of Control*, vol. 29, pp. 51–61, 2016, ISSN: 0947-3580. DOI: [10.1016/j.ejcon.2016.02.002](https://doi.org/10.1016/j.ejcon.2016.02.002).

- [9] J. Xie and S. Dubljevic, “Discrete-time modeling and output regulation of gas pipeline networks,” *Journal of Process Control*, vol. 98, pp. 30–40, 2021, ISSN: 0959-1524. DOI: [10.1016/j.jprocont.2020.12.002](https://doi.org/10.1016/j.jprocont.2020.12.002).
- [10] L. Zhang, J. Xie, and S. Dubljevic, “Tracking model predictive control and moving horizon estimation design of distributed parameter pipeline systems,” *Computers & Chemical Engineering*, vol. 178, p. 108381, 2023, ISSN: 0098-1354. DOI: [10.1016/j.compchemeng.2023.108381](https://doi.org/10.1016/j.compchemeng.2023.108381).
- [11] L. Zhang, J. Xie, and S. Dubljevic, “Dynamic modeling and model predictive control of a continuous pulp digester,” *AICHE Journal*, vol. 68, no. 3, e17534, 2022. DOI: [10.22541/au.164841554.43817131/v1](https://doi.org/10.22541/au.164841554.43817131/v1).
- [12] P. D. Christofides, *Nonlinear and robust control of PDE systems* (Systems & Control: Foundations & Applications). New York, NY: Springer, Oct. 2012.
- [13] S. Dubljevic, N. H. El-Farra, P. Mhaskar, and P. D. Christofides, “Predictive control of parabolic PDEs with state and control constraints,” *International Journal of Robust and Nonlinear Control*, vol. 16, no. 16, pp. 749–772, 2006, ISSN: 1049-8923. DOI: [10.1002/rnc.1097](https://doi.org/10.1002/rnc.1097).
- [14] G. O. Cassol, D. Ni, and S. Dubljevic, “Heat exchanger system boundary regulation,” *AICHE Journal*, vol. 65, no. 8, e16623, 2019, ISSN: 0001-1541. DOI: [10.1002/aic.16623](https://doi.org/10.1002/aic.16623).
- [15] S. Khatibi, G. O. Cassol, and S. Dubljevic, “Model predictive control of a non-isothermal axial dispersion tubular reactor with recycle,” *Computers & Chemical Engineering*, vol. 145, p. 107159, 2021, ISSN: 0098-1354. DOI: [10.1016/j.compchemeng.2020.107159](https://doi.org/10.1016/j.compchemeng.2020.107159).
- [16] K. A. Morris, *Controller design for distributed parameter systems*. Springer, 2020. DOI: [10.1007/978-3-030-34949-3_7](https://doi.org/10.1007/978-3-030-34949-3_7).
- [17] R. Curtain and H. Zwart. Springer Nature, 2020. DOI: [10.1007/978-1-0716-0590-5_1](https://doi.org/10.1007/978-1-0716-0590-5_1).
- [18] I. Aksikas, L. Mohammadi, J. F. Forbes, Y. Belhamadia, and S. Dubljevic, “Optimal control of an advection-dominated catalytic fixed-bed reactor with catalyst deactivation,” *Journal of Process Control*, vol. 23, no. 10, pp. 1508–1514, 2013, ISSN: 0959-1524. DOI: [10.1016/j.jprocont.2013.09.016](https://doi.org/10.1016/j.jprocont.2013.09.016).
- [19] L. Mohammadi, I. Aksikas, S. Dubljevic, and J. F. Forbes, “LQ-boundary control of a diffusion-convection-reaction system,” *International Journal of Control*, vol. 85, no. 2, pp. 171–181, 2012, ISSN: 0959-1524. DOI: [10.1080/00207179.2011.642308](https://doi.org/10.1080/00207179.2011.642308).

- [20] I. Aksikas, “Spectral-based optimal output-feedback boundary control of a cracking catalytic reactor PDE model,” *International Journal of Control*, vol. 97, no. 12, pp. 1–10, 2024, ISSN: 0020-7179. DOI: [10.1080/0207179.2024.2302057](https://doi.org/10.1080/0207179.2024.2302057).
- [21] M. Krstić (Systems & control). Birkhäuser, 2009.
- [22] G. O. Cassol and S. Dubljevic, “Discrete output regulator design for a mono-tubular reactor with recycle,” in *2019 American Control Conference (ACC)*, IEEE, 2019, pp. 1262–1267. DOI: [10.23919/acc.2019.8815250](https://doi.org/10.23919/acc.2019.8815250).
- [23] J. Qi, S. Dubljevic, and W. Kong, “Output feedback compensation to state and measurement delays for a first-order hyperbolic PIDE with recycle,” *Automatica*, vol. 128, p. 109565, 2021, ISSN: 0005-1098. DOI: [10.1016/j.automatica.2021.109565](https://doi.org/10.1016/j.automatica.2021.109565).
- [24] O. Levenspiel, *Chemical reaction engineering*. John Wiley & Sons, 1998.
- [25] K. F. Jensen and W. H. Ray, “The bifurcation behavior of tubular reactors,” *Chemical Engineering Science*, vol. 37, no. 2, pp. 199–222, 1982, ISSN: 0009-2509. DOI: [10.1016/0009-2509\(82\)80155-3](https://doi.org/10.1016/0009-2509(82)80155-3).
- [26] P. V. Danckwerts, “Continuous flow systems: Distribution of residence times,” *Chemical Engineering Science*, vol. 2, no. 1, pp. 1–13, 1953, ISSN: 0009-2509. DOI: [10.1016/0009-2509\(53\)80001-1](https://doi.org/10.1016/0009-2509(53)80001-1).
- [27] J. M. Ali, N. H. Hoang, M. A. Hussain, and D. Dochain, “Review and classification of recent observers applied in chemical process systems,” *Computers & Chemical Engineering*, vol. 76, pp. 27–41, 2015, ISSN: 0098-1354. DOI: [10.1016/j.compchemeng.2015.01.019](https://doi.org/10.1016/j.compchemeng.2015.01.019).
- [28] J. R. Dormand and P. J. Prince, “A family of embedded Runge-Kutta formulae,” *Journal of computational and applied mathematics*, vol. 6, no. 1, pp. 19–26, 1980, ISSN: 0377-0427. DOI: [10.1016/0771-050x\(80\)90013-3](https://doi.org/10.1016/0771-050x(80)90013-3).
- [29] L. F. Shampine, “Some practical Runge-Kutta formulas,” *Mathematics of computation*, vol. 46, no. 173, pp. 135–150, 1986, ISSN: 0025-5718. DOI: [10.2307/2008219](https://doi.org/10.2307/2008219).
- [30] P. Virtanen *et al.*, “SciPy 1.0: Fundamental Algorithms for Scientific Computing in Python,” *Nature Methods*, vol. 17, no. 3, pp. 261–272, 2020, ISSN: 1548-7091. DOI: [10.1038/s41592-019-0686-2](https://doi.org/10.1038/s41592-019-0686-2).
- [31] B. Moadeli and S. Dubljevic, “Model predictive control of axial dispersion tubular reactors with recycle: Addressing state-delay through transport PDEs,” in *2025 American Control Conference (ACC)*, 2025.

- [32] B. Moadeli and S. Dubljevic, “Observer-based MPC design of an axial dispersion tubular reactor: Addressing recycle delays through transport PDEs,” in *2025 European Control Conference (ECC)*, 2025.
- [33] D. Dochain, “State observers for tubular reactors with unknown kinetics,” *Journal of process control*, vol. 10, no. 2-3, pp. 259–268, 2000, ISSN: 0959-1524. DOI: [10.1016/s0959-1524\(99\)00020-7](https://doi.org/10.1016/s0959-1524(99)00020-7).
- [34] D. Dochain, “State observation and adaptive linearizing control for distributed parameter (bio) chemical reactors,” *International Journal of Adaptive Control and Signal Processing*, vol. 15, no. 6, pp. 633–653, 2001, ISSN: 0890-6327. DOI: [10.1002/acs.691](https://doi.org/10.1002/acs.691).
- [35] A. A. Alonso, I. G. Kevrekidis, J. R. Banga, and C. E. Frouzakis, “Optimal sensor location and reduced order observer design for distributed process systems,” *Computers & chemical engineering*, vol. 28, no. 1-2, pp. 27–35, 2004, ISSN: 0098-1354. DOI: [10.1016/s0098-1354\(03\)00175-3](https://doi.org/10.1016/s0098-1354(03)00175-3).
- [36] P. D. Christofides and P. Daoutidis, “Feedback control of hyperbolic PDE systems,” *AIChE Journal*, vol. 42, no. 11, pp. 3063–3086, 1996, ISSN: 0001-1541. DOI: [10.1002/aic.690421108](https://doi.org/10.1002/aic.690421108).
- [37] S. Dubljevic and P. D. Christofides, “Predictive control of parabolic PDEs with boundary control actuation,” *Chemical Engineering Science*, vol. 61, no. 18, pp. 6239–6248, 2006, ISSN: 0009-2509. DOI: [10.1016/j.ces.2006.05.041](https://doi.org/10.1016/j.ces.2006.05.041).
- [38] S. Hiratsuka and A. Ichikawa, “Optimal control of systems with transportation lags,” *IEEE Transactions on Automatic Control*, vol. 14, no. 3, pp. 237–247, 1969, ISSN: 0018-9286. DOI: [10.1109/TAC.1969.1099175](https://doi.org/10.1109/TAC.1969.1099175).
- [39] V. Havu and J. Malinen, “The Cayley transform as a time discretization scheme,” *Numerical Functional Analysis and Optimization*, vol. 28, no. 7-8, pp. 825–851, 2007, ISSN: 0163-0563. DOI: [10.1080/01630560701493321](https://doi.org/10.1080/01630560701493321).
- [40] Q. Xu and S. Dubljevic, “Linear model predictive control for transport-reaction processes,” *AIChE Journal*, vol. 63, no. 7, pp. 2644–2659, 2017, ISSN: 0001-1541. DOI: [10.1002/aic.15592](https://doi.org/10.1002/aic.15592).
- [41] E. Hairer, M. Hochbruck, A. Iserles, and C. Lubich, “Geometric numerical integration,” *Oberwolfach Reports*, vol. 3, no. 1, pp. 805–882, 2006, ISSN: 1660-8933. DOI: [10.4171/owr/2011/16](https://doi.org/10.4171/owr/2011/16).
- [42] B. Moadeli and S. Dubljevic, “Advanced control of non-isothermal axial dispersion tubular reactors with recycle-induced state delay,” *The Canadian Journal of Chemical Engineering*, 2025.

- [43] V. Hlaváček and H. Hofmann, “Modeling of chemical reactors—XVII steady state axial heat and mass transfer in tubular reactors numerical investigation of multiplicity,” *Chemical Engineering Science*, vol. 25, no. 1, pp. 187–199, 1970, ISSN: 0009-2509. DOI: [10.1016/0009-2509\(70\)85031-x](https://doi.org/10.1016/0009-2509(70)85031-x).
- [44] V. Hlaváček and H. Hofmann, “Modeling of chemical reactors—XVI steady state axial heat and mass transfer in tubular reactors an analysis of the uniqueness of solutions,” *Chemical Engineering Science*, vol. 25, no. 1, pp. 173–185, 1970, ISSN: 0009-2509. DOI: [10.1016/0009-2509\(70\)85030-8](https://doi.org/10.1016/0009-2509(70)85030-8).
- [45] D. S. Cohen and A. B. Poore, “Tubular chemical reactors: The “lumping approximation” and bifurcation of oscillatory states,” *SIAM Journal on Applied Mathematics*, vol. 27, no. 3, pp. 416–429, 1974, ISSN: 0036-1399. DOI: [10.1137/0127032](https://doi.org/10.1137/0127032).
- [46] C. Georgakis, R. Aris, and N. R. Amundson, “Studies in the control of tubular reactors-I general considerations,” *Chemical Engineering Science*, vol. 32, no. 11, pp. 1359–1369, 1977, ISSN: 0009-2509. DOI: [10.1016/0009-2509\(77\)85032-x](https://doi.org/10.1016/0009-2509(77)85032-x).
- [47] D. Luss and N. R. Amundson, “Stability of loop reactors,” *AICHE Journal*, vol. 13, no. 2, pp. 279–290, 1967, ISSN: 0001-1541. DOI: [10.1002/aic.690130218](https://doi.org/10.1002/aic.690130218).
- [48] C. S. Bildea, A. C. Dimian, S. C. Cruz, and P. D. Iedema, “Design of tubular reactors in recycle systems,” *Computers & chemical engineering*, vol. 28, no. 1-2, pp. 63–72, 2004, ISSN: 0098-1354. DOI: [10.1016/s0098-1354\(03\)00170-4](https://doi.org/10.1016/s0098-1354(03)00170-4).
- [49] P. D. Christofides and P. Daoutidis, “Finite-dimensional control of parabolic PDE systems using approximate inertial manifolds,” *Journal of Mathematical Analysis and Applications*, vol. 216, no. 2, pp. 398–420, 1997, ISSN: 0022-247X. DOI: [10.1006/jmaa.1997.5649](https://doi.org/10.1006/jmaa.1997.5649).
- [50] A. Armaou and P. D. Christofides, “Dynamic optimization of dissipative PDE systems using nonlinear order reduction,” *Chemical Engineering Science*, vol. 57, no. 24, pp. 5083–5114, 2002, ISSN: 0009-2509. DOI: [10.1016/s0009-2509\(02\)00419-0](https://doi.org/10.1016/s0009-2509(02)00419-0).
- [51] I. Aksikas, A. A. Moghadam, and F. Forbes, “Optimal linear-quadratic control of coupled parabolic–hyperbolic PDEs,” *International Journal of Control*, vol. 90, no. 10, pp. 2152–2164, 2017. DOI: [10.1109/icca.2017.803083](https://doi.org/10.1109/icca.2017.803083).

- [52] M. J. Balas, “Feedback control of linear diffusion processes,” *International Journal of Control*, vol. 29, no. 3, pp. 523–534, 1979. DOI: [10.1016/b978-0-12-734250-4.50041-2](https://doi.org/10.1080/002071790890412).
- [53] R. Curtain, “Finite-dimensional compensator design for parabolic distributed systems with point sensors and boundary input,” *IEEE Transactions on Automatic Control*, vol. 27, no. 1, pp. 98–104, 1982, ISSN: 0018-9286. DOI: [10.1109/tac.1982.1102875](https://doi.org/10.1109/tac.1982.1102875).
- [54] J. Xie, J.-P. Humaloja, C. R. Koch, and S. Dubljevic, “Constrained receding horizon output estimation of linear distributed parameter systems,” *IEEE Transactions on Automatic Control*, vol. 68, no. 8, pp. 5103–5110, 2022, ISSN: 0018-9286. DOI: [10.1109/tac.2022.3217111](https://doi.org/10.1109/tac.2022.3217111).
- [55] R. F. Heinemann and A. B. Poore, “The effect of activation energy on tubular reactor multiplicity,” *Chemical Engineering Science*, vol. 37, no. 1, pp. 128–131, 1982, ISSN: 0009-2509. DOI: [10.1016/0009-2509\(82\)80079-1](https://doi.org/10.1016/0009-2509(82)80079-1).
- [56] A. Hastir, F. Lamoline, J. J. Winkin, and D. Dochain, “Analysis of the existence of equilibrium profiles in nonisothermal axial dispersion tubular reactors,” *IEEE Transactions on Automatic Control*, vol. 65, no. 4, pp. 1525–1536, 2020, ISSN: 0018-9286. DOI: [10.1109/tac.2019.2921675](https://doi.org/10.1109/tac.2019.2921675).

Appendix A

Additional Example Figures

Each of the following pages will provide an example of a different figure configuration. In addition to the examples the code that generates the figure will be provided and explanations of what the different parts of the code do will be included. From all of the included information in this Appendix it should be possible to even develop your own figures that potentially suit your needs best.

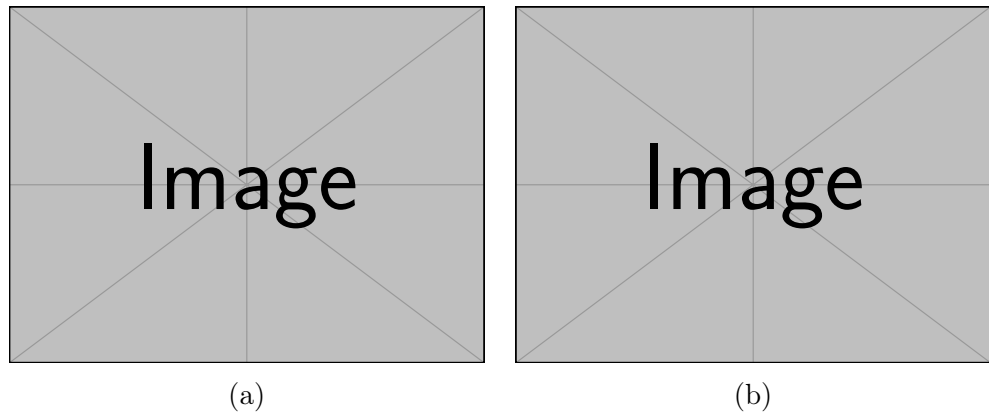


Figure A.1: This is an example of a double image figure.

```
\begin{figure}[H]
\centering
\begin{subfigure}{0.45\linewidth}
\includegraphics[width=\linewidth]{example-image}
\caption{} % Leave blank for just letter
\label{fig:doubleImage2:a}
\end{subfigure}
\begin{subfigure}{0.45\linewidth}
\includegraphics[width=\linewidth]{example-image}
\caption{} % Leave blank for just letter
\label{fig:doubleImage2:b}
\end{subfigure}
\caption{This is an example of a double image figure.}
\label{fig:doubleImage2}
\end{figure}
```

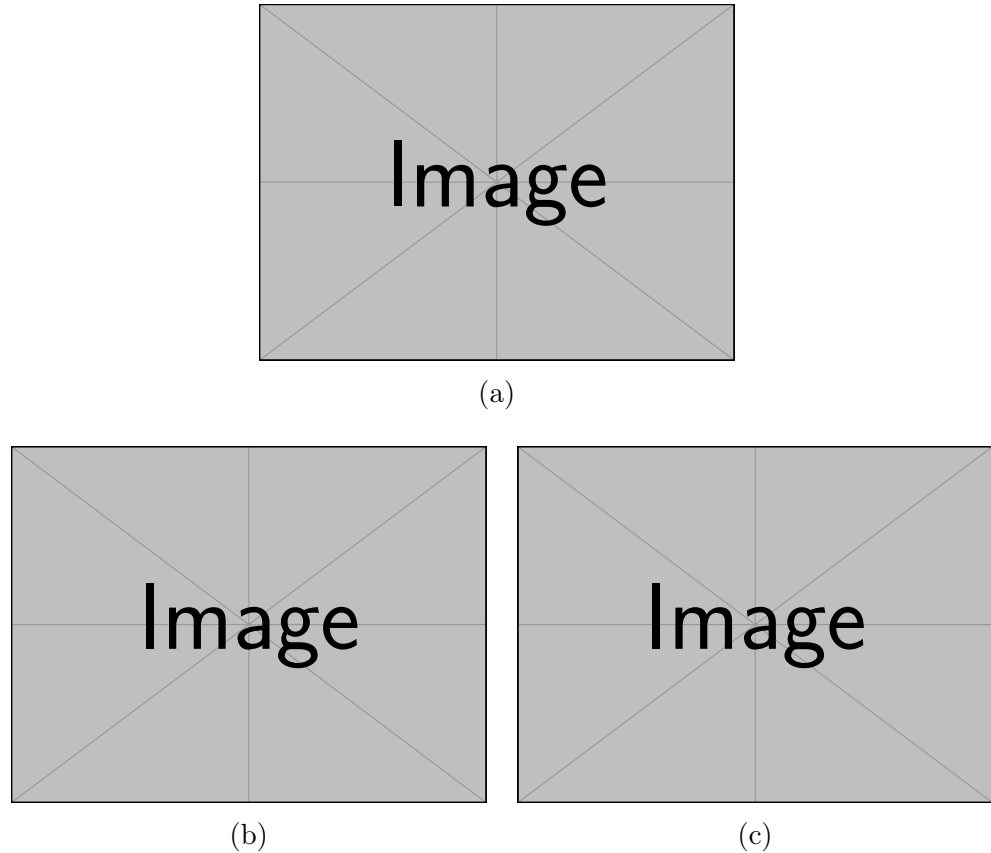


Figure A.2: This is an example of a triple image figure.

```
\begin{figure}[H]
    \centering
    \hspace*{\fill}\% Adds space to left of top image (prevents two images from going to top)
    \begin{subfigure}{0.45\linewidth}
        \includegraphics[width=\linewidth]{example-image}
        \caption{} \% Leave blank for just letter
        \label{fig:tripleImage1:a}
    \end{subfigure}
    \hspace*{\fill}\% Adds space to right of top image (prevents two images from going to top)
    \par\vspace{1em}\% Adds space between upper and lower images
    \begin{subfigure}{0.45\linewidth}
        \includegraphics[width=\linewidth]{example-image}
        \caption{} \% Leave blank for just letter
        \label{fig:tripleImage1:b}
    \end{subfigure}
    \% Adds space between the two lower figures
    \begin{subfigure}{0.45\linewidth}
        \includegraphics[width=\linewidth]{example-image}
        \caption{} \% Leave blank for just letter
        \label{fig:tripleImage1:c}
    \end{subfigure}
    \caption{This is an example of a triple image figure.}
    \label{fig:tripleImage1}
\end{figure}
```

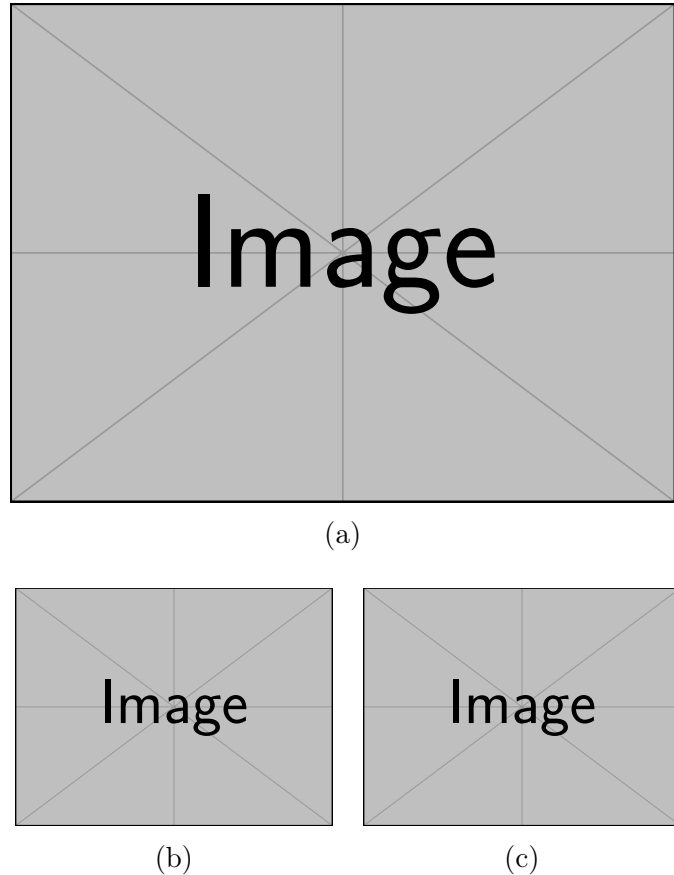


Figure A.3: This is a second example of a triple image figure.

```
\begin{figure}[H]
\centering
\hspace*{\fill}\% Adds space to left of top image (prevents two images from going to top)
\begin{subfigure}{0.90\linewidth+1em} \% 0.9 = 0.45 + 0.45, and 1em is the width of ~
    \includegraphics[width=\linewidth]{example-image}
    \caption{} \% Leave blank for just letter
    \label{fig:tripleImage2:a}
\end{subfigure}
\hspace*{\fill}\% Adds space to right of top image (prevents two images from going to top)
\par\vspace{1em}\% Adds space between upper and lower images
\begin{subfigure}{0.45\linewidth}
    \includegraphics[width=\linewidth]{example-image}
    \caption{} \% Leave blank for just letter
    \label{fig:tripleImage2:b}
\end{subfigure}
\% Adds space between the two lower figures
\begin{subfigure}{0.45\linewidth}
    \includegraphics[width=\linewidth]{example-image}
    \caption{} \% Leave blank for just letter
    \label{fig:tripleImage2:c}
\end{subfigure}
\caption{This is a second example of a triple image figure.}
\label{fig:tripleImage2}
\end{figure}
```

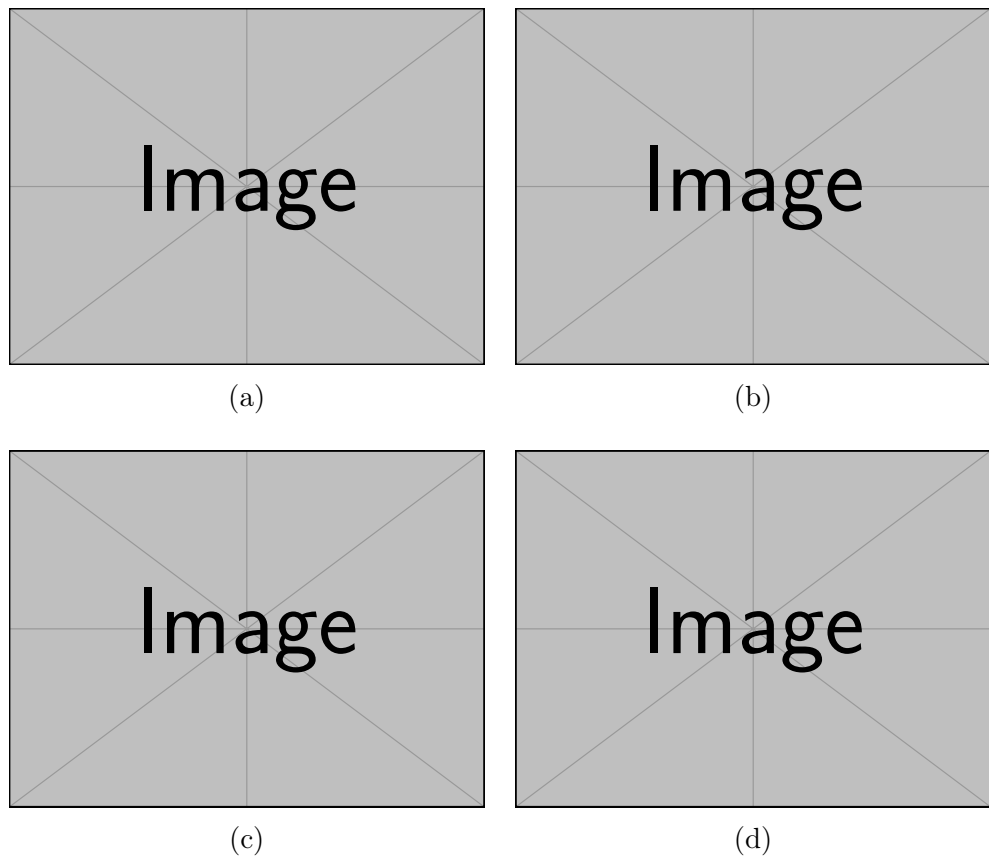


Figure A.4: This is an example of a quad image figure.

```
\begin{figure}[H]
    \centering
    \begin{subfigure}{0.45\linewidth}
        \includegraphics[width=\linewidth]{example-image}
        \caption{} % Leave blank for just letter
        \label{fig:quadImage:a}
    \end{subfigure}
    ~ % Adds space between the two top figures
    \begin{subfigure}{0.45\linewidth}
        \includegraphics[width=\linewidth]{example-image}
        \caption{} % Leave blank for just letter
        \label{fig:quadImage:b}
    \end{subfigure}
    \par\vspace{1em} % Adds space between upper and lower images
    \begin{subfigure}{0.45\linewidth}
        \includegraphics[width=\linewidth]{example-image}
        \caption{} % Leave blank for just letter
        \label{fig:quadImage:c}
    \end{subfigure}
    ~ % Adds space between the two lower figures
    \begin{subfigure}{0.45\linewidth}
        \includegraphics[width=\linewidth]{example-image}
        \caption{} % Leave blank for just letter
        \label{fig:quadImage:d}
    \end{subfigure}
    \caption{This is an example of a quad image figure.}
    \label{fig:quadImage}
\end{figure}
```

Appendix B

Additional Example Tables

B.1 Section 1

Nullam eleifend justo in nisl. In hac habitasse platea dictumst. Morbi nonummy. Aliquam ut felis. In velit leo, dictum vitae, posuere id, vulputate nec, ante. Maecenas vitae pede nec dui dignissim suscipit. Morbi magna. Vestibulum id purus eget velit laoreet laoreet. Praesent sed leo vel nibh convallis blandit. Ut rutrum. Donec nibh. Donec interdum. Fusce sed pede sit amet elit rhoncus ultrices. Nullam at enim vitae pede vehicula iaculis.

Class aptent taciti sociosqu ad litora torquent per conubia nostra, per inceptos hymenaeos. Aenean nonummy turpis id odio. Integer euismod imperdiet turpis. Ut nec leo nec diam imperdiet lacinia. Etiam eget lacus eget mi ultricies posuere. In placerat tristique tortor. Sed porta vestibulum metus. Nulla iaculis sollicitudin pede. Fusce luctus tellus in dolor. Curabitur auctor velit a sem. Morbi sapien. Class aptent taciti sociosqu ad litora torquent per conubia nostra, per inceptos hymenaeos. Donec adipiscing urna vehicula nunc. Sed ornare leo in leo. In rhoncus leo ut dui. Aenean dolor quam, volutpat nec, fringilla id, consectetur vel, pede.

Nulla malesuada risus ut urna. Aenean pretium velit sit amet metus. Duis

iaculis. In hac habitasse platea dictumst. Nullam molestie turpis eget nisl. Duis a massa id pede dapibus ultricies. Sed eu leo. In at mauris sit amet tortor bibendum varius. Phasellus justo risus, posuere in, sagittis ac, varius vel, tortor. Quisque id enim. Phasellus consequat, libero pretium nonummy fringilla, tortor lacus vestibulum nunc, ut rhoncus ligula neque id justo. Nullam accumsan euismod nunc. Proin vitae ipsum ac metus dictum tempus. Nam ut wisi. Quisque tortor felis, interdum ac, sodales a, semper a, sem. Curabitur in velit sit amet dui tristique sodales. Vivamus mauris pede, lacinia eget, pellentesque quis, scelerisque eu, est. Aliquam risus. Quisque bibendum pede eu dolor.

B.2 Section 2

Fusce suscipit cursus sem. Vivamus risus mi, egestas ac, imperdiet varius, faucibus quis, leo. Aenean tincidunt. Donec suscipit. Cras id justo quis nibh scelerisque dignissim. Aliquam sagittis elementum dolor. Aenean consectetur justo in pede. Curabitur ullamcorper ligula nec orci. Aliquam purus turpis, aliquam id, ornare vitae, porttitor non, wisi. Maecenas luctus porta lorem. Donec vitae ligula eu ante pretium varius. Proin tortor metus, convallis et, hendrerit non, scelerisque in, urna. Cras quis libero eu ligula bibendum tempor. Vivamus tellus quam, malesuada eu, tempus sed, tempor sed, velit. Donec lacinia auctor libero.

Appendix C

Including Code Listings

This appendix provides guidelines for including code listings in your thesis. Code listings are often used to demonstrate algorithms, data processing scripts, or other relevant programming content. Proper formatting ensures that code is both readable and aesthetically pleasing.

C.1 Using the `listings` Package

The `listings` package is a powerful tool for displaying code in LaTeX. It supports syntax highlighting for a wide variety of programming languages and offers many customization options.

C.1.1 Basic Usage

To include a simple code listing, you can use the following command:

```
\begin{lstlisting}[language=Python]
    # Your code here
    print("Hello, world!")
\end{lstlisting}
```

The `language` option specifies the programming language, which enables syntax highlighting. Replace `Python` with the appropriate language for your

code.

C.1.2 Customizing Listings

The `listings` package allows for extensive customization. You can adjust the appearance of your code by setting options such as `frame`, `backgroundcolor`, `keywordstyle`, and more.

Here is an example of how to customize your code listing:

```
\lstset{
    language=Python ,
    frame=single ,
    backgroundcolor=\color{gray!10} ,
    keywordstyle=\color{blue}\bfseries ,
    commentstyle=\color{green} ,
    stringstyle=\color{red} ,
    basicstyle=\ttfamily ,
    breaklines=true
}
```

This configuration adds a single-line frame around the code, sets a light gray background, and defines styles for keywords, comments, and strings.

Listing C.1: This is a caption for the inserted code

```
function [outputs] = functionName(inputs)
%
% This is a Comment Block
% That
% can
% span
% multiple
% lines.
%

% This is a regular comment
a = 1 + 2 * sin(angle);
b = 'This is a String';
```

Listing C.2: This is a caption for the inserted code

```
#include <iostream>
using namespace std;
/* This function adds two integer values
* and returns the result
*/
```

```

int sum( int num1, int num2){
    int num3 = num1 + num2; return num3;
}

void main(){
    //Calling the function
    cout << 'The sum is:' << sum(1,99);
}

```

C.2 Advanced Features

C.2.1 Including External Files

The `listings` package allows you to include code from external files. This is particularly useful if you have long code files that you want to reference directly.

```
\lstinputlisting[language=Python]{path/to/your/code.py}
```

Replace `path/to/your/code.py` with the actual path to your file. Or you can use the `\addmedia{./99_Inclusions/}` and `\addcode{Code/}` commands to define the location for code files, then you can just use `\insertcode{filename.ext}` command instead of the full path. You can customize the display in the same way as inline listings.

C.2.2 Handling Special Characters

If your code contains special characters (*e.g.*, #, %, \$), you may need to escape them or use the `literate` option to ensure proper display.

```
\lstset{
    literate={~} {$\sim$}{1}
```

This command, for example, replaces the tilde symbol with the appropriate LaTeX command.

C.3 Line Breaks in Long Code Lines

To automatically break long lines of code, use the `breaklines=true` option as shown in the earlier examples. This prevents code from running off the page and maintains readability.

C.4 Conclusion

Including well-formatted code listings in your thesis can enhance the clarity of your work and demonstrate your technical skills. By following the guidelines in this appendix, you can ensure that your code is presented professionally.

Appendix D

Including PDFs

⚠ WARNING While it is possible to have horizontal pages with the page numbers centered on the bottom long edge, I *DO NOT* recommended it. This is because, while it looks okay in a digital format, this is not suitable for printing... this would print page numbers on the side of the page rather than consistently on the bottom or in the heading.

The package that is used to include PDF's is `pdfpages`. This provide the main command `\includepdf` that can be used to include a PDF. Further, this package provides another command, `\includepdfset`, that can be used in the start of the document to pre-set some of the default values. This class file detects the presence of this package and invokes this command as follows:

```
\includepdfset{pages=-, scale=0.85, pagecommand=\  
    thispagestyle{STYLE}}
```

Where `pages=-` defaults to including all pages from the PDF and `scale=0.85` scales the inserted PDF to 85% of its original size, so that the documents fit within the page's margins, headers, and footers.

Further, the option `pagecommand=\cmd {thispagestyle}\mopt {STYLE}` sets the pagestyle for the PDF pages, where, `STYLE` is replaced with the current

pagestyle¹ that is in use.

D.1 How to Insert a Portrait PDF

To insert a portrait-oriented PDF into your LaTeX document, you can use the `pdfpages` package, which provides a convenient way to include external PDF files. The following code snippet demonstrates how to include a portrait PDF with the specified options:

```
\includepdf{./99_Inclusions/PDFs/examplePDF}
```

¹To change the pagestyle of this one can add or remove the class option `fancyheaders`.

This is an Example PDF that is Portrait

This is the second page

D.2 How to Insert a Landscape PDF

Inserting a landscape-oriented PDF is similarly straightforward using the `pdfpages` package. The code snippet below demonstrates how to include a landscape PDF:

```
\includepdf[landscape=true]{./99_Inclusions/PDFs/  
landscapePDF}
```

Here, `landscape` sets the orientation to landscape. This configuration ensures that your landscape PDF is correctly oriented and properly sized within your document.

This is an Example PDF that is Landscape

This is the second page

Appendix E

Math Lettering

Table E.1: Math Mode Greek Letters

Command	Output	Command	Output	Command	Output
<code>\alpha</code>	α	<code>\beta</code>	β	<code>\gamma</code>	γ
<code>\delta</code>	δ	<code>\epsilon</code>	ϵ	<code>\zeta</code>	ζ
<code>\eta</code>	η	<code>\theta</code>	θ	<code>\iota</code>	ι
<code>\kappa</code>	κ	<code>\lambda</code>	λ	<code>\mu</code>	μ
<code>\nu</code>	ν	<code>\xi</code>	ξ	<code>\o</code>	\o
<code>\pi</code>	π	<code>\rho</code>	ρ	<code>\sigma</code>	σ
<code>\tau</code>	τ	<code>\upsilon</code>	υ	<code>\phi</code>	ϕ
<code>\chi</code>	χ	<code>\psi</code>	ψ	<code>\omega</code>	ω
A	A	B	B	<code>\Gamma</code>	Γ
<code>\Delta</code>	Δ	E	E	Z	Z
H	H	<code>\Theta</code>	Θ	I	I
K	K	<code>\Lambda</code>	Λ	M	M
N	N	<code>\Xi</code>	Ξ	O	O
<code>\Pi</code>	Π	P	P	<code>\Sigma</code>	Σ
T	T	<code>\Upsilon</code>	Υ	<code>\Phi</code>	Φ
X	X	<code>\Psi</code>	Ψ	<code>\Omega</code>	Ω

Table E.2: Blackboard Bold Letters

Command	Output	Command	Output	Command	Output
<code>\mathbb{A}</code>	\mathbb{A}	<code>\mathbb{B}</code>	\mathbb{B}	<code>\mathbb{C}</code>	\mathbb{C}
<code>\mathbb{D}</code>	\mathbb{D}	<code>\mathbb{E}</code>	\mathbb{E}	<code>\mathbb{F}</code>	\mathbb{F}
<code>\mathbb{G}</code>	\mathbb{G}	<code>\mathbb{H}</code>	\mathbb{H}	<code>\mathbb{I}</code>	\mathbb{I}
<code>\mathbb{J}</code>	\mathbb{J}	<code>\mathbb{K}</code>	\mathbb{K}	<code>\mathbb{L}</code>	\mathbb{L}
<code>\mathbb{M}</code>	\mathbb{M}	<code>\mathbb{N}</code>	\mathbb{N}	<code>\mathbb{O}</code>	\mathbb{O}
<code>\mathbb{P}</code>	\mathbb{P}	<code>\mathbb{Q}</code>	\mathbb{Q}	<code>\mathbb{R}</code>	\mathbb{R}
<code>\mathbb{S}</code>	\mathbb{S}	<code>\mathbb{T}</code>	\mathbb{T}	<code>\mathbb{U}</code>	\mathbb{U}
<code>\mathbb{V}</code>	\mathbb{V}	<code>\mathbb{W}</code>	\mathbb{W}	<code>\mathbb{X}</code>	\mathbb{X}
<code>\mathbb{Y}</code>	\mathbb{Y}	<code>\mathbb{Z}</code>	\mathbb{Z}		

Table E.3: Calligraphic Letters

Command	Output	Command	Output	Command	Output
<code>\mathcal{A}</code>	\mathcal{A}	<code>\mathcal{B}</code>	\mathcal{B}	<code>\mathcal{C}</code>	\mathcal{C}
<code>\mathcal{D}</code>	\mathcal{D}	<code>\mathcal{E}</code>	\mathcal{E}	<code>\mathcal{F}</code>	\mathcal{F}
<code>\mathcal{G}</code>	\mathcal{G}	<code>\mathcal{H}</code>	\mathcal{H}	<code>\mathcal{I}</code>	\mathcal{I}
<code>\mathcal{J}</code>	\mathcal{J}	<code>\mathcal{K}</code>	\mathcal{K}	<code>\mathcal{L}</code>	\mathcal{L}
<code>\mathcal{M}</code>	\mathcal{M}	<code>\mathcal{N}</code>	\mathcal{N}	<code>\mathcal{O}</code>	\mathcal{O}
<code>\mathcal{P}</code>	\mathcal{P}	<code>\mathcal{Q}</code>	\mathcal{Q}	<code>\mathcal{R}</code>	\mathcal{R}
<code>\mathcal{S}</code>	\mathcal{S}	<code>\mathcal{T}</code>	\mathcal{T}	<code>\mathcal{U}</code>	\mathcal{U}
<code>\mathcal{V}</code>	\mathcal{V}	<code>\mathcal{W}</code>	\mathcal{W}	<code>\mathcal{X}</code>	\mathcal{X}
<code>\mathcal{Y}</code>	\mathcal{Y}	<code>\mathcal{Z}</code>	\mathcal{Z}		

Table E.4: Fraktur Letters

Command	Output	Command	Output	Command	Output
<code>\mathfrak{a}</code>	a	<code>\mathfrak{b}</code>	b	<code>\mathfrak{c}</code>	c
<code>\mathfrak{d}</code>	d	<code>\mathfrak{e}</code>	e	<code>\mathfrak{f}</code>	f
<code>\mathfrak{g}</code>	g	<code>\mathfrak{h}</code>	h	<code>\mathfrak{i}</code>	i
<code>\mathfrak{j}</code>	j	<code>\mathfrak{k}</code>	k	<code>\mathfrak{l}</code>	l
<code>\mathfrak{m}</code>	m	<code>\mathfrak{n}</code>	n	<code>\mathfrak{o}</code>	o
<code>\mathfrak{p}</code>	p	<code>\mathfrak{q}</code>	q	<code>\mathfrak{r}</code>	r
<code>\mathfrak{s}</code>	s	<code>\mathfrak{t}</code>	t	<code>\mathfrak{u}</code>	u
<code>\mathfrak{v}</code>	v	<code>\mathfrak{w}</code>	w	<code>\mathfrak{x}</code>	x
<code>\mathfrak{y}</code>	y	<code>\mathfrak{z}</code>	z		
<code>\mathfrak{A}</code>	A	<code>\mathfrak{B}</code>	B	<code>\mathfrak{C}</code>	C
<code>\mathfrak{D}</code>	D	<code>\mathfrak{E}</code>	E	<code>\mathfrak{F}</code>	F
<code>\mathfrak{G}</code>	G	<code>\mathfrak{H}</code>	H	<code>\mathfrak{I}</code>	I
<code>\mathfrak{J}</code>	J	<code>\mathfrak{K}</code>	K	<code>\mathfrak{L}</code>	L
<code>\mathfrak{M}</code>	M	<code>\mathfrak{N}</code>	N	<code>\mathfrak{O}</code>	O
<code>\mathfrak{P}</code>	P	<code>\mathfrak{Q}</code>	Q	<code>\mathfrak{R}</code>	R
<code>\mathfrak{S}</code>	S	<code>\mathfrak{T}</code>	T	<code>\mathfrak{U}</code>	U
<code>\mathfrak{V}</code>	V	<code>\mathfrak{W}</code>	W	<code>\mathfrak{X}</code>	X